Space Weather
Science and Observation Gap Analysis for the National Aeronautics and Space Administration (NASA)

A Report to NASA's Space Weather Science Application Program

Compiled by APL
Sep.2020 - Apr.2021

Committee Members and Acknowledgments

Committee

Angelos Vourlidas (chair), Drew Turner (co-chair), Doug Biesecker, Anthea Coster, Alec Engell, George Ho, Tom Immel, Catherine Keys, Lou Lanzerotti, Gang Lu, Noé Lugaz, Janet Luhmann, Leila Mays, Paul O'Brien, Eddie Semones, Harlan Spence, Lisa Upton, Stephen White

Ex-officio: Jim Spann, Elsayed Talaat, Mike Wiltberger, James Favors, Reiner Friedel

Acknowledgments

The committee thanks the external experts and referees for their valuable input that has enhanced the report: Doug Brinkman, Manolis Georgoulis, Justin Likar, Jeffrey Love, Slava Merkin, Jeff Newmark, Phil Quinn, Ian Richardson, Dimitrios Vasiliadis, Kathryn Whitman, Harry Warren.

Table of Contents

List of Figures

List of Tables

Executive Summary

This document describes the results of a science and measurement gap analysis for the Space Weather Science Application Program (SWxSA) within NASA's Heliophysics Division (HPD). The analysis was performed by a committee of space weather (SWx) experts from academia, the commercial sector, and the space weather operational and end-user community under a NASA task order to the Johns Hopkins Applied Physics Laboratory (APL). The study informs on how measurements from NASA observatories will advance forecasting, nowcasting, and hindcasting (collectively referred to as "*-casting") capabilities by focusing on two tasks: (1) assess the current state of NASA's observational capability to address the science of SWx and improve accuracy of predictive SWx *-casting models and (2) identify high-priority measurements critical to improved *-casting that are either at risk or currently unavailable (Section 1.2).

In identifying measurements and assigning priorities, the committee considered both Earth-based SWx users and NASA's space exploration needs (Sections 2 and 3), particularly in cislunar, interplanetary space, and Mars locations. The committee determined that measurement requirements could be naturally split into those related to the solar drivers and hazards, such as flare radiation, coronal mass ejections (CMEs) or solar energetic particles (SEPs), and those related to the response to those drivers plus internal drivers of SWx in the geospace environment (Section 4). Solar and heliospheric (SH) measurements tend to be associated with the full range of forecasting needs, from minutes (SEPs) to days (arrival of CMEs), while geospace measurements are generally relevant to nowcasting and short-term forecasting requirements (current conditions to minutes to hours in advance). The committee also took into account longer-term climatological concerns, such as flare/CME prediction and solar-cycle variations (Section 4.3) as these fall squarely under NASA HPD's purview. Space weather hazards that occur very frequently (e.g., daily) but have relatively low societal and cost impacts (e.g., ionospheric disturbances affecting satellite communications) were considered comparably as important as those that occur quite infrequently but have potentially very consequential societal and cost impacts (e.g., large geomagnetic storms and geomagnetically induced currents [GICs]). It should be noted here too that prediction accuracy of "all clear" environmental conditions are of equivalent value and importance to prediction accuracy of adverse and hazardous conditions.

The detailed measurement gap analysis is described in Section 5 and summarized in Table 5-1 (for SH measurements) and Figures 5-1 through 5-10 (for geospace measurements). Based on the details presented in Section 5, and weights derived from metrics on breadth and level of SWx impact and scientific value/interest (Section 6), the committee identified the following top-level, highest priority observational gaps in rank order. Table 1 consists of the seven highest priority observable/measurement categories out of over 40 considered. Measurements or observables pertaining to each gap in the table below are detailed in Section 5 and summarized in Section 6.

Summary Table 1. Top-ranked current SWx observation and research gap categories

Rank	Current Observation Gaps	Research Gaps
1	Solar/solar wind observations, including off Sun–Earth line (SEL) (e.g., Sun–Earth L4 and L5) and beyond 1 AU	SEP occurrence and properties at a given inner heliospheric location; interplanetary (IP) propagation of solar transients (e.g., B_z, time of arrival [ToA])

Rank	Current Observation Gaps	Research Gaps
2	Ionospheric key observables	Response to variable solar, interplanetary, thermospheric, and magnetospheric conditions; high resolution global state; cross-scale and -altitude dependencies and variability; driving from lower atmosphere
3	Solar wind in peri-geospace (i.e., within ~20 R_E of Earth's dayside bow shock)	Fine-scale structure of SW-transients; spatiotemporal evolution and turbulence
4	Thermospheric key observables	Expansion, heating, and cooling processes over a range of scales (<100 km to global) and altitudes; response to variable solar, ionospheric, and magnetospheric conditions; driving from lower atmosphere
5	Ionospheric D- and E-region energetic particle precipitation (EPP) and E- and F-region cusp and auroral precipitation	Impacts of energetic particle, cusp, and auroral precipitation on ionosphere–thermosphere system; cross-scale (<100 km to global) and spatiotemporal nature of precipitation and consequences on ionosphere–thermosphere system (e.g., conductivity, heating, chemistry and cooling)
6	Ring current and radiation belt electrons	Role of magnetospheric dynamics, mesoscale injections, and variety of wave-particle interactions acting in concert to shape these trapped energetic particle populations, driving geomagnetic storms and radiation belt enhancements and depletions
7	Plasma sheet electrons and injections/bursts from cislunar into geosynchronous and medium Earth orbit (GEO and MEO) regions	Nature of kinetic- to mesoscale processes (e.g., reconnection, turbulence) affecting global-scale magnetospheric dynamics and magnetosphere–ionosphere coupling

Solar and solar wind observables from off the Sun–Earth line (SEL), respectively, provide information on active regions, coronal holes, and other structures on the "farside" (i.e., around the left-hand [eastern] and right-hand [western] horizons of the solar disk as viewed from an Earth-based perspective, including at the Sun–Earth L1 point) that may be affecting, or may eventually affect, Earth. In particular, the L4 and L5 Sun–Earth Lagrange points offer ideal locations to extend our solar observable horizons around the eastern and western limbs, respectively. Because of the pervasiveness of solar and solar wind driving, and sources, on so many aspects (essentially all) of SWx, solar and solar wind observation gaps ranked high in this priority scheme.

Often, significant errors occur when solar wind quantities from observations made around L1 (~240 R_E upstream of Earth along the SEL) are propagated to Earth's subsolar magnetopause at 1 AU. The average transit time for a typical packet of solar wind plasma is ~45 min from L1 to Earth's subsolar magnetopause. Propagation errors result from the frequent complexity of solar wind structures and the spatiotemporal evolution of the turbulent solar wind as it propagates between L1 and Earth's magnetopause. For this reason, a dedicated and continuous solar wind monitoring system in *peri-geospace* (i.e., the space around geospace, approximately corresponding to cislunar range) also ranks high on this prioritization scheme, since reducing errors in solar wind input conditions will also reduce error in SWx predictive-model outputs driven by solar wind conditions. Whenever possible, observables that can contribute as real-time boundary conditions for operational models (e.g., solar wind in peri-geospace as a real-time boundary condition for magnetosphere–ionosphere–thermosphere systems models) should also be improved and populated; such real-time, observation-driven model boundary conditions should lead to improved performance and accuracy of nowcasting and forecasting models.

There remain key observation gaps in solar disk and coronal monitoring from Earth's perspective (and at other solar longitudes), such as more global solar magnetic field maps and solar spectral irradiance (SSI) from ultraviolet (UV) to X-rays. These gaps also remain at relatively high priority considering the important aspects of these observables as model inputs for thermospheric density, for example. The most direct observational way to improve the lead time for geospace modeling

is to use model inputs for the solar wind parameters (typically velocity, density, temperature, and vector magnetic field) and the SSI. Full-disk magnetograms, and global maps constructed from them, are the primary basis for both of these models. These also allow monitoring of active region emergence and evolution and, if available for the farside and/or from L5, can provide both improved synoptic maps for longer-lead solar wind predictions as well as possible flare and CME-alerts. For additional activity forecasts, solar radiation monitors (solar radio burst [SRB], flare, and solar energetic particles [SEP] monitoring) should also be conducted from a distributed network of solar/solar wind monitoring, including at the L4, L5, and L1 Lagrange points and in peri-geospace; such monitors will be of increasing importance as humanity returns to the Moon and expands its presence further to Mars and beyond.

Ionospheric effects on satellite communications and navigation signals plus the threat of spacecraft charging due to enhanced current systems and electron precipitation around low Earth orbit (LEO) result in the next highest priority category of observation gaps. Similarly, key observables for quantifying and predicting thermospheric expansion and contraction also ranked high. This is because of the threat of enhanced atmospheric drag affecting satellite lifetimes and orbit prediction uncertainty, all of which lead to higher possibilities of satellite collisions and the proliferation of debris fields around LEO. Energetic particle precipitation (EPP) and auroral (i.e., lower-energy, <100 keV) precipitation into the upper layers of Earth's atmosphere results in enhanced and often localized ionospheric heating and conductivity plus thermospheric heating. Measurements of that precipitation rounds off the top seven priorities related to SWx hazards in Earth's ionosphere–thermosphere system, including aspects of magnetosphere–ionosphere coupling. Precipitating electrons and electrons corresponding to ionospheric and field-aligned current (FAC) systems also pose a hazard to spacecraft surface and subsurface/hybrid charging in the proliferated LEO environment. Major gaps are looming in the near future with the discontinuation of the Defense Meteorological Satellite Program (DMSP) and Polar Operational Environmental Satellites (POES) program. Filling these gaps will require new and innovative solutions. Such solutions could potentially leverage hosted payloads and data buys from the proliferating LEO satellite environment, considering that all of these geospace effects can be highly localized (<100 km scales) yet are distributed over the full globe. Thus, future observatory systems to fill the needed critical measurement gaps will have to rely on a network of many observatories providing a combination of in situ and remote sensing measurements.

With the end of NASA's Van Allen Probes mission, several major and critical observational gaps remain in peri-geospace. These gaps concern various radiation hazards to both crewed (including both the spacecraft and the astronauts onboard them) and uncrewed spacecraft. The final categories in the top seven list pertain to those radiation hazards. Priorities include continued, comprehensive monitoring of key observables in Earth's ring current and radiation belts, energetic electrons in the near-Earth plasma sheet, and injections and bursts of energetic electrons from cislunar space into GEO and MEO.

Finally, the committee's analysis resulted in a list of lessons learned that arose during its deliberations and the prioritization exercise (Section 7). The main important take-away messages are: (1) most of the observational gaps can be addressed with *current technology and capabilities* deployed to close spatial/temporal/spectral coverage gaps rather than any lack of measurement capability; (2) the prioritization showed that coordinated concurrent measurements are the only way

to significantly increase the impact of NASA's measurements to SWx *-casting capability; a *systems approach* is the most effective and efficient path forward; (3) the analysis uncovered a few areas where novel measurement approaches could potentially lead to leaps in *-casting certain SWx hazards, such as the remote sensing of "seed" solar particles (for high-energy SEPs), grids of closely spaced in situ measurements at ≥0.1 AU from Earth (for CME magnetic and dynamic content), and embracing the use of hosted payloads, small-satellite technology, and rideshares for populating future observatory networks around geospace.

The committee believes that its thorough analyses will be useful in informing the Program's future strategy and plans.

1 Introduction

As humanity continues to become more dependent on space-based technology and global-scale infrastructure, our technological civilization is increasingly vulnerable to the hazards of space weather, defined as the conditions and disturbances in the region of space that surrounds Earth and adversely affect human systems. The defense of our nation and its economic stability also depends on the use of space-based technology. Despite recognized vulnerabilities, many critical gaps still exist in key observables needed for an effective space weather forecasting and nowcasting system sufficient to protect the security of our nation, the economy, and critical infrastructure and therefore ensure the well-being of our people.

In response to the recommendations of the 2013 National Academies of Sciences, Engineering, and Medicine Decadal Survey for Solar and Space Physics and the actions delineated in the 2019 National Space Weather Strategy and Action Plan, NASA's Heliophysics Division (HPD) commissioned a space weather science and measurement gap analysis consistent with NASA's role in space science and exploration.

1.1 Scope and Statement of Task

To conduct the gap analysis, the Johns Hopkins Applied Physics Laboratory (APL) was tasked with convening a space weather expert committee composed of representatives from academia, the commercial sector, and the space weather operational and user communities. The committee's analysis was confined to the following two tasks:

1. Assessing the current state of NASA's observational capability to address the science of space weather and its capacity to provide data input that significantly advances forecasting and nowcasting capability
2. Identifying high-priority observations that are at risk or not currently available that are required to significantly advance forecasting and nowcasting capability

1.2 Report Organization

The report follows the standard plan of a gap analysis (i.e., focus area, current state, desired state, gap, plan of action). First, we identify the scope of the analysis: *NASA observing capability to advance SWx forecasting/nowcasting* (Section 1.2) and the set of specific *SWx hazards* (Section 2) for which improved fore/now/hindcasting (*-casting, hereafter) is desired. Next, we summarize the *SWx users' needs* (Section 3) regarding the degree of *-casting accuracy for the various SWx hazards. We use this information to aid in identifying and prioritizing gaps. Then we list the *focus areas* for the analysis; namely, the solar drivers, relevant geospace phenomena, and the long-term space climate (Section 4).

Section 5 contains the detailed gap analysis. For each physical phenomenon within the three focus areas, we determine:

1. The physical quantities most relevant to SWx *-casting, either because they are used as inputs to operational models or because they are markers of activity used by forecasters
2. The corresponding *-casting requirement, if known (*desired state*)
3. The current *-casting status (*current state*)
4. The most important measurement gap(s)
5. Required measurements to close the gaps organized in terms of increasing value (i.e., maintain current status, improve, advance, close)

Finally, we summarize and prioritize common measurement themes in Section 6. We identify the highest priority measurements that can lead to significant advances in SWx *-casting across multiple focus areas.

We note that the determination of "significant advancement" is based on the committee's expertise and experience. No effort was made to quantify the degree of improvement in SWx *-casting (unless it was straightforward) from a particular measurement, as this effort was beyond the scope of the report.

2 Space Weather Hazards

Our hazard list stems from the Next Step Space Weather Benchmarks report and includes five hazards, as follows (in random order; see also Figure 2-1):

1. Geomagnetically induced currents (GIC) affecting power grids, pipelines, non-optical communication cables, and rail networks
2. Radiation effects affecting operations, functionality, and health and safety of uncrewed and crewed spacecraft, stations, and aircraft. Specific hazards include event total dose (ETD), single event effects (SEE), and internal, subsurface/hybrid, and external charging and discharge (see Figure 2-2 below)
3. Disturbances of the ionospheric D-, E-, and F-regions affecting communications and navigation via electromagnetic signal disruptions through the ionosphere
4. Thermospheric expansion and neutral density structures affecting satellite drag, orbit estimation and prediction, and collision avoidance
5. Solar radio bursts affecting communications and navigation

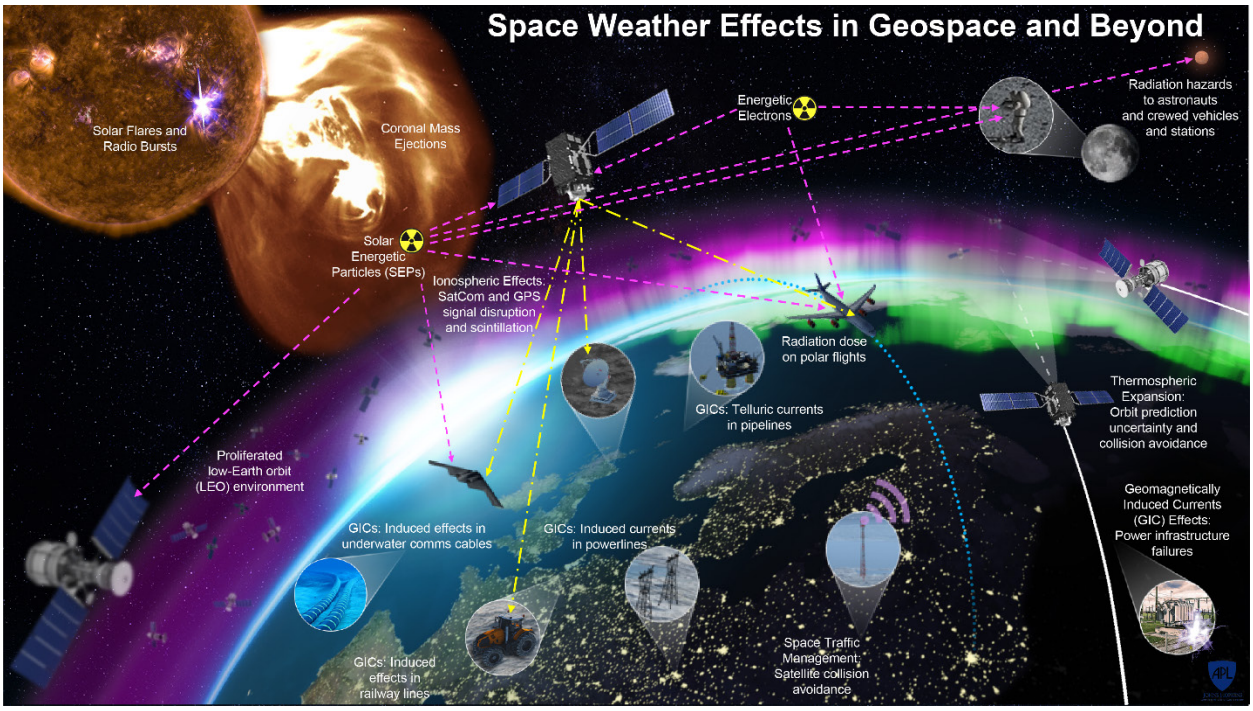

Figure 2-1. Space weather effects in geospace and beyond. This is an illustrative graphic showing various space weather effects and hazards from the Sun to Earth and geospace to the Moon and elsewhere in the heliosphere (e.g., Mars).

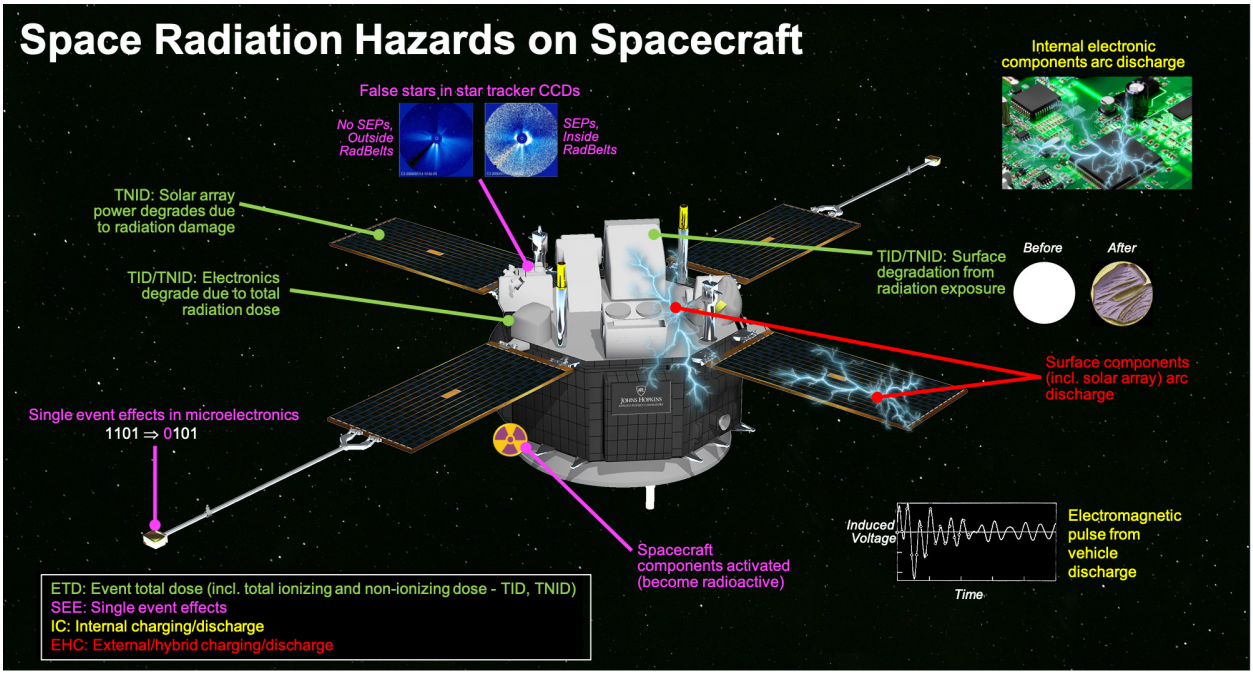

Figure 2-2. Radiation hazards on spacecraft in the space environment.

These hazards can be crudely categorized and prioritized based on likelihood and consequence, as shown in Figure 2-3. Here, likelihood is quantified by frequency or probability of occurrence (here, rough order of magnitude frequency of corresponding space weather hazards), and consequence is

quantified by approximate societal impacts on worst-case cost of damages and level of scale. It is impossible to assign a cost to human life, and astronaut health is placed in the highest tier of societal impact, consistent with the scale of human spaceflight program budgets. These hazards and priorities formed a key basis for the prioritization of the SWx gaps detailed in this report. Space weather hazards that occur very frequently (e.g., daily) but have relatively low societal and cost impacts (e.g., ionospheric disturbances affecting satellite communications) are considered comparably as important as those that occur quite infrequently but have potentially very consequential societal and cost impacts (e.g., large geomagnetic storms and GICs).

These SWx hazards and their resulting consequences on society, our infrastructure, and our endeavors form the underlying motivational basis for this gap analysis. With the details presented further in this report, and using the above defined hazards and prioritization plus metrics on breadth and level of impact and scientific value/interest to weight different observables, the following top-level, highest priority observational gaps were identified in ranked order. Table 2-1 consists of the seven highest priority observable categories out of over 40 categories of and individual observables considered (see Figure 5-1 through Figure 5-10). Particular observables pertaining to each category of observation gap are detailed further in the report (see Section 5) and summarized in the Executive Summary and Section 6.

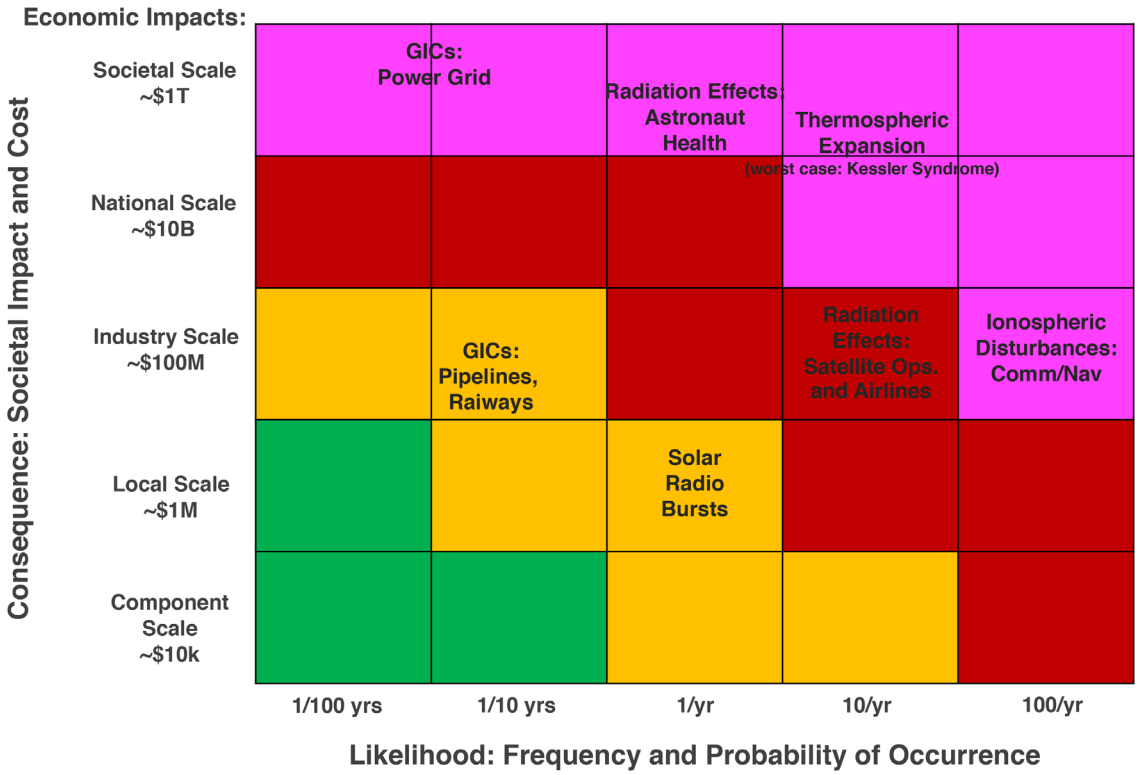

Figure 2-3. Top-level space weather hazard categories organized by likelihood (rough order of magnitude frequency of occurrence) and societal consequence (rough order of magnitude cost and impact level). Color coding approximately corresponds to worst-case damages.

Table 2-1. Top-ranked current SWx observation gap categories and corresponding research gaps

Rank	Current Observation Gaps	Research Gaps
1	Solar/solar wind observations, including off-SEL (e.g., Sun–Earth L4 and L5) and beyond 1 AU	SEP occurrence and properties at a given inner heliospheric location; interplanetary (IP) propagation of solar transients (e.g., B_z, time of arrival [ToA])
2	Ionospheric key observables	Response to variable solar, solar wind, thermospheric, and magnetospheric conditions; high resolution global state; cross-scale and -altitude dependencies and variability; driving from lower atmosphere
3	Solar wind in peri-geospace (dayside, magnetic local time [MLT]~ 10–14)	Fine-scale structure of solar wind (SW)-transients; spatiotemporal evolution and turbulence
4	Thermospheric key observables	Expansion, heating, and cooling processes over a range of scales (<100 km to global) and altitudes; response to variable solar, ionospheric, and magnetospheric conditions; driving from lower atmosphere
5	Ionospheric D- and E-region EPP and E- and F-region cusp and auroral precipitation	Impacts of energetic particle, cusp, and auroral precipitation on ionosphere–thermosphere system; cross-scale (<100 km to global) and spatiotemporal nature of precipitation and consequences on ionosphere–thermosphere system (e.g., conductivity, heating, chemistry and cooling)
6	Ring current and radiation belt electrons	Role of magnetospheric dynamics, mesoscale injections, and variety of wave-particle interactions acting in concert to shape these trapped energetic particle populations, driving geomagnetic storms and radiation belt enhancements and depletions
7	Plasma sheet electrons and injections/bursts from cislunar into GEO and MEO regions	Nature of kinetic- to mesoscale processes (e.g., reconnection, turbulence) affecting global-scale magnetospheric dynamics and magnetosphere–ionosphere coupling

3 Needs of SWx Users

We use the *-casting needs of the terrestrial SWx user community as a guide for assigning priorities to the scientific measurements we considered. To simplify this exercise, we considered the six most widely recognized civil and commercial user groups (power grid, satellite operations, navigation, aviation, Federal Emergency Management Agency (FEMA)/emergency managers, and NASA) since their concerns capture the majority of SWx requirements across the various user communities (Abt Report). The National Oceanic and Atmospheric Administration (NOAA) is the agency responsible for addressing these user needs. Since this is a NASA-focused report, we include NASA's needs for SWx impacts on robotic and human exploration missions. The Department of Defense (DoD) needs are addressed implicitly (without direct attributions or justification, due to the sensitive nature of such concerns) by the DoD-affiliated committee members.

We extract the most pertinent requirements for our analysis in Table 3-1. The terrestrial user needs or requirements are taken from the Customer Needs and Requirements for Space Weather Products and Services report, which was focused on the five key sectors (electric power, satellites, global navigation satellite systems [GNSS], aviation, and emergency management). The NASA requirements are taken from the Space Weather Architecture Options to Support Human and Robotic Deep Space Exploration report.

Table 3-1 leads to a key observation. The user *-casting needs can be summarized in just three areas: longer lead time, improved accuracy, and regional (including heliospheric locations) *-casts. Therefore, any NASA measurement that improves on any one (or preferably more) of these areas demonstrates SWx value.

Table 3-1. SWx needs and requirements of SWx users from NOAA and NASA reports

Need	Requirement
Electric Power	
increased granularity	• Granularity in the NOAA's G5 (G5+) - nowcast or hindcast considered most likely • Regional (e.g., state- and county-level) forecast for GIC threat to power grid infrastructure
actionable forecasts	Geoelectric potential forecasts >1 h (24 h desired, 3–6 h would be an improvement)
historical data access	• Geomagnetic Storm Ranked Lists • Access to relevant measurements (data) quantifying power grid impacts from historical storms
Satellites	
actionable forecasts	• Establish measures of uncertainty for nowcasts and forecasts of degraded satellite communications through the ionosphere; thermospheric drag, orbit prediction, and collision avoidance; and radiation threats to spacecraft systems • Improve forecast lead time for each of the above-mentioned actionable forecasts
data availability	Provide data products required for nowcasts/forecasts of degraded satellite communications; thermospheric drag; and radiation threats for LEO, MEO, geosynchronous transfer orbit (GTO), GEO, high Earth orbit (HEO), cislunar, and lunar orbits, as relevant to each
spacecraft operations	Spacecraft charging. Create 3D representations (latitude, longitude, Alt or magnetic latitude [MLat], magnetic local time [MLT], and L-shell) of high-energy (>100 keV, internal charging) and lower-energy (~100 eV to 100 keV, surface charging) electrons in near real time (within the last 5 min to 1 h) and forecast at 1-h to 1-day range
spacecraft operations	Satellite communications. Improved nowcast and forecast (1-h to 2-day range) of SRBs and ionospheric disturbances down to regional scales over the globe affecting satellite communications (signal absorption, phase and amplitude scintillation, usable frequencies, etc.)
spacecraft operations	Improved resiliency to single event effects (SEE) requiring more robust electronics design and improved nowcasts and forecasts of SEP events
spacecraft operations and longevity	Satellite drag and collision avoidance: improved real-time knowledge and 1-h to 2-day forecasts of thermospheric density over globe
spacecraft operations and longevity	Improved resiliency and mission design considerations for total ionizing (TID) and non-ionizing (TNID) dose requiring better climatological models of the radiation environment in near-Earth space
spacecraft longevity	Improved resiliency and design considerations (e.g., materials selection, surface coatings) for corrosion from exposure to low-energy plasma
historical data access	Provide long-term historical information (data) on satellite communications performance, orbit degradation, and on-orbit satellite anomalies
GNSS	
actionable forecasts	Improved nowcast and forecast (1-h to 2-day range) of ionospheric disturbances down to regional scales over full globe affecting GNSS availability and accuracy
increased granularity	• Regional alerts • Warning for enhanced scintillation
historical data access	Provide long-term historical information (data) on GNSS accuracy (position and timing error) and signal disruptions attributed to space weather activity
Aviation	
increased granularity	Regional/geographically targeted alerts/warnings for solar radio bursts and communications disruptions over full globe and increased radiation exposure over polar latitudes
actionable forecasts	• Forecast potential hours to days for communications disruptions and increased radiation levels • Develop measures of uncertainty for those forecasts
historical data access	Provide historical information (data) on aircraft component and crew radiation doses accumulated over polar routes under a range of geomagnetic conditions
Emergency Management	
actionable forecasts	Provide forecasts with 1- to 2-day lead time
increased granularity	• Tailor warning to specific geographies • Develop hazard maps for different phenomena

Need	Requirement
NASA Robotic Exploration	
spacecraft operations	Improve radiation threat nowcast and forecast accuracy at spacecraft locations throughout heliosphere
data availability	Include critical SWx instrumentation (radiation and solar activity monitors) on future robotic/unscrewed missions
NASA Human Exploration	
actionable forecasts	• 10-to 30-min lead time for critical radiation exposure • >30 min warning for SEPs; see SRAG/USAF requirements
data availability	Include critical SWx instrumentation (radiation and solar activity monitors) on future Mars and Lunar Gateway missions
increased granularity	• Predict 10 MeV to 1 GeV proton fluxes and SEP events; nowcast current state of threatening radiation levels on crewed vehicles (including radiation belts and SEPs) • Develop ≥6-h forecasting window to pre-eruptive models

4 Focus Areas

Our analysis focuses on three areas: the external drivers of SWx, the internal drivers and physical phenomena that manifest as SWx, and the long-term aspects and considerations of space climate. Below, we briefly describe the physical phenomena we have examined for each area to provide some background for the more detailed gap analysis in Section 5 and Section 6. Each phenomenon is described in a short paragraph pointing to recent and/or SWx-focused reviews for more information.

4.1 External Drivers of Space Weather

This section highlights *external* drivers of space weather, primarily the solar and solar wind drivers, but also including cosmic rays, and driving from "below" the system via the lower atmosphere. The magnetosphere–ionosphere–thermosphere system is driven by the dynamic solar irradiance and solar wind, including each of the drivers discussed in this section, but due to the complexity and highly nonlinear, coupled nature of processes in Earth's magnetosphere, ionosphere, and thermosphere, most SWx nowcasts and forecasts of the geospace environment are inaccurate if driven using solar and solar wind inputs alone. On account of internal energy storage and instabilities that trigger its release, the timing and quantitative details of energy and material flows in the magnetosphere–ionosphere–thermosphere system depend not only on external drivers but also on internal driving through delay and feedback mechanisms. Details on those relevant magnetosphere–ionosphere–thermosphere internal processes are covered in Section 4.2.

A **CME** is the explosive expulsion of magnetized plasma from the solar corona into the heliosphere. CMEs are the most energetic phenomena in the solar system. They reach kinetic energies of 10^{25} J as they expel $10^{12–13}$ kg of coronal material at speeds observed up to 3400 km/s over the span of a few hours. As a result, many CMEs drive shocks throughout the corona and inner heliosphere, which in turn can accelerate particles to relativistic energies. CMEs, and their associated shocks and sheath regions, are the main drivers of intense SWx in geospace, and one of the main safety concerns for space exploration activities. At Earth, about 50% of CMEs drive shocks. Further information can be found in reviews on CME observations (Webb & Howard, 2012), theory (Chen, 2011), and SWx effects (Schwenn, 2006; Pulkkinen, 2007; Kilpua et al., 2019).

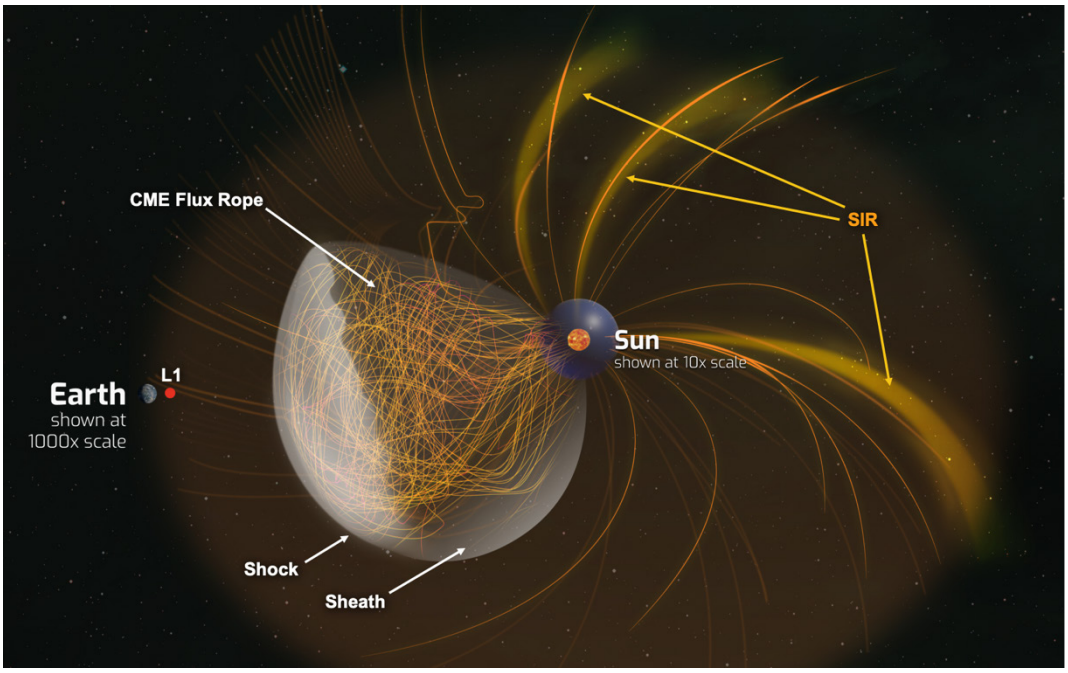

Figure 4-1. Snapshot from a simulation of a shock-driving CME interacting with solar wind structures on its way to Earth. The spatial scale and internal complexity of the solar drivers of SWx and the vastness of the Sun–Earth system demonstrate the challenges facing SWx forecasting systems. Simulation courtesy of E. Provornikova. (SIR: Stream Interaction Region) Image credit: APL.

Solar flares are sudden brightening of coronal loops over a broad range of the electromagnetic spectrum caused by the impulsive heating of coronal plasmas, believed to be due to magnetic reconnection. The energy released in a flare can result in the acceleration of electrons and protons to high energies (MeV for electrons, hundreds of MeV for protons) as well as heating that produces temperatures reaching 10–20 million K in the solar corona, resulting in intense radiation from X-rays to radio wavelengths that can last from a few minutes to several hours. Flares can be associated with CMEs, SRBs, and SEPs, which are also relevant events for SWx. Flares associated with these events are known as eruptive flares and are energetically comparable to CMEs (Emslie et al., 2012; Aschwanden et al., 2017). Further information can be found in reviews of flare observations (Benz, 2008) and the SWx effects of flares (Pawloski & Ridley, 2011).

Solar Energetic Particle (SEP) events are associated with solar eruptions that result in high fluxes of energetic protons (1–500 MeV), electrons (up to MeV), and heavier elements (tens of MeV per nucleon) that flood through interplanetary space across a wide range of longitudes. They produce radiation levels elevated by orders of magnitude that can last for days. SEPs with energies greater than 10 MeV are capable of penetrating space suits, and SEPs with energies greater than 100 MeV can penetrate spacecraft—making SEP events a risk for crew health, safety, and the success of human exploration missions (e.g., Jiggens et al., 2014). Electronics onboard spacecraft can suffer during SEP events from degradation, data corruption, noise in imaging, system shutdowns, and circuit damage. Less common are Ground Level Enhancements (GLEs) that are so intense that nuclear interactions in the atmosphere at energies above 500 MeV produce neutron fluxes that are readily measurable at ground level.

At Earth, SEPs can be trapped in the geomagnetic field, particularly during intense geomagnetic storms (see Section 4.2.2) when they can gain access to lower radial distances in the magnetosphere. Such trapped SEPs contribute to the proton (and heavier ion) radiation belts and represent a time-variable source of that radiation population in the inner magnetosphere. SEPs are in general a significant radiation hazard throughout geospace and the heliosphere. The dipole nature of Earth's magnetic field means that impacts on the atmosphere from SEPs are most pronounced in the polar regions. Airlines flying polar routes during SEP events therefore pose a risk to the health and safety of the crew and passengers and total radiation dose on aircraft systems and components.

Solar irradiance at UV and shorter wavelengths is an important driver of conditions in Earth's atmosphere and ionosphere where those wavelengths are absorbed. Most of the energy in the Sun's irradiance is at optical and near-infrared (IR) wavelengths (>300 nm) that pass through or reflect from the atmosphere and have no significant space weather impacts. However, wavelengths shorter than 300 nm are strongly absorbed by the upper atmosphere and are primarily responsible for its structure and composition (e.g., Fuller-Rowell et al, 2004). Solar emission between 300 and 120 nm reaches down to about the 100 km height level (the E-layer) where it is absorbed by O_2 and O_3, but these wavelengths are dominated by emission from layers just above the photosphere that do not vary much with time and so do not play a strong role in transient events.

Shorter wavelengths, despite transporting much less energy, are highly variable and act as a major driver of space weather phenomena in Earth's atmosphere. They are able to photoionize atomic and molecular species, thus producing and disturbing the ionosphere. Solar emission at wavelengths shorter than 100 nm is dominated by lines from the hot plasma in the chromosphere, transition region and corona. The coronal component (temperatures > 10^6 K) dominates below 30 nm and varies greatly with solar activity levels, playing a significant role in total electron content (TEC) variations in the ionosphere. Solar flares produce orders of magnitude variation at X-ray wavelengths. Wavelengths from 20 to 100 nm deposit their energy at heights between about 120 and 400 km, and the heating they produce creates the increase in temperature with height that represents the thermosphere. Variation in the heat input in this range controls expansion of the thermosphere and thus impacts satellite drag.

Wavelengths shorter than a few nanometers (i.e., X-ray wavelengths) can reach heights of 90 km and lower: this is the D-layer ionosphere, where the neutral density is so high that electron-neutral collisions can provide significant opacity at radio wavelengths.

SRBs are produced by flares and CMEs. Three main types of radio burst are relevant for SWx. At metric wavelengths, the plasma emission mechanism produces intense radio bursts such as Type II, III, and IV. At shorter centimeter wavelengths, the same electrons that produce hard X-rays and gamma rays also radiate by the synchrotron emission mechanism. In between, in the widely used decimetric wavelength range (cell phones and GPS), there are occasional very intense bursts thought to be due to the electron cyclotron maser mechanism. We emphasize that while most observations of these phenomena can be taken more effectively from the ground and therefore do not require NASA resources, apart from emissions below the ionospheric cutoff, it is appropriate to mention them here since they can both affect NASA assets directly (e.g., radio bursts can impact satellite telemetry) and are used in models forecasting other impacts to space assets (such as SEPs).

Cosmic rays are very energetic (kinetic energies ≥ 10s of MeV/nucleon) protons and atomic nuclei present throughout the heliosphere; they pose a non-negligible radiation hazard to crewed and uncrewed systems operating outside of Earth's atmosphere. In this report, cosmic rays are considered as energetic particles of extrasolar origin, separate from SEPs. The flux of cosmic rays in the heliosphere, including throughout the magnetosphere and geospace, is modulated by solar magnetic fields and solar wind transients (e.g., coronal mass ejections [CMEs], corotating interaction regions [CIRs], discussed above), resulting in a solar-cycle modulation of cosmic ray intensities. In the heliosphere, cosmic rays are more intense during solar minimum than they are during solar maximum, and solar wind transients result in shorter-scale decreases in cosmic ray intensities (known as Forbush decreases) during the passage of those transients through the heliosphere. See Hill et al. (2020) and references therein for more detail.

Solar wind structures are spatial structures within the solar wind that last from hours to days and corotate with the Parker spiral. This includes the reversal of the interplanetary magnetic field (IMF) in Alfvénic turbulence and at the heliospheric current sheet (HCS) and the associated heliospheric plasma sheet, slow and fast solar wind streams, and changes in the solar wind density and dynamic pressure. Of high importance for space weather are **stream interaction regions (SIRs)**, also referred to as **CIRs**, which can recur over multiple Carrington rotations (CRs) (months). SIRs and CIRs form due to the interaction between regions of slow and fast solar wind, as fast solar wind overtakes slower solar wind ahead of it, resulting in a compressed interface region of high density, dynamic pressure and magnetic field. Shock waves form with this interaction, typically at distances farther than 1 AU, but ~25% of SIRs/CIRs have shocks at 1 AU. Further information about SIRs/CIRs can be found in Richardson (2018).

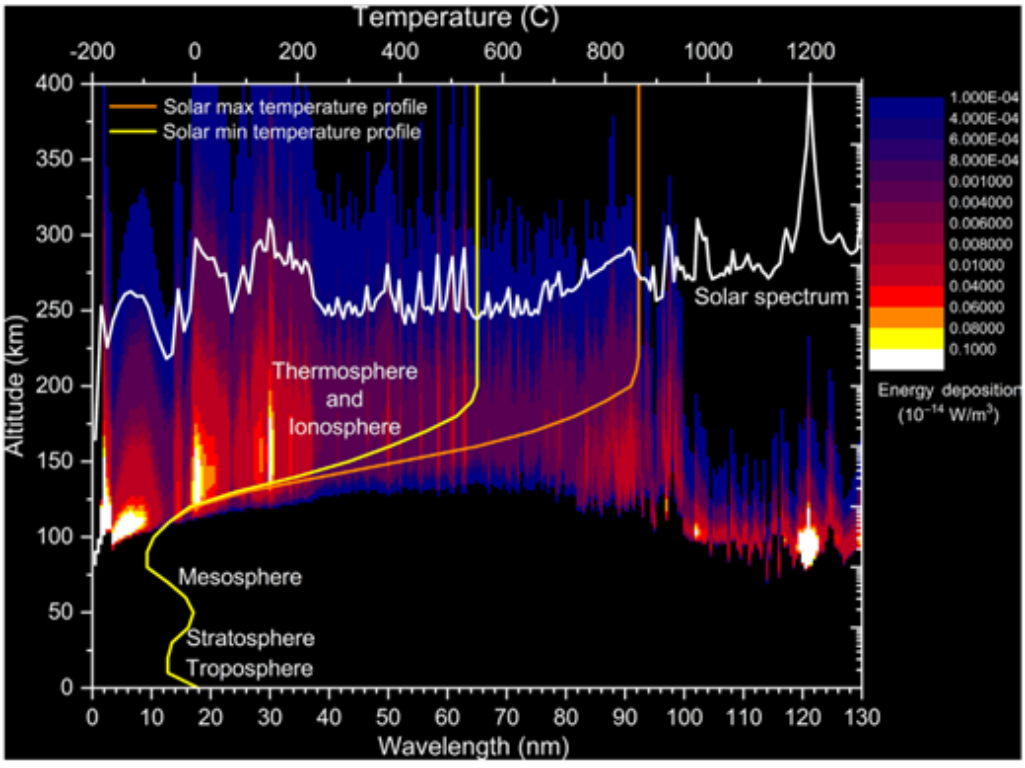

Figure 4-2. Energy deposition by the solar short wavelength irradiance (colors) as a function of wavelength and altitude, with the solar spectrum overlaid in white. From Machol et al. (2020).

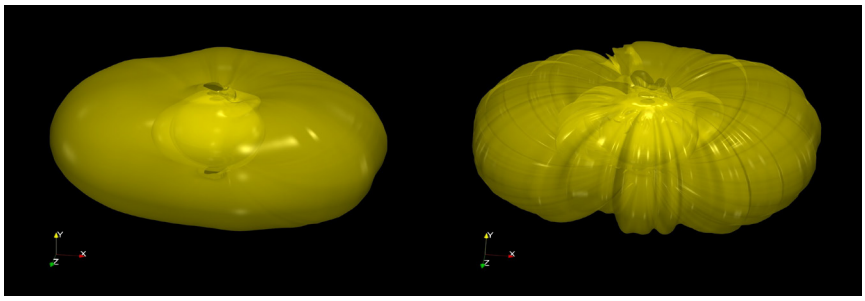

Figure 4-3. Electron density isosurfaces in the plasmasphere affected by gravity waves of tropospheric origin. Simulations of Earth's plasma environment shown here have two lower boundary specifications; a climatological wind model (left) and the WACCM-X model (right) which simulates the spectrum of gravity waves propagating upward from the troposphere. Small-scale changes in the electrodynamics of the mid-latitude ionosphere introduce significant structuring of plasmaspheric density (Figure courtesy of J. Huba)

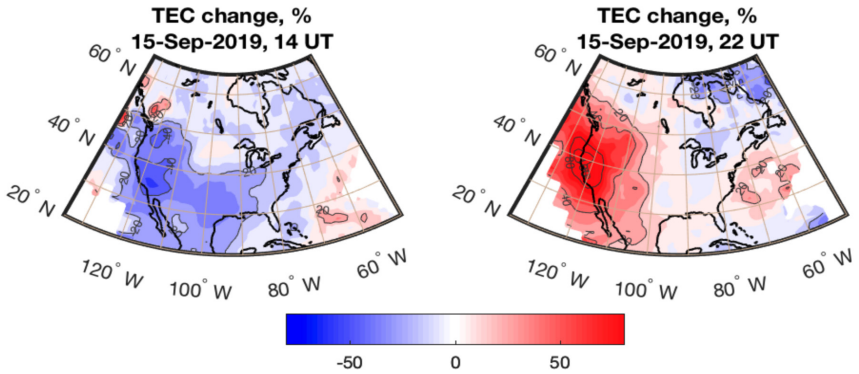

Figure 4-4. Effects of a rare Antarctic stratospheric warming on ionospheric densities over North America. Departures of TEC from seasonal averages are shown at two times. A remarkable change with local time is seen in the western United States, while the central and eastern United States are much less disturbed. The repeated observation of significant, global-scale changes in the ionosphere with every stratospheric warming event demonstrates the strong connection of planetary waves in the stratosphere to conditions in space.

Lower atmospheric waves directly impact the plasma environment around Earth, with imprints on electron density extending from the D-region to the plasmasphere. The spectrum of tides, planetary waves, and gravity waves changes seasonally, but also varies on timescales of days. These waves produce a remarkable set of effects on ionospheric plasma densities, driving modifications of both the F-layer density and height at equatorial altitudes, while driving related changes at middle latitudes. The entire plasmasphere is modified as well, with the tidal spectrum present in the E-region being impressed on plasmaspheric densities (Pedatella et al., 2011). A recent remarkable finding (see Figure 4-2) suggests that the structure of the plasmapause is highly sensitive to gravity waves forcing, originating almost completely in tropospheric weather events.

Stratospheric warming events are a remarkable case of driving by the lower atmosphere where the ionosphere is seriously perturbed by major changes in polar stratospheric circulation. These changes are tied directly to modification of the atmospheric planetary wave spectrum (Siddiqui et al., 2015). Due to their large wavelength, these waves can propagate into the space environment and modify the development of the ionosphere directly, while also modifying the spectrum of tides in the thermosphere. These translate to remarkable changes in the ionosphere, with high plasma

concentrations and F-peak densities shifting from afternoon to near sunrise at low latitudes, often paired with a remarkable depression in the afternoon and nighttime densities.

4.2 Space Weather Phenomena and Processes Internal to the Magnetosphere–Ionosphere–Thermosphere Systems

4.2.1 The Coupled Geospace System and Internal Drivers of Space Weather

Global magnetospheric convection, magnetosphere–ionosphere–thermosphere coupling, and magnetic reconnection are broad terms for physical processes that collectively encompass and govern a complex and tightly coupled system of systems in geospace that is responsible (either directly or indirectly) for most SWx hazards. Magnetospheric processes result in many of the radiation hazards throughout geospace, such as the Van Allen radiation belts, while ionospheric and thermospheric disturbances can result in communications and navigation signal disruptions, and derail LEO satellites. Magnetosphere–ionosphere–thermosphere coupling is ultimately what drives GICs. The intensity and frequency of geomagnetic storms and substorms and their associated SWx hazards throughout the magnetosphere–ionosphere–thermosphere system can vary wildly for seemingly comparable solar wind driving conditions. Thus, it is critical to SWx to understand and be able to successfully model Earth's magnetosphere–ionosphere–thermosphere system and provide low-latency observations of key quantities throughout the magnetosphere–ionosphere–thermosphere system. These observations can be used as data inputs (more accurate preconditioning of the systems) and data assimilative modeling (i.e., time-dependent updates of model parameterization and state conditions to optimally match model output to corresponding current best estimate [CBE] observation updates).

Magnetospheric convection describes plasma motion throughout Earth's magnetosphere. The plasma convection is critically driven by the solar wind and linked by magnetic reconnection along Earth's magnetopause, which opens up magnetospheric field lines to the solar wind on the upstream, driving side (dayside), and magnetic reconnection in Earth's magnetotail, which reestablishes closed magnetic field lines on the downstream side (nightside) and generates plasma flows and energy transport back into and around the inner magnetosphere. With the convection of closed field-lines around the inner magnetosphere from the nightside to the dayside again, replenishing magnetic flux lost to magnetopause reconnection, the global convection cycle is complete. This entire global convection process is known as the Dungey cycle, and it processes plasma throughout Earth's magnetosphere over timescales of ~1 h. Since all magnetospheric field lines close on at least one end through Earth, plasma coupling to and from the ionosphere is critical to this entire process, as is evident in the spectacular visible displays of aurora. Due to the complex, coupled nature of the magnetosphere–ionosphere–thermosphere system, magnetospheric convection is not a global, laminar process; a wide range of small-scale to mesoscale processes (e.g., magnetic reconnection at electron-kinetic scales of ~10 km to bursty bulk flows and substorms at hundreds to thousands of kilometers) are relevant, many of which behave nonlinearly and are explosive in nature. For some good recent reviews of these topics, see: Eastwood et al. (2015), Milan et al. (2017), Pfaff et al. (2012), Ebihara & Miyoshi (2010), and Li & Hudson (2019).

4.2.2 Geomagnetic Storms and Inner Magnetospheric Activity

Geomagnetic storms (see Katus et al., 2015; Gonzalez et al., 1999; Kamide et al., 1998) are hours-to-daylong periods of intense, global magnetospheric activity, and they can be responsible for generating or enhancing multiple SWx hazards (including GICs, radiation hazards, ionospheric disturbances, and thermospheric expansion). Storms occur frequently: several (~1/week on average) storms occur each month around solar maximum, while around solar minimum, the occurrence rate is approximately one to two storms per month. These storms are most often driven by large transient structures (e.g., CMEs, SIRs/CIRs) in the solar wind, and their activity level is correlated to the time-integrated product of the solar wind speed and southward magnetic field of the driving transient. The storms are manifested on Earth's surface by strong decreases in the magnetic field intensity in the equatorial and low latitude regions, characterized in the disturbance storm-time (D_{st}) index compiled from a global network of ground-based magnetometers. Those magnetic field variations observed on the ground result from an intense buildup and enhancement of the ring current in Earth's inner magnetosphere. Storms are broken into distinct phases, each with a clear behavior of the D_{st} index: (1) sudden storm commencement, involving a sudden compression of the magnetosphere and corresponding positive enhancement of the D_{st} index; (2) storm main phase, involving a rapid and precipitous decrease in the D_{st} index; and (3) recovery phase, involving a slower, nonlinear increase in D_{st} index back to pre-storm levels over a several day period. Storm intensity is quantified by the minimum D_{st} and the point in time that occurs delineates the end of the main phase from the beginning of the recovery phase.

Sudden storm commencement is often initiated by an impulsive event in the solar wind, such as a CME shock or sudden pressure pulse at the leading edge of a CIR/SIR, and those impulsive changes in solar wind dynamic pressure result in sudden magnetopause motion (compression) and enhancements of the magnetopause currents. Magnetopause incursions can drive sudden losses of outer radiation belt electrons and ring current ions. Such impulsive compressions also coincide with sudden enhancement of the global convection electric field resulting in the development of a plasmaspheric drainage plume. Under extreme compression, the magnetopause might even move Earthward of dayside GEO, posing a threat to geostationary spacecraft that rely on magnetotorquers for attitude control.

Storm-time variability of coupled magnetospheric and ionospheric current systems ultimately results in rapid changes of the electric potentials that can drive GICs, endangering critical ground-based infrastructure such as power grids. Those current systems are most intense during geomagnetic storms, when energy inputs and internal processes driving ionospheric disturbances and thermospheric expansion are also severe. Storm-time variations in the ring current and inner magnetospheric pressure can also couple back to the magnetotail, resulting in strong substorm and auroral activity, often persistent through the main phase and sometimes into and throughout the recovery phase of storms, and field-aligned currents (FACs) around LEO. Such activity poses a threat to spacecraft throughout geospace via surface charging, internal charging, and ETD. During storms, magnetospheric erosion and compression are also most extreme, enabling SEP access to lower latitudes/L-shells. Many of these systems and processes are detailed further in subsections below.

Enhancements and/or strong variability of magnetosphere–ionosphere coupling, substorm and auroral activity, the energy content of the plasma sheet and inner magnetospheric plasmas, radiation belt electrons, and rapid thermospheric heating and cooling all occur during geomagnetic storms.

Due to the highly nonlinear, coupled nature of the magnetosphere–ionosphere-thermosphere system, accurate predictability of the global magnetospheric response during any particular geomagnetic storm remains elusive. In the following paragraphs, we detail some of the key aspects of the magnetosphere–ionosphere-thermosphere system response to geomagnetic storms. It should also be noted that the geomagnetic K_p index is most widely used for space weather forecasting since it more broadly reflects global magnetospheric activity, unlike the D_{st} index which just represents changes in the ring current.

Ring current: Earth's ring current, consisting largely of protons and electrons at energies of ~100s eV to ~10s keV, circulates westward in the near-equatorial region around Earth at radial distances ranging from order 10,000 to order 60,000-km altitude (see Figure 4-5). Oxygen ions from Earth's ionosphere and the interplanetary medium can often comprise a small yet significant component of the ring current population and energy density. The intensity of the ring current varies greatly, depending upon the level of disturbance of Earth's magnetosphere by the external forcing of the interplanetary conditions (solar wind and its embedded magnetic field). The enhanced, storm-time ring current also significantly modifies the magnetic field in the magnetosphere itself, which in turn dictates the motion of the radiation belt particles trapped in the magnetic field. Instabilities in the distribution functions of the ions (largely the protons) in the ring current can produce electromagnetic and electrostatic plasma waves that affect radiation belt particles—energizing them and/or causing their losses via scattering into Earth's atmosphere or escape through the magnetopause. Understanding the generation, dynamics, and decay of the ring current is essential in understanding how Earth's magnetosphere evolves and develops during storms.

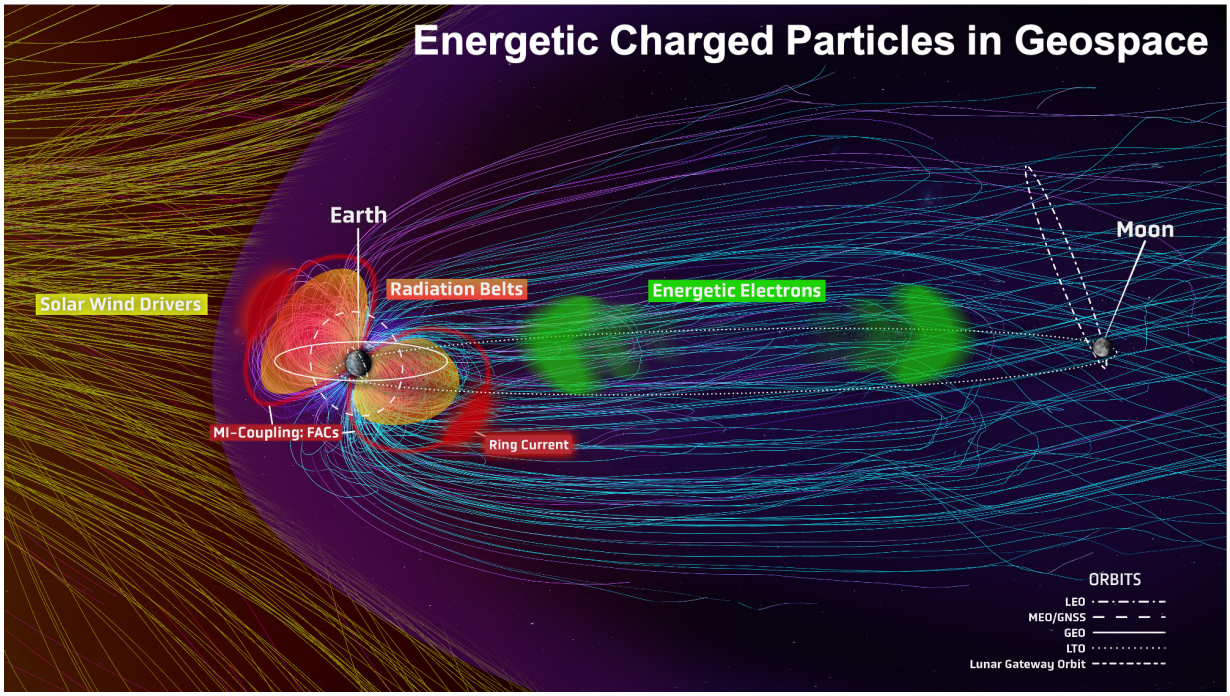

Figure 4-5. Energetic charged particle environment around geospace. Earth's magnetosphere (blue magnetic field lines) and solar wind driver (yellow magnetic field lines) are shown from a high resolution magnetohydrodynamic simulation, with various energetic charged particle populations (ring current, field-aligned currents [FACs], radiation belts, and bursts of energetic electrons) also shown in their typical locations. Several examples of common orbits are also shown (see legend) with Earth and the Moon to scale. Image credit: APL

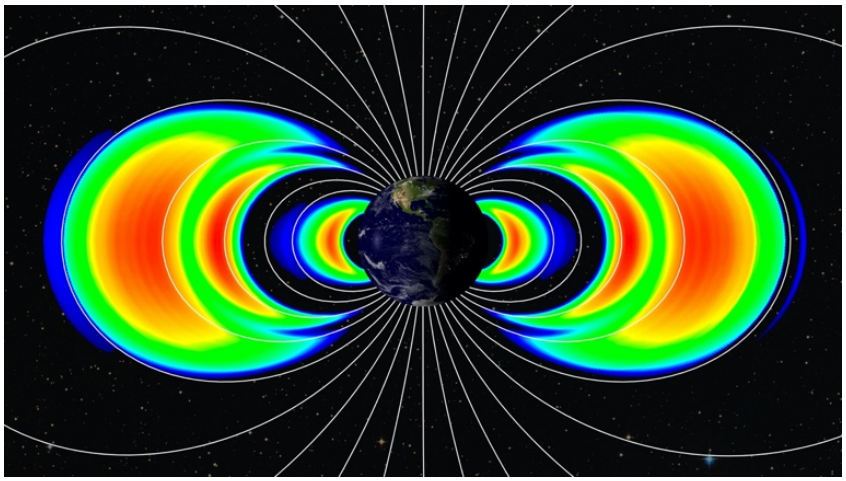

Figure 4-6. Earth's electron radiation belts. Intensity shown in color, with red being most intense and blue being least using a logarithmic scale ranging several decades. Image credit: APL.

Radiation belts: Earth's radiation belts consist of intense populations of very energetic particles (100s keV to several MeV for electrons; MeV to GeV for protons) that are quasi-stably trapped by Earth's dipole-like magnetic field in the inner magnetosphere. Radiation belt particles are generally organized by magnetic field lines (i.e., not just by geocentric distance), and intensities are highest near the magnetic equator and fall off by up to several orders of magnitude in intensity as one goes to higher latitudes along magnetic field lines. The electron radiation belts consist of two distinct and energy-dependent zones (inner and outer belts) that are most often separated by a "slot" region that is generally devoid of such electrons. The inner radiation belt ranges from a few-hundred-kilometer altitude to about 7,000-km altitude in the equatorial plane, while the outer belt ranges from around 12,000- to 40,000-km altitude in the equatorial plane. Radiation belt electrons are extremely variable, with intensities varying by several orders of magnitude observed over a wide range of timescales, from seconds (e.g., energetic particle injections during substorms) to hours and days (e.g., depletions and enhancements during geomagnetic storms) to years and decades (e.g., solar-cycle periodicities). The proton radiation belt is mostly limited to the same region as the inner electron radiation belt. The proton belt is mostly very stable over long time periods (i.e., decades), except at its outermost edge, where SEPs can become stably trapped during strong storm events, contributing as a time-variable source. Radiation belt losses to Earth's atmosphere contribute as a non-negligible energy input for thermospheric heating plus a source of ionization to the ionosphere.

Plasmasphere: Earth's plasmasphere is a region of cold (few electronvolts), relatively dense (>100 cm^{-3}) plasma that corotates with the magnetic field closest to Earth. The plasmapause is the outer boundary of the plasmasphere, and it is a dynamic boundary, changing sometimes very rapidly with geomagnetic activity. The plasmapause is ultimately the balance point between the solar wind driven convection electric field that permeates the magnetosphere and the corotation electric field resulting from the rotation of the planet. Typically, the plasmapause is located between ~25,000 and ~40,000 km in the equatorial plane, but during the sudden commencement and main phases of geomagnetic storms, the plasmapause can "erode" rapidly inward to much lower radial distances as the convection electric field in the solar wind is enhanced by increased magnitudes of solar wind speed and/or southward IMF (B_z). During storm recovery phases, the plasmasphere is replenished by ionospheric plasma and expands back to pre-storm levels. The plasmapause is not a symmetric boundary, particularly during storm times when a plasmaspheric "drainage plume"

(called that since it is responsible for the loss of plasmaspheric plasma during erosion) might extend in the afternoon local time sector out to the magnetopause. The dynamic plasmasphere is a critical region for space weather since it is an important boundary for spacecraft surface charging; is an important region concerning variability of outer radiation belt electrons; and represents one of several key aspects of magnetosphere–ionosphere coupling.

4.2.3 Magnetospheric Substorms

Magnetospheric substorms consist of the rapid (approximately tens of minutes) and explosive reconfiguration of Earth's magnetotail and dipolarization of the near-Earth magnetic field via nonlinear cascade of energy conversion from magnetic energy stored in the magnetotail lobes into kinetic and thermal plasma energy in the plasma sheet and inner magnetosphere. Substorms occur frequently, several per day, and are often independent of geomagnetic storms. However, during storms, the frequency and intensity of substorms are amplified. The auroral electrojet lower (AL) index is an effective rough proxy for substorm activity level. Magnetic reconnection in the magnetotail and magnetosphere–ionosphere coupling via FACs are both fundamentally critical to substorm activity.

Substorms are most widely recognized for the intense auroral and geomagnetic activity that accompanies them. Of highest relevance to space weather, substorms also involve significant ionospheric disturbances, enhanced ionospheric current systems (a potential charging threat to spacecraft in LEO), and injections of energetic particles (10s keV to MeV electrons, protons, and heavier ions) into the inner magnetosphere (into and inside of GEO), which can pose a significant threat to satellites via spacecraft charging. Substorm activity is also related to the drivers of (and thus well correlated with) enhancements of Earth's outer radiation belt electrons and transient belts within what is usually the slot region; thus, substorm activity is also highly relevant to internal charging and total dose space weather hazards. Energetic particle injections during substorms also result in non-negligible energy inputs into Earth's ionosphere and thermosphere via EPP and may contribute further to associated space weather hazards related to those systems.

4.2.4 Ionospheric Disturbances

Earth's ionosphere extends from about 50 km above the surface to ~1000 km in altitude (though note that arguably, the plasmasphere is the uppermost extent of the ionosphere in geospace). The ionosphere consists of electrically charged particles (electrons and ions). It is formed by the ionization of atmospheric neutral gases due to solar UV radiation and also EPP from the magnetosphere.

The ionosphere constitutes the important near-Earth space environment through which radio waves for satellite navigation (GNSS) and communication signals have to propagate. Ionospheric electrons directly impact radio wave propagation. Radio wave interaction with the ionospheric plasma leads to changes in propagation paths due to refraction, reflection of high frequency (HF) and very high frequency (VHF) waves depending on the maximum electron density, added range delay due to the changes in the group velocity, and occasionally complete absorption of HF radio waves in the ionospheric D-region (defined below).

Small-scale irregularities in the electron density can impact the reception of both the phase and amplitude signatures of radio waves. In certain cases, this can cause receivers to be unable to track

satellites as in the case of loss-of-lock of the GNSS signals. Refracted wave-paths, range delay, and changes in phase result directly in accuracy errors for GNSS position solutions, which can become quite significant (approximately tens of meters or more [Moreno et al., 2010]) under highly disturbed ionospheric conditions. Large-scale structures such as the storm-enhanced density (SED) feature that can be observed over the continental United States and elsewhere and traveling ionospheric disturbances that propagate globally during geomagnetic storms can seriously impact GNSS positioning. Another important space weather effect in the ionosphere is the variation/fluctuation of ionospheric currents, which is the root cause of GICs and also connect to FACs from the magnetosphere, which can pose a surface charging threat to spacecraft in LEO.

The ionosphere can be separated into several layers or regions based on the altitude profile of the electron density distribution (see Figure 4-7). The F-region extends from ~150 to 500 km in altitude, and is where the largest electron density of the ionosphere can be observed. The peak in F-region electron density is referred to as NmF2, and the corresponding altitude of that peak density is called HmF2. The E-region ionosphere is defined from 85 to ~150 km. The D-region is the lowermost layer of the ionosphere, ranging from 50 to 85 km in altitude.

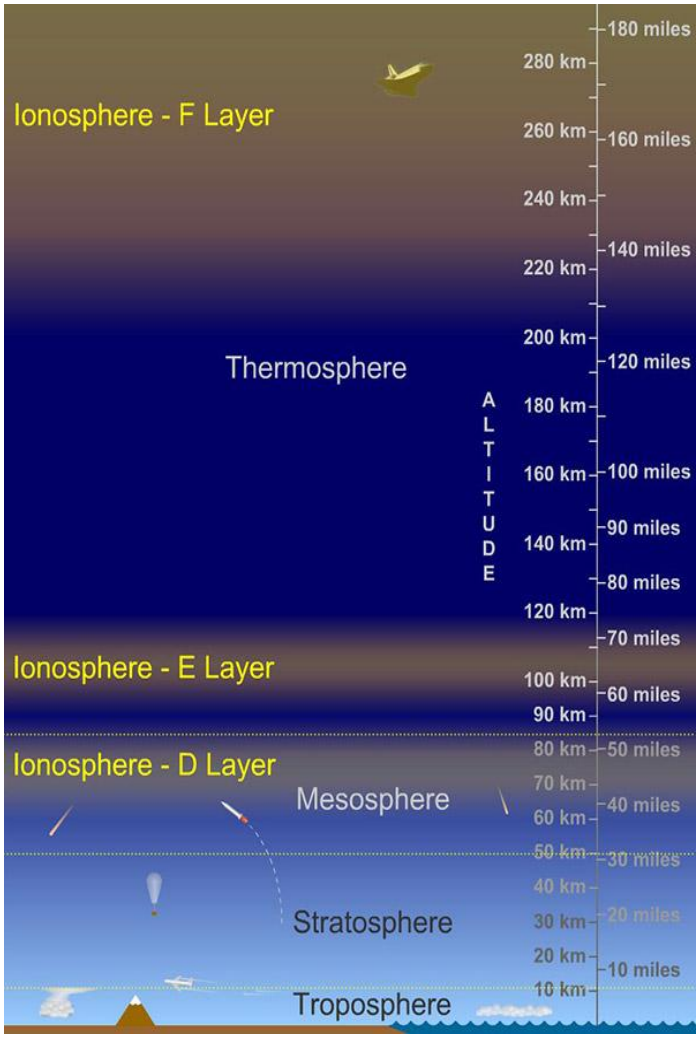

Figure 4-7. Regions of the ionosphere, showing the D-, E-, and F-layers. Credit: UCAR Center for Science Education staff (Randy Russell)

D-region ionosphere: Electron production in the D-region is from solar X-rays and also very-high-energy EPP (e.g., 100s keV to ≥MeV electrons and protons) from both the Sun and the magnetosphere. Ionization of this region is primarily due to the ionization of nitric oxide (NO), and molecular nitrogen and oxygen (N_2 and O_2). The ionization of NO is due to the hydrogen Ly-α radiation at a wavelength of 121.6 nm and EPP. High solar activity levels generate X-rays (wavelength <1 nm) that ionize N_2 and O_2. Recombination rates are high in the D-layer, so the D-region exists primarily in the daytime. The few electrons that remain in the D-region at night are those generated by cosmic rays and EPP from the magnetosphere, and in the particular instances described below, those produced during SEP events.

Medium frequency (MF) and lower HF radio waves are significantly attenuated within the D-region ionosphere, due to the high collision rates of electrons with neutral molecules. Of particular interest are SEP events, when D-region ionization can reach unusually high levels at high latitudes. Such events are known as polar cap absorption (PCA) events because the increased ionization significantly enhances the absorption of radio signals passing through the region. In fact, absorption levels can increase by many tens of dB during intense events, which is enough to absorb most (if not all) transpolar HF radio signal transmissions. Such events typically last less than 24–48 h.

E-region ionosphere: The normal E-region is composed mostly of oxygen and nitric oxide ions. Ionization is due to X-ray UV (XUV) (1–10 nm) and far UV solar radiation. In addition, EPP (e.g., 100s eV to 100s keV electrons and 10s to ~100 keV protons) from the magnetosphere are the main source of ionization in the high-latitude auroral zones. The E-region ionosphere impacts all radio wave propagation via refraction, absorption, and range delay. However, under typical conditions, this layer can only reflect radio waves with frequencies lower than about 10 MHz. The vertical structure of the E-layer is primarily determined by the competing effects of ionization and recombination. At night, the E-layer weakens and decays rapidly for two reasons: (1) the primary source of ionization (solar radiation) is no longer present, and (2) due to the high level of collisions. After sunset, the peak height of the E-layer rises, causing an increase in the range that HF radio waves can travel due to reflection from the E-region.

Occasionally, thin layers of very high levels of ionization are embedded in the lower E-region (typically between 100 and 110 km). These layers are known as sporadic E (Es) composed mostly of metallic ions from meteorites. The level of ionization in these layers may be up to five times greater than those normally achieved at the peak of the sunspot cycle. During intense sporadic E events, the Es-layer can reflect frequencies up to 50 MHz and higher. These layers vary greatly in size, although typically they are 1–2 km in thickness, and can be elongated by as much as 100 km or more. Es-layers can form in the equatorial region where they are associated with plasma instabilities in the equatorial electrojet. In the auroral region, Es-layers are associated with auroral precipitation and EPP into the E-layer. In mid-latitudes, the layers likely form due to wind shear in the lower thermosphere. Es-layers in the mid-latitudes exhibit pronounced seasonal and latitudinal dependence (Haldoupis et al., 2007).

F-region ionosphere: The F-region region of the ionosphere consists of the highest electron densities in the ionosphere (including the plasmasphere), and it is the most important region for long distance HF radio communications. The highest electron densities can typically be found between 160 and 500 km, although during storm-time conditions they can be lifted higher. During the daytime, the F-region often splits into two regions, with the lower one being the F1-region and the

higher one, the F2-region. Typically, the F1-layer is found at an altitude of 250–300 km and the F2-layer above it at ~350–400 km. After sunset, the two regions merge into one. Electrons in the F-region are produced by solar extreme UV radiation as well as auroral and soft EPP from the magnetosphere and solar wind (e.g., 100s eV electrons and a few keV protons), such as those that flow into the dayside cusp regions. In addition to production, the F-region electron density is also subject to transport by electric fields and neutral winds, and chemical reactions with neutrals through changes in neutral composition and temperature.

There are a variety of major space weather effects in the ionospheric F-region. All radio waves that propagate through the F-region are impacted by both a range delay and a refractive bending due to the dispersive nature of the ionospheric index of refraction. A number of specific F-region features induce space weather effects. Among these are the mesoscale (100–1000 km) features associated with large electron density gradients. An example of these features are the mid-latitude storm-enhanced density plumes and the polar region tongue of ionization and plasma density patches. Another example is the equatorial anomaly, which during large geomagnetic storms (e.g., minimum D_{st} ~-100s of nT) is greatly enhanced. These large features have specific implications for navigation, high precision positioning, and in particular, the Wide Area Augmentation System (WAAS) used in aviation. Other F-region features related to space weather include traveling ionospheric disturbances, which possess a wide range of spatial and temporal scales, with medium-scale traveling ionizing disturbances having horizontal wavelengths of tens to hundreds of kilometers and periods from 10 min up to 1 h, and large-scale traveling ionizing disturbances of >1000-km wavelengths and 30 min to 3 h in periods (Hunsucker, 1982). Traveling ionizing disturbances have implications for high precision differential positioning and for HF-wave propagation. A final space weather feature of the F-region ionosphere is small-scale electron density irregularities that induce amplitude and phase scintillation. These irregularities are found in the equatorial region, thought to be seeded by tropospheric waves and wind perturbations. Irregularities are also found in the high-latitude regions, associated with auroral precipitation and ionospheric density gradients associated with the tongue of ionization feature as well as polar cap patches. Ionospheric storm conditions can also lead to irregularities in the mid-latitudes. Scintillation can induce loss-of-lock of satellite signals that traverse the ionosphere and can also impact radar tracking of objects.

4.2.5 Thermospheric Dynamics

The thermosphere is the outermost layer of the neutral atmosphere, extending from ~90–600 km above Earth's surface. It is the region where many LEO satellites operate. Thermospheric neutral density is the main contributor to satellite drag in the LEO environment (not just limited to LEO spacecraft, since some higher altitude elliptical orbits have perigee in this altitude range and are thus also affected by drag there). The overall distribution of thermospheric density is determined by the balance between heating (such as absorption of solar radiation, Joule frictional heating, and heating by EPP) and cooling through infrared radiative emissions by carbon dioxide (CO_2) and NO. The excessive Joule and particle heating during geomagnetic storms causes the atmosphere to expand, leading to increases in neutral mass density and also changes in neutral composition due to the rising of the heavier, molecular-rich air from the lower atmosphere. In addition, impulsive Joule heating launches large-scale gravity waves that propagate equatorward toward middle and low latitudes, even into the opposite hemisphere, altering the mean global circulation of the thermosphere. This phenomenon is termed as a traveling atmosphere disturbance (TAD).

Under quiet conditions, the thermosphere experiences a general upwelling in the summer hemisphere and downwelling in the winter hemisphere, and the neutral winds flow toward the winter hemisphere. This means the global circulation pattern of the thermosphere is altered during geomagnetic storms when enhanced auroral heating produces strongly equatorward winds. At midlatitudes, the increased equatorward winds tend to push the ionosphere higher up along the magnetic fields lines, which can then produce a positive storm effect (e.g., an increase in NmF_2) owing to the lower loss rate at higher altitudes. The increased equatorward winds also carry the molecular-rich air resulting from upwelling due to auroral heating to midlatitudes. At lower latitudes, the subsequent downwelling reduces the concentration of molecular species. Changes in neutral composition have a direct impact on the ionosphere since the loss rate of ions depends strongly on neutral composition.

Infrared radiative emission by CO_2 and NO gases is the primary energy output in the thermosphere that counteracts the energy input from the Sun via solar irradiance and from the magnetosphere in the forms of Joule heating and EPP. Although both NO and CO_2 have been shown to respond to geomagnetic storms (Mlynczak et al., 2008), NO reacts more promptly to the incident energy input from the magnetosphere, which often varies on shorter time scales, from hours to days. As a result, NO cooling appears to play a more important role in regulating thermospheric temperature under short-term disturbed conditions such as during geomagnetic storms. It has been postulated that NO radiative cooling serves as a "natural thermostat" for the thermosphere (Mlynczak et al., 2008). NO radiative cooling is the main factor determining how fast the thermosphere returns to its pre-storm state during the recovery phase of geomagnetic storms, and that in turn dictates how much altitude loss satellites experience during each geomagnetic storm. NO's role in thermospheric cooling represents another area of connectivity between the solar and magnetospheric and thermospheric systems, since NO production can be enhanced by EPP (Randall et al., 2015).

Atmospheric drag affects satellites in all altitude regimes—from low altitudes to beyond geosynchronous altitudes. In fact, atmospheric drag is the largest source of error in modeling the force on many of these satellites. Precision orbit determination, needed for collision avoidance, is of increasing importance due to the proliferation and exponential increase of LEO satellites. While knowledge of atmospheric drag is most important for LEO satellites, its effects can be observed at all altitudes. If one assumes three different spheres with equal *A/M* ratios of 0.1 cm^2/gr, the time for the drag to change the satellite position by 12 km along track is ~1 day for a satellite at 300 km, 23 days for a satellite at 800 km, and 39 days for a satellite at 2800 km.

The equation describing atmospheric drag is expressed as: $F = 1/2\ C_d(A/M)\rho Vs^2$, where C_d is the ballistic coefficient, *A/M* is the area-to-mass ratio of the satellite, ρ is the atmospheric density, and *Vs* is the speed of the satellite with respect to the atmosphere (i.e., the vector sum of the speed of the satellite, V_{sat}, and the speed of the atmosphere/wind speed, V_{atmos}). On average, the ballistic coefficient is about 2.2, but in reality it must be determined for each satellite depending on the type of scattering (specular, diffuse, or some combination) that takes place between the surface of the satellite and the neutral particles in the atmosphere. The *A/M* ratio can be determined from the satellite's geometric design. The two key parameters that define atmospheric drag are neutral density and *Vs*, and the latter depends on the speed of the satellite with respect to the atmospheric winds. Since the atmospheric composition is involved in the determination of C_d, the density of the individual constituents is preferred. The speed of a satellite with respect to Earth is known with fairly high precision. However, the atmospheric winds vary drastically in latitude, longitude, and altitude, especially during geomagnetic storms. Winds can have speeds of several hundred meters

per second and sometimes greater, and therefore winds represent a non-negligible fraction of the satellite orbital velocity (around 7 km/s at LEO). Any advances in modeling satellite drag will depend on better estimation of thermospheric density as well as the neutral winds in the thermosphere.

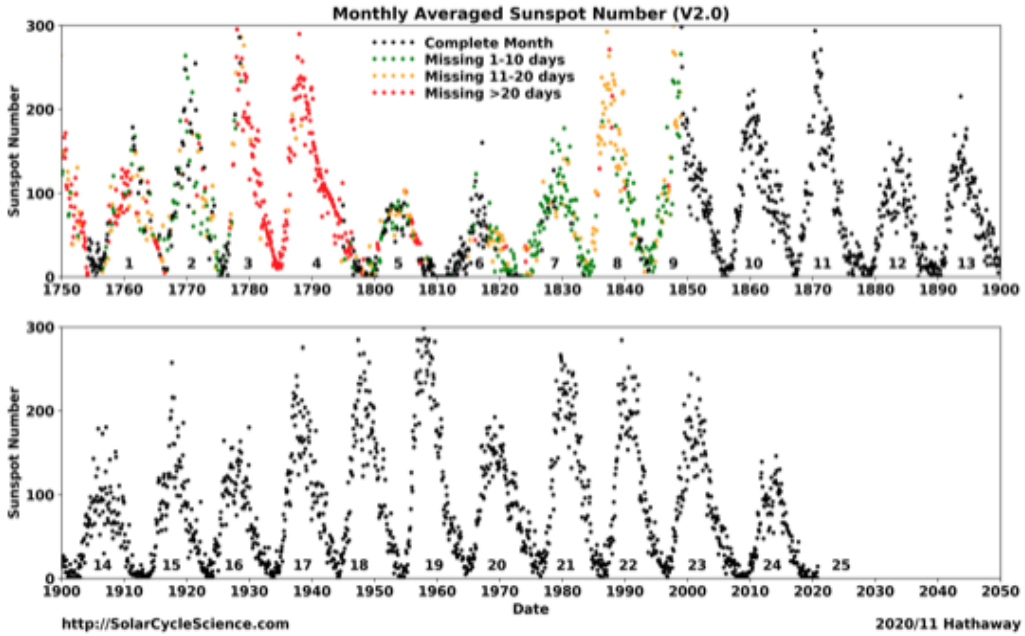

Figure 4-8. Monthly averaged sunspot numbers. This shows monthly averaged sunspot numbers (SILSO v2.0) since 1750. Color indicates the number of missing days in each monthly average, with the black dot representing complete months.

4.3 Long-Term Space Weather and Space Climate

On average, the solar cycle has a period of about 11 years and typically features a faster rising phase (~3–4 years) up to the solar maximum phase followed by a slower declining phase (~6–7 years) down to the solar minimum phase. This cycle can be quantified using sunspot numbers. The sunspot cycle is typically measured by counting the number of sunspots that appear each month and smoothed over 13 months. As new forms of solar activity (e.g., flares, CMEs, coronal holes) were discovered, it was found that their frequency of occurrence also varies with the sunspot cycle, and thus the sunspot number has become the standard for tracking the solar activity cycle.

The Solar Influences Data Analysis Center (SIDC) maintains the Sunspot Index and Long-term Solar Observations (SILSO) database, which includes the official record of the sunspot number (SSN). The amplitude of the cycle, as measured by the peak in the 13-month smoothed SSN version 2.0, typically ranges in values from about 80 up to nearly 300, with an average amplitude of ~180.

Active regions (ARs) are magnetic in nature (Borrero & Ichimoto, 2011), typically composed of a leading polarity sunspot emerging through the surface and a following polarity sunspot where the magnetic fields submerge into the interior again. The ARs tend to be tilted such that the leading polarity spot is more equatorward than the following polarity spot; this is known as the **Joy's Law** tilt. The polarity of the spots is opposite across the hemispheres and this polarity changes from one cycle to the next (thus, a full solar cycle is actually ~22 years); this is known as **Hale's Law**. At the

beginning of the 11-year sunspot cycle, the ARs tend to emerge at midlatitudes (~30°) and as the solar cycle progresses, they emerge closer and closer to the equator; this is known as **Spörer's Law**.

Another way to view the solar cycle is to average the magnetic field over all longitudes and to plot it as a function of latitude and time, i.e., the magnetic butterfly diagram. When this is done, the combination of Joy's, Hale's, and Spörer's laws form chevron-like patterns that resemble the wings of butterflies. Furthermore, additional characteristics of the Sun's magnetic field become apparent. Streams of flux, typically of following polarity, can be seen migrating from the AR belts to the Sun's poles. This flux collects at the poles, forming the **polar fields** (Petrie, 2015), and reverses polarity at about the time of solar-cycle maximum. The magnetic butterflies and the reversal of the polar fields reveal the full solar cycle is really a 22-year magnetic cycle (consisting of two 11-year sunspot cycles). The cycle polarity is known to have an impact on the influx of galactic cosmic rays (GCRs) into the heliosphere and may have additional ramifications that need to be explored.

Studying the motions of the Sun's plasma reveals the flows that guide the magnetic fields. The rotation of the Sun creates an east–west flow. The Sun is not a solid body, and thus rotates at a different rate at each latitude. This differential rotation (DR) is faster at the equator and slower at the poles. In addition to the east–west DR, the Sun also has a north–south flow known as the meridional circulation (MC), which is poleward at the surface. Together, the DR and the MC are referred to as the zonal flows or the axisymmetric flows. In addition to the axisymmetric flows, the Sun's plasma motions include the convective flows (CFs). These turbulent motions are the most complex of the Sun's flows, acting on multiple temporal, spatial, and velocity scales as well as moving in all directions.

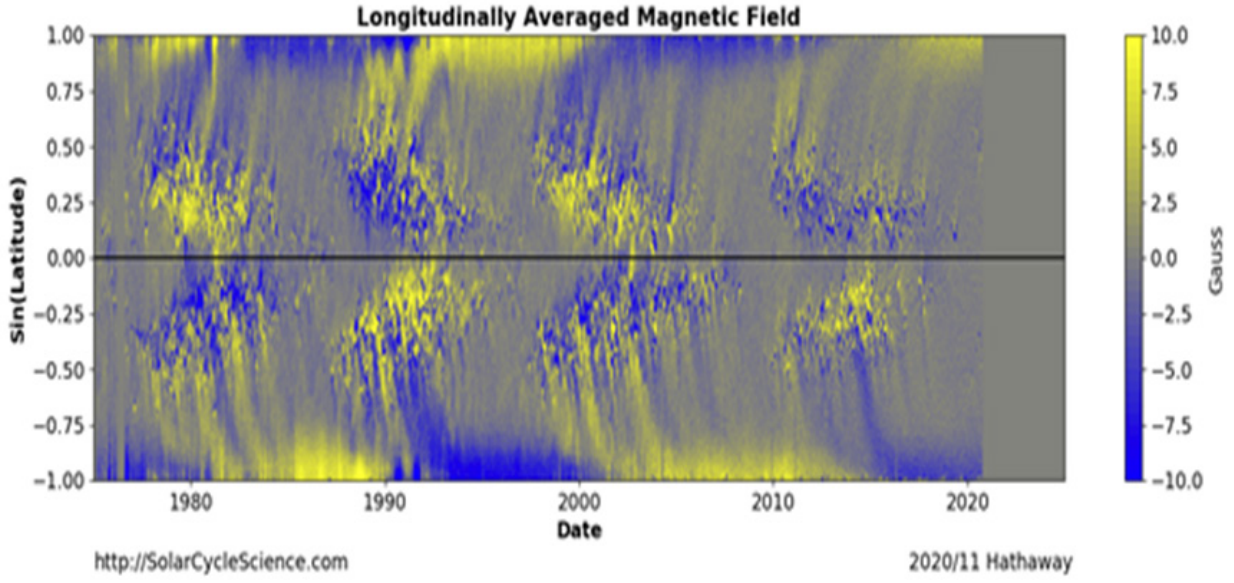

Figure 4-9. Magnetic butterfly diagram. This shows the distribution of the surface magnetic field (longitudinally averaged) over the last four solar cycles. The poles have opposite polarities that switch from one cycle to the next near the time of solar maximum.

Collectively, all of these fields and flows work together in a process known as the **Babcock–Leighton mechanism** (Charbonneau, 2020) to create the solar cycle. Through this dynamo process, the Sun's global magnetic field is converted from a poloidal to toroidal configuration and

back again through a series of stages. During solar minimum, the Sun begins with a relatively weak poloidal magnetic field which is oriented in a north–south configuration through the convection zone and which emerges from the poles, forming a dipole. The DR shears the submerged magnetic field in the toroidal direction, which strengthens the magnetic field. As the field gets stronger, it becomes buoyant and emerges through the surface, forming bipolar ARs with Joy's tilt and Hale's polarity. Magnetic flux in the ARs is shredded off of and dispersed by the turbulent convective motions. While most of the flux cancels with the opposite polarity, the residual magnetic flux (which is predominately the following polarity and opposite in sign to the poles) is transported to the poles by the meridional flow. Over the course of the solar cycle, the residual flux cancels the old poloidal field and creates a new poloidal field with opposite polarity. From there, the 11-year sunspot cycle repeats itself.

Long-term solar activity prediction. This term addresses the long-term aspect of SWx forecasting, which we define as the prediction of eruptive solar phenomena (flares or CMEs) on time scales of days to weeks. This is an area of exploration driven primarily by basic research. It mostly focuses on understanding photospheric magnetic flux emergence and evolution (e.g., van Driel-Gesztelyi & Green, 2015) with the purpose of developing the capability to predict AR emergence, flaring, and eruptions. Analysis techniques, such as helioseismology, machine learning, and sophisticated modeling (3D radiative transfer, data-driven, ambipolar diffusion, etc.) are being employed to elucidate the transfer of magnetic flux and energy from the convection zone to the corona, where it is liberated in the form of flares and CMEs.

Solar climate prediction. For longer time scales, "climate" is a more appropriate term. Climatology is the study of the long-term, statistical behavior of weather systems and in particular patterns or trends that occur on any type of periodicity (even roughly—such as 1/100-year occurrence probability). Hence, space climate refers to the prediction of changes in solar activity that occur on longer time scales (e.g., months, years, or decades), such as the solar cycle (Hathaway, 2015; Usoskin, 2017). The prediction for "solar cycle"–scale activity typically relies on the average properties of the fields and flows to provide a probabilistic basis for SWx in the coming years, which is essential for mission planning. Several methods exist for long-term solar-cycle predictions (Petrovay, 2020). The most successful are the physics-based methods that rely on the fact that the polar fields at solar-cycle minimum are the best predictor of the amplitude of the next cycle. Over the last decade, dynamo models and surface flux transport models have become more favorable. These models simulate the evolution of the Sun's magnetic field using our current understanding of the observed fields and flows with the aim of improving the predictive range by deriving the polar fields at minimum several years in advance.

Geospace climate. Solar-cycle variability is reflected in the geospace environment, where the majority of space weather hazards to human systems occur. The long-term systems behavior that are SWx-relevant can be considered as "geospace climate." However, geospace climatology represents a major space weather gap, mostly because of the limited (less than one solar cycle) time series of many relevant geospace phenomena. A good example of a successful and valued climatological space weather model is the AE9/AP9/IRENE model characterizing the radiation environment in near-Earth space. To develop such reliable climatological models, statistically significant quantities of data on key observables must be obtained, spanning at least one solar cycle and ideally spanning more. The most relevant phenomena, from a climatological perspective, are: radiation belt proton/electron intensities (i.e., contributing to statistical development of AE9/AP9/IRENE), energetic

particle injection occurrence rates as a function of location and activity levels (solar wind driving conditions, geomagnetic indices) throughout the inner magnetosphere and plasma sheet, plasmaspheric density structure and variability as a function of location (L-shell, magnetic local time [MLT], magnetic latitude [MLat]), ranges and occurrence rates of thermospheric properties (density, temperature, composition) as a function of location (latitude, longitude, altitude) and activity levels (solar wind driving conditions, geomagnetic indices), and ranges and occurrence rates of ionospheric quantities (D-region absorption, Es-layer and scintillation, and F-region density structure, variability, and gradients) as a function of latitude/longitude at some reasonably high resolution and activity levels (solar wind driving conditions, geomagnetic indices). Climatological models represent a high-value product for space weather end-users, including the insurance sector, in particular for occurrence rates and confidence levels used in risk assessment and for space mission design and operations planning. While geospace SWx climatology is of interest to note here and consider as a factor in observational gap prioritization, additional details on geospace SWx climatology and climate model development are beyond the scope of this task and not included here.

5 Gap Analysis

We perform the gap analysis on the quantities most relevant to SWx (see Section 2 and Section 3) and derived from observations of the physical phenomena described in Section 4. The quantities are selected via literature review and discussions with the SWx experts and end-user community representatives within the committee. Some of these quantities are used as inputs to research and operational models while others are used directly for forecasting (i.e., “all clear” or ToA).

For each quantity, we briefly describe how they are derived and/or used, list the current and desired fore/nowcasting status, identify the research and/or measurement gaps and then proceed to describe the required measurement for closing the gap in order of increasing value.

The following set of block diagrams trace key observable quantities or sets pertinent to specifications and end user needs for each SWx hazard identified in Section 2. Some of the observable boxes are intentionally vague here (intended as top-level placeholders), and each observable gap is described and detailed further in this section. Each diagram also identifies which observables are currently satisfactory (green observable boxes) or qualify as either partial (yellow) or full (red) gaps in our existing observatory network, and a priority, low to high, is assigned to each gap observable.

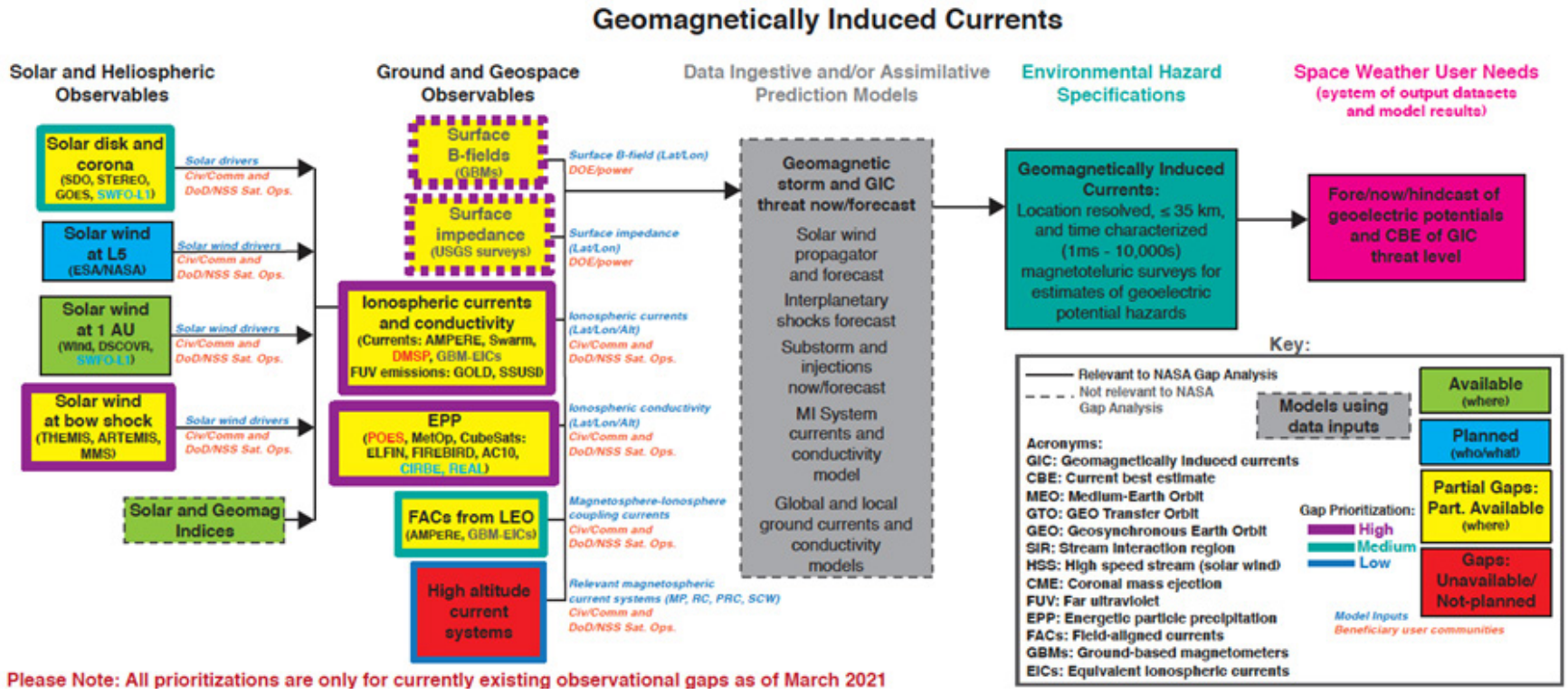

Figure 5-1. Key observables to end-user products traceability diagram. Observables are split between “solar and heliospheric” (leftmost column) and “ground and geospace” (second column from left). In the traceability, data from those observables feed forward into data-ingestive and/or -assimilative prediction models relevant to particular environmental hazard specifications and finally to end-user needs and products. Models are not detailed further in this report since they are outside of the scope of this task. For each observable, the gap status (full gap in red, partial gap in yellow, no gap in blue or green for planned and currently available assets, respectively) and priority (high priority with thick purple outlines, medium with turquoise, and low with thin blue) are indicated on the boxes themselves. Only solid outlines, indicating observations made from spacecraft, are considered in this report, with dashed outlines indicating ground-based observables. See the key for additional details for SWx effects from GICs.

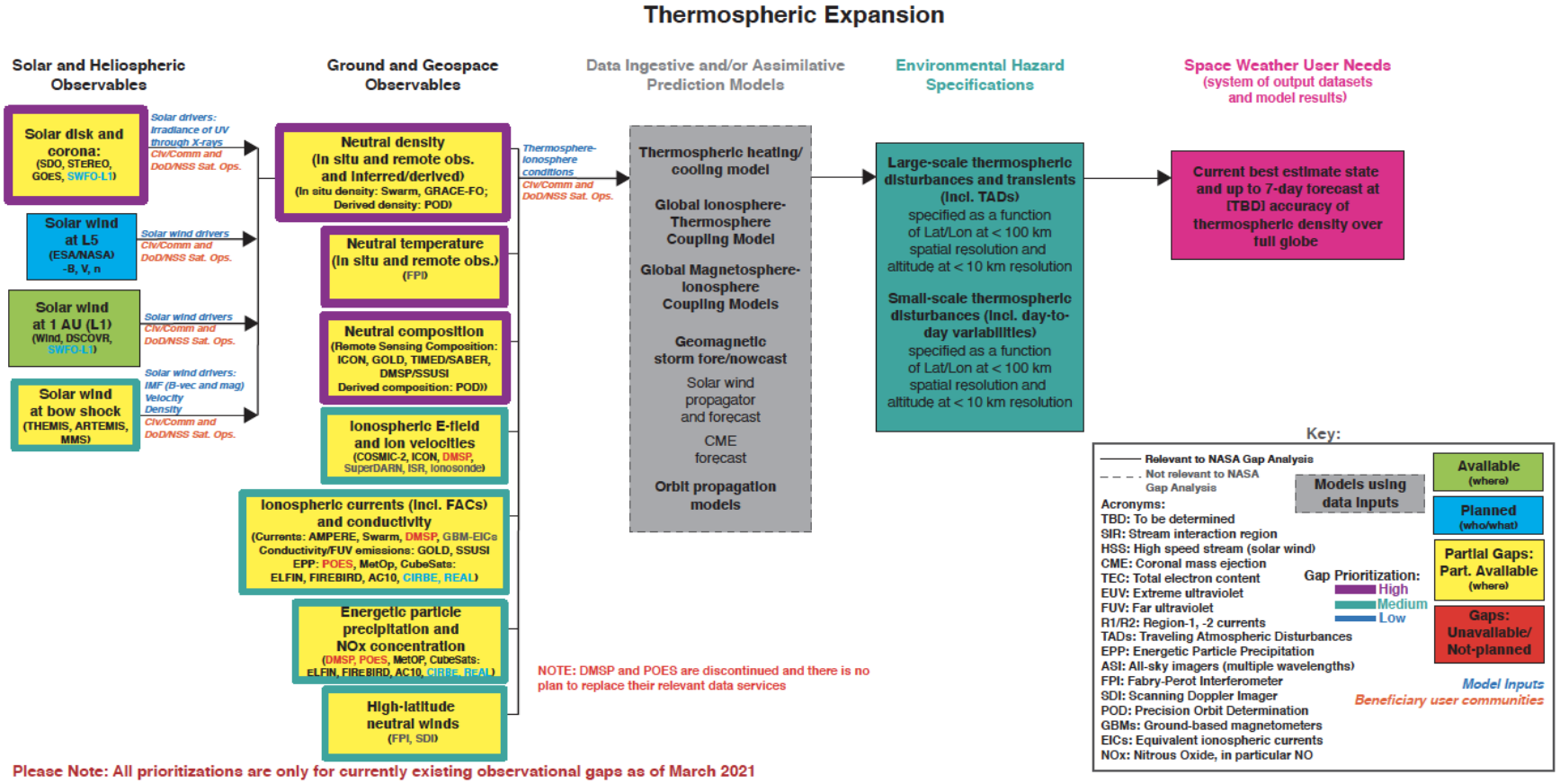

Figure 5-2. Key observables to end-user products traceability diagram for SWx effects from thermospheric expansion.

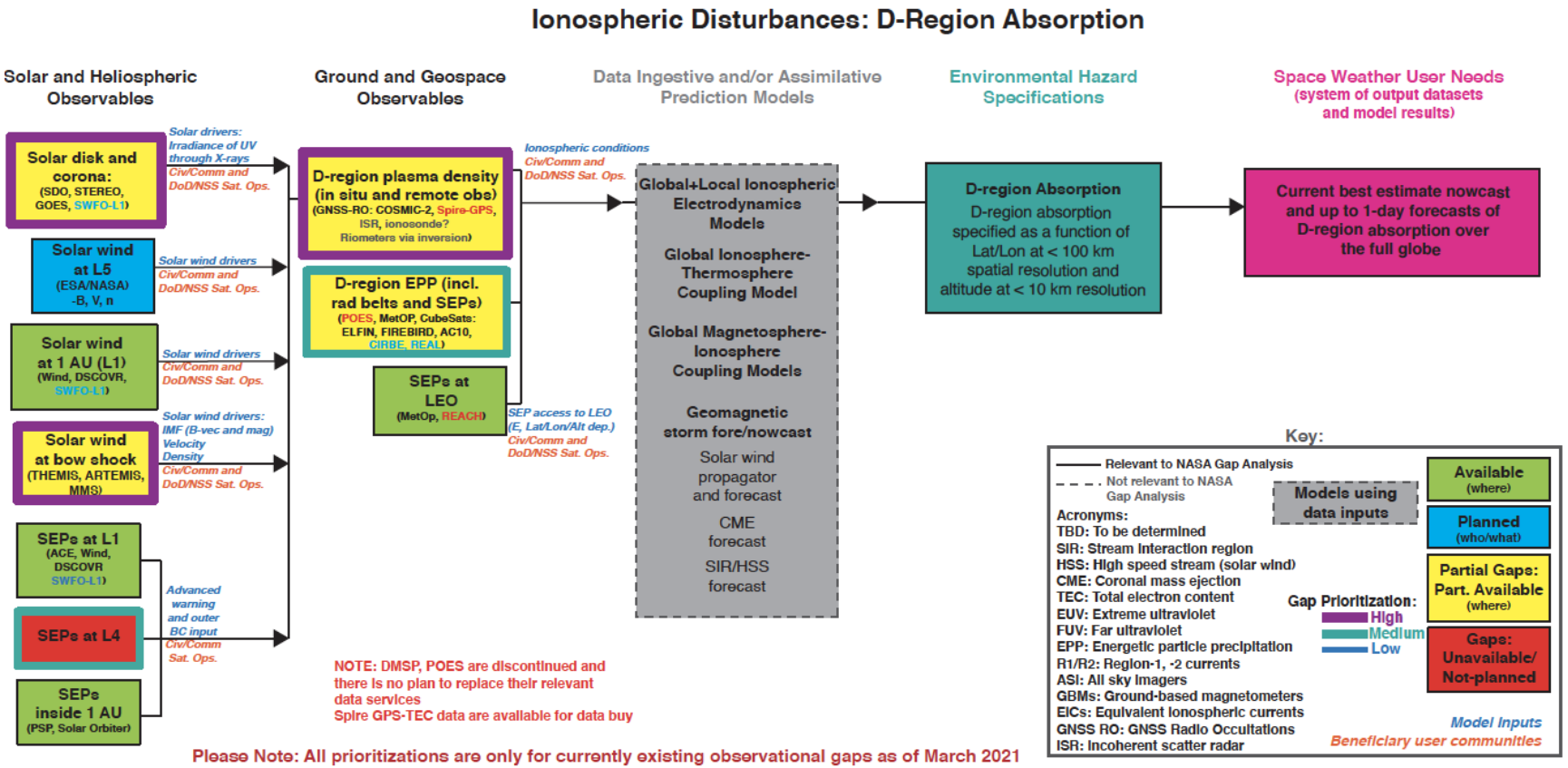

Figure 5-3. Key observables to end-user products traceability diagram for SWx effects from ionospheric D-region absorption.

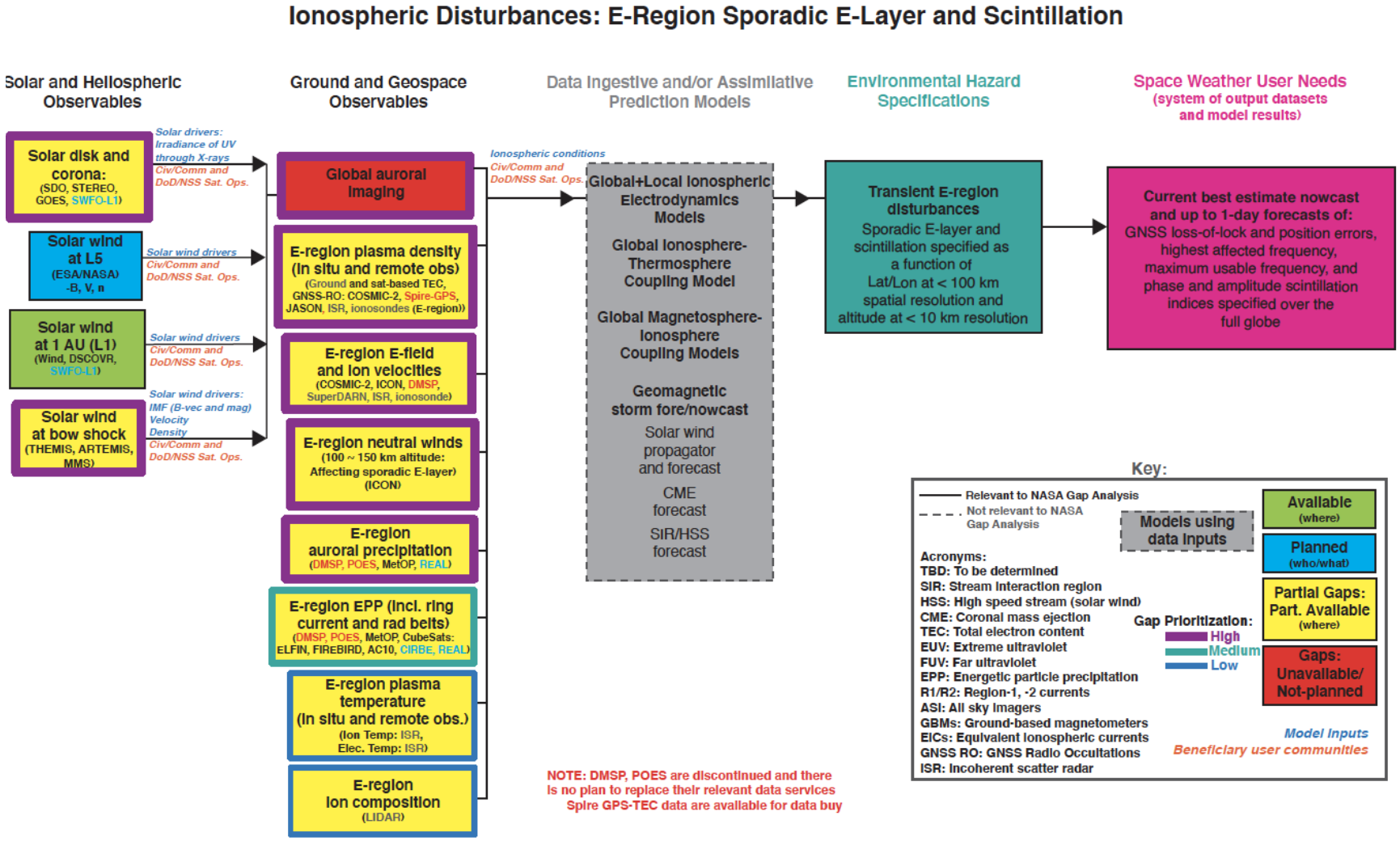

Figure 5-4. Key observables to end-user products traceability diagram for SWx effects from ionospheric E-region Es-layer and scintillation.

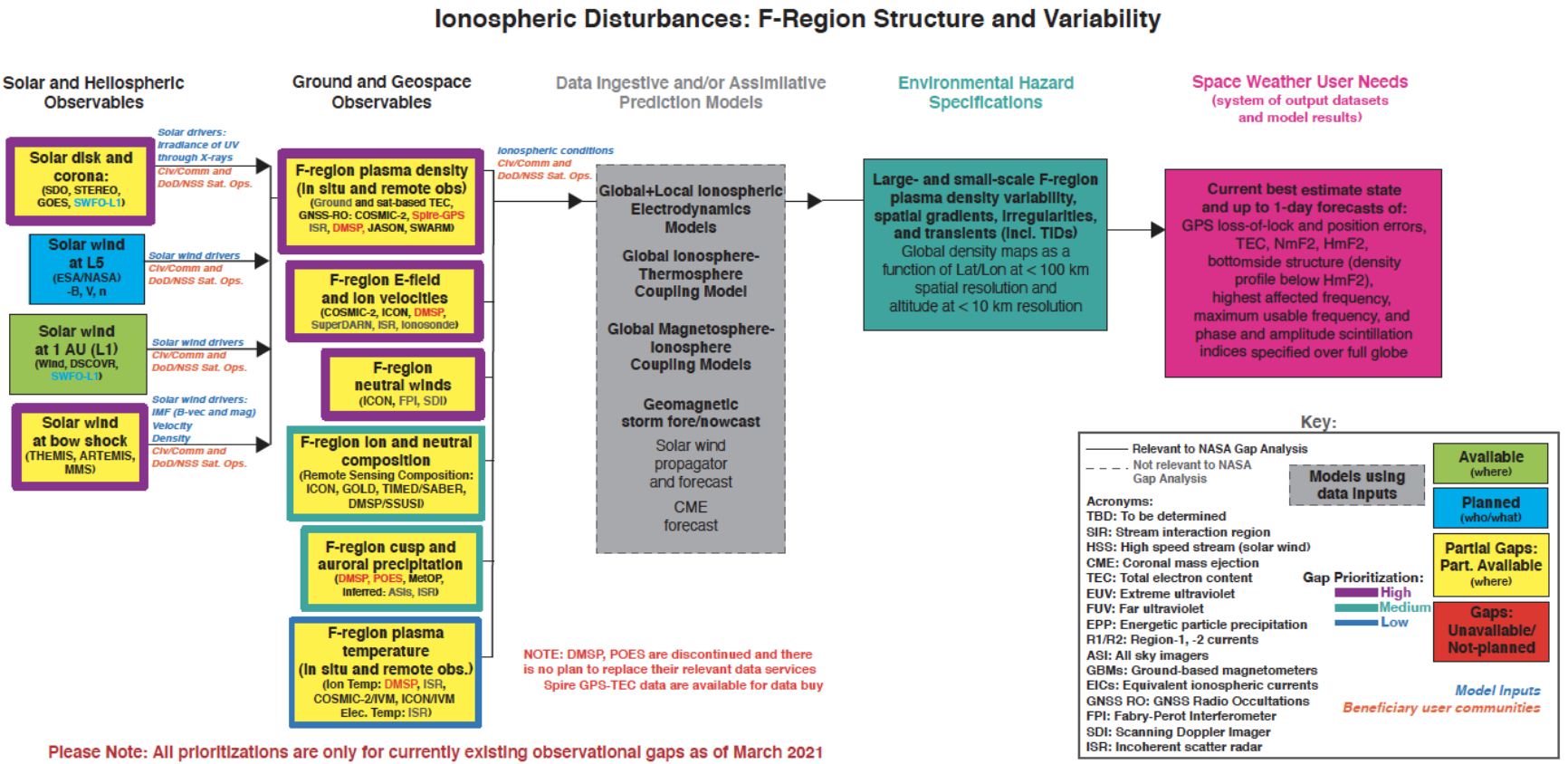

Figure 5-5. Key observables to end-user products traceability diagram for SWx effects from ionospheric F-region structure and variability.

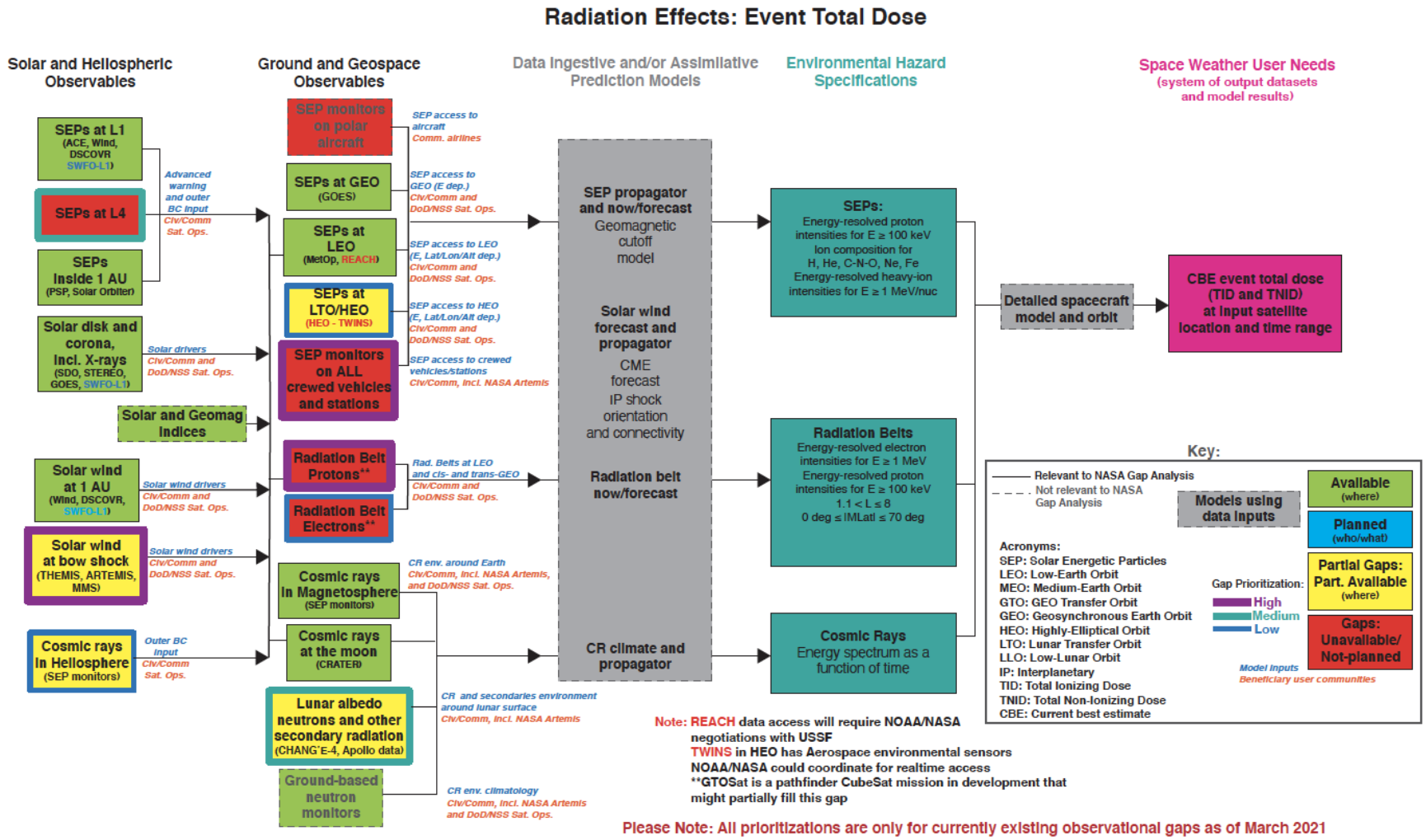

Figure 5-6. Key observables to end-user products traceability diagram for SWx effects from total radiation dose.

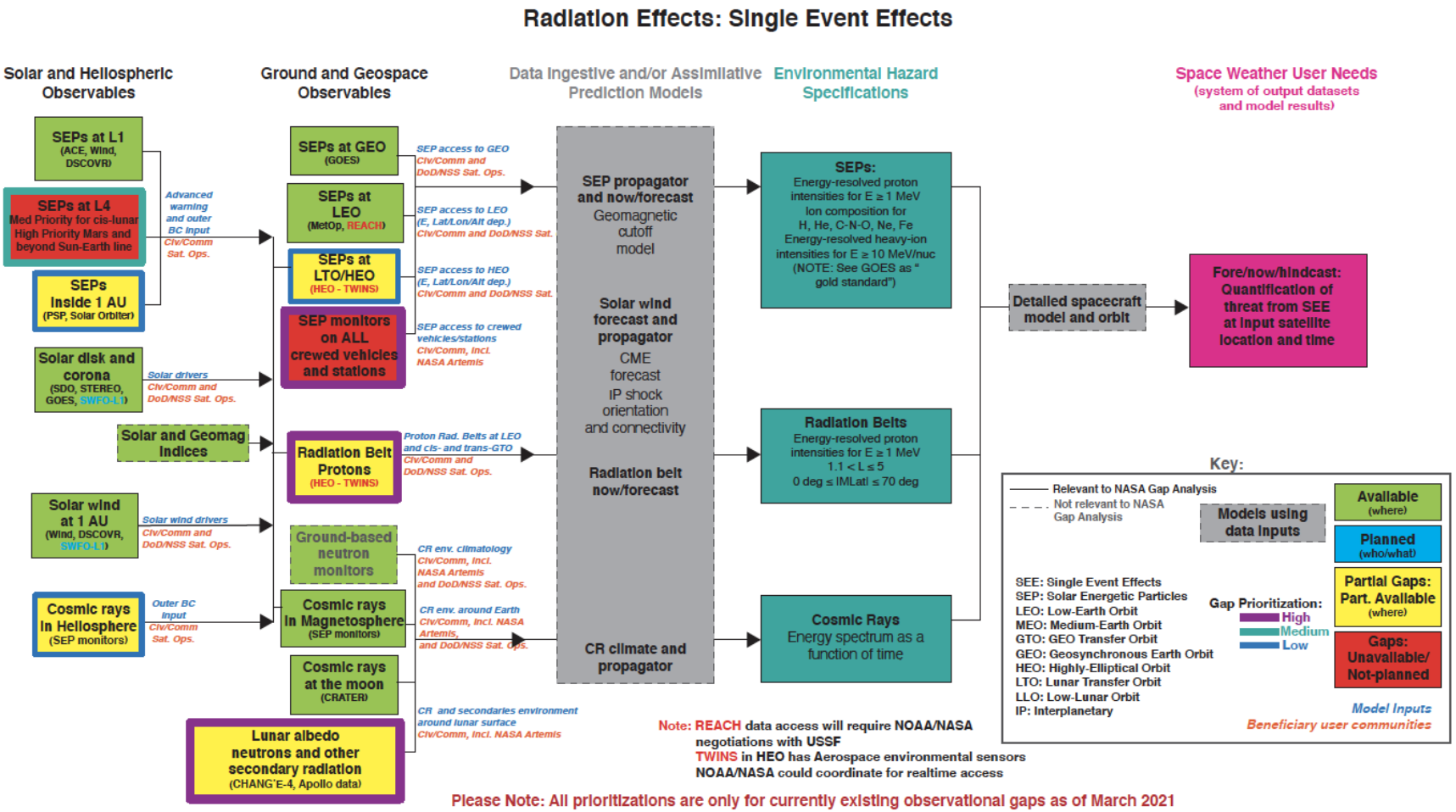

Figure 5-7. Key observables to end-user products traceability diagram for SWx effects from total radiation dose.

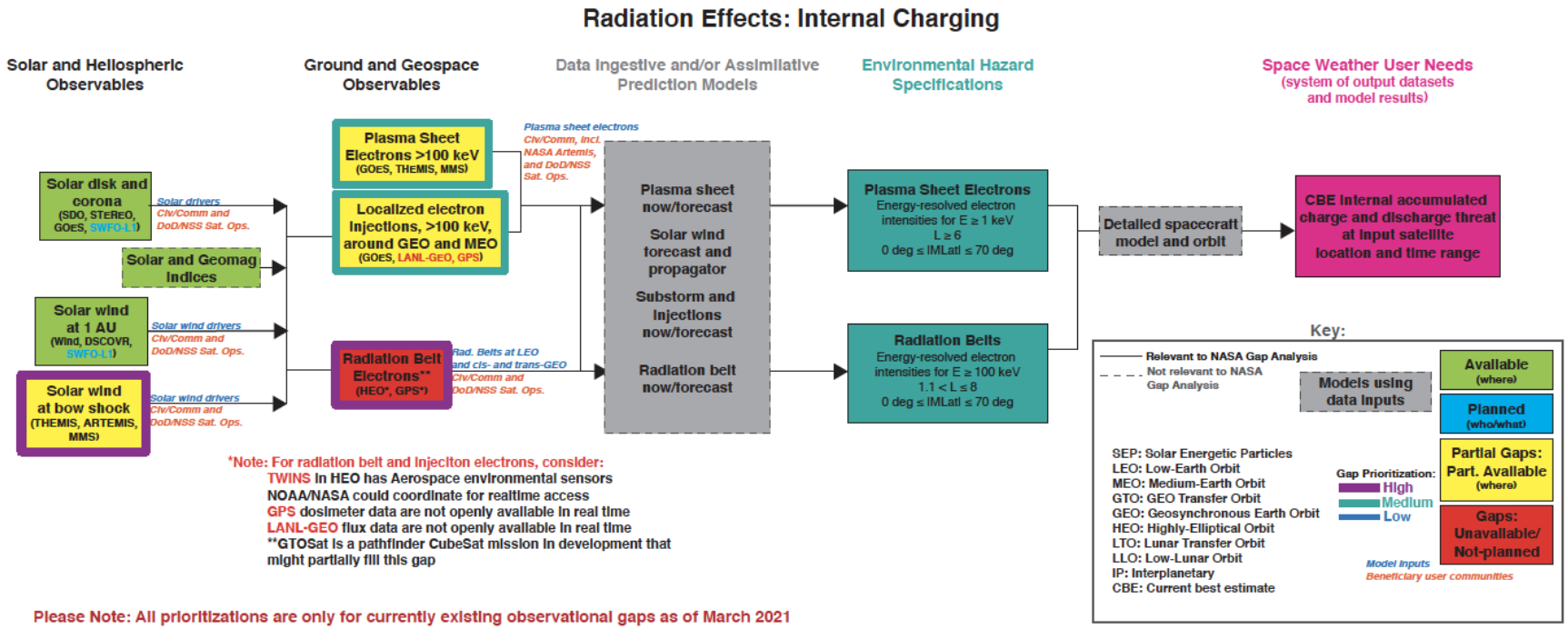

Figure 5-8. Key observables to end-user products traceability diagram for SWx effects from spacecraft internal charging from radiation.

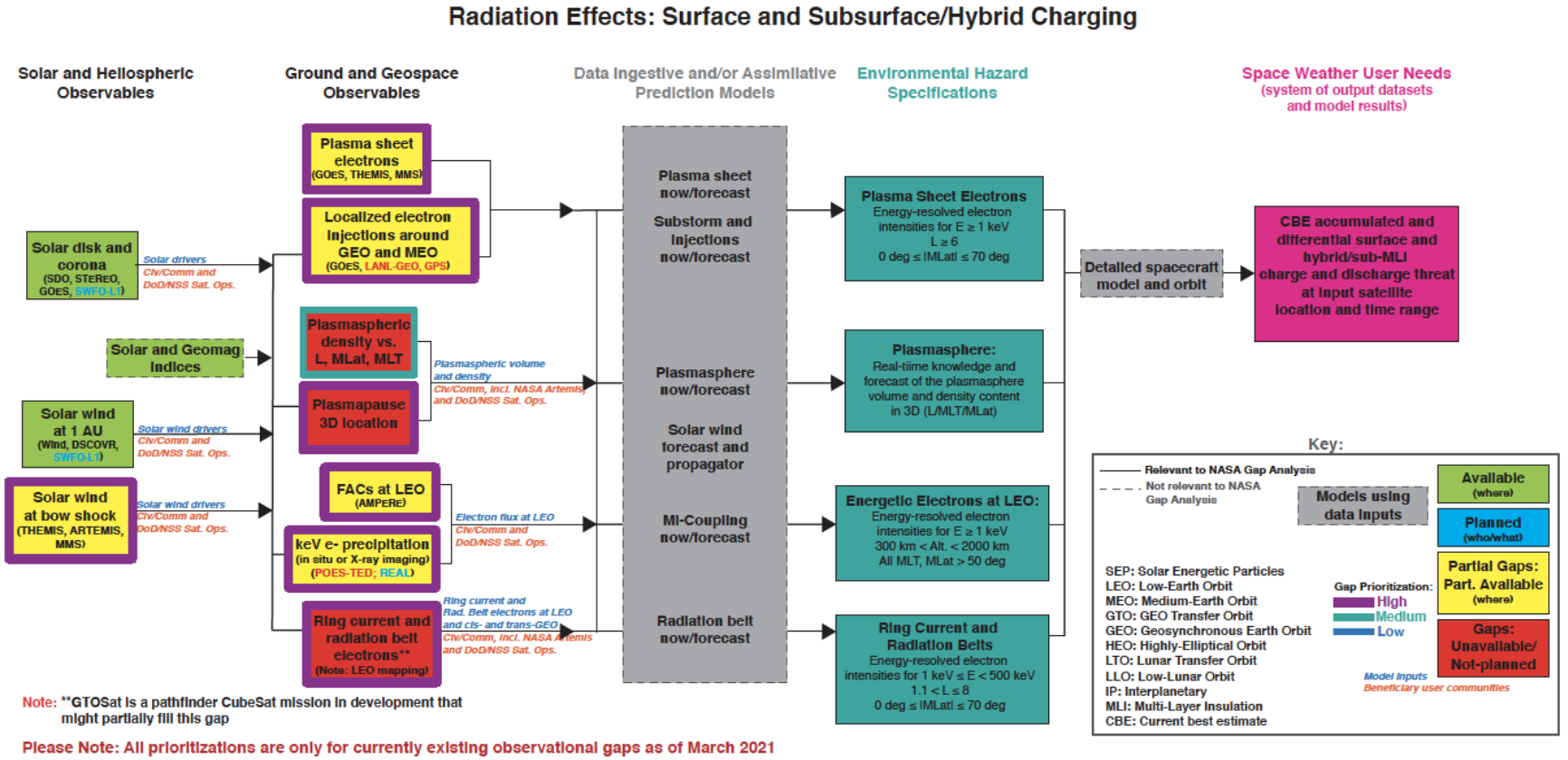

Figure 5-9. Key observables to end-user products traceability diagram for SWx effects from spacecraft surface and subsurface/hybrid charging from radiation.

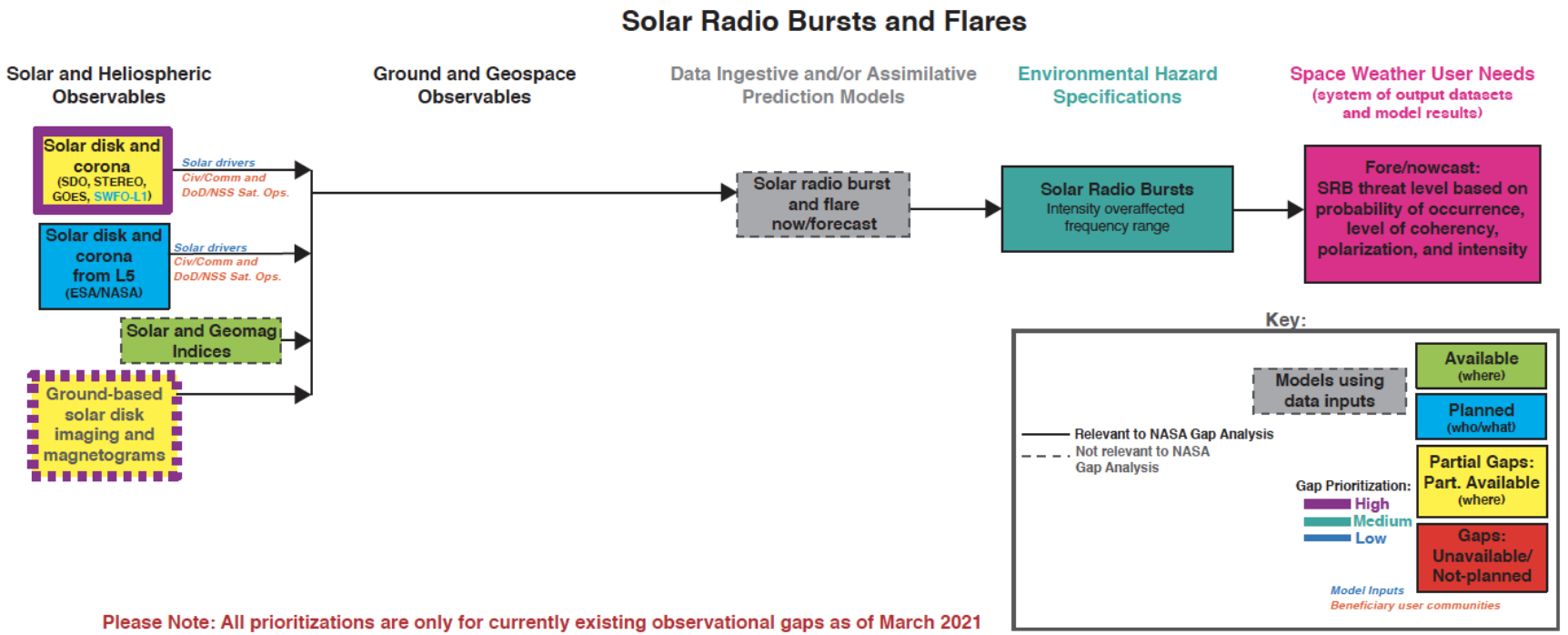

Figure 5-10. Key observables to end-user products traceability diagram for SWx effects from SRBs and flares.

5.1 Solar and Heliospheric Observables

The following sections walk through the details on relevant SWx drivers and phenomena and the key observables that qualify as gaps pertaining to each. The closure of these gaps by future observations should lead to higher performance of space weather predictive models (*-casting). Section 5.1 starts with solar and heliospheric (SH) observables, and Section 5.2 covers geospace observables. These distinctions are important since the SH sections largely revolve around those observables corresponding to drivers of SWx both at Earth and throughout the heliosphere (e.g., at Mars), as detailed earlier in this report (e.g., Figure 4-1). Meanwhile, the geospace observables correspond to a combination of internal drivers and actual SWx effects/consequences throughout the ground and atmosphere (on Earth) and geospace (in space, including cislunar) environments.

The SH gap analysis is summarized in Table 5-1 shown in the foldout. The gap analysis adopts a flowdown structure. It starts with the solar phenomenon, followed by its key observables and then traces the current state (forecast status), the desired state (forecast requirement, if known), and a brief outline of the knowledge gaps responsible for the current state. The flowdown then proceeds to outline four categories of required observations to (1) maintain the current *-casting status; (2) partially improve it; (3) advance it significantly, and (4) to provide possible closure—defined as leading to actionable forecasts. The rationale for the flowdown is discussed in the following sections. Section 5.2 follows a similar structure, using Figure 5-1 through Figure 5-10 for the flowdown.

Table 5-1. Top-level summary of gap analysis for SH observables

Phenomenon	Parameter of Value to Models & SWx*-Casting Products	Forecasting Status (If Known)	Forecasting Requirement	Research Gaps	Maintain	Improve	Advance	Close (Actionable Forecasting)
CME/Shocks	All Clear	97% of CMEs detected from SEL	100% of user-directed CMEs within 2 h of eruption	• "stealth" events (from Sun-observer viewpoint) • overlapping events • low duty cycle	SEL EUV disk imaging + VIS coronagraphic imaging to >20 $R_\odot$ with 95% duty cycle	off-SEL VIS coronagraphic imaging to >20 $R_\odot$ + EUV imaging disk to 1.5 $R_\odot$ with 95% duty cycle	2-view (90°) off-SEL VIS coronagraph imaging >20 $R_\odot$ + EUV disk imaging to 1.5 $R_\odot$ with 95% duty cycle	• 3-view (120°) off-SEL coronagraphic imaging >20 $R_\odot$ + EUV disk imaging >1.5 $R_\odot$ • off-ecliptic (>60°) VIS coronagraphic imaging to >80 $R_\odot$ with 95% duty cycle • msrt of coronal currents in ARs
	Direction (Hit/Miss)	80% (from off-SEL VIS imaging)	24-h warning of a hit	• IP evolution • line-of-sight effects • "stealth" events	SEL EUV disk imaging + VIS coronagraphic imaging to >20 $R_\odot$ with 95% duty cycle + L1 in situ (P&F)	• off-SEL VIS imaging to >80 $R_\odot$ + off-SEL EUV disk imaging to >1.5 $R_\odot$ with 95% duty cycle • >50% long. coverage of B_{phot} (east limb preferred)	• off-ecliptic (>60°) VIS coronagraphic imaging to >80 $R_\odot$ with 95% duty cycle • in situ P&F msrts upstream of L1 • 2-view off-SEL EUV disk imaging to >1.5 $R_\odot$ + off-SEL VIS coronagraphic imaging to >80 $R_\odot$ with 95% duty cycle	• 3-view (120° apart) + off-ecliptic (>60°) VIS imaging to >80 $R_\odot$ + distributed in situ P&F msrts upstream of Earth • multipoint in situ P&F msrt at ~0.3 AU from Earth • distributed in situ P&F msrt from Earth to 0.3 AU upstream
	Time of Arrival	9.8 ±2 h (from off-SEL VISimaging). It reduces to >17 h for SEL VIS imaging	0 ±2 h (for actionable electric grid measures)	• IP propagation • CME/shock shape and size at 1 AU	SEL EUV disk imaging + off-SEL VIS coronagraphic imaging to >30 $R_\odot$	• multipoint in situ P&F msrts >0.1 AU upstream • 2-view off-SEL VIS coronagraphic imaging >80 $R_\odot$ • >50% long. coverage of B_{phot} (east limb preferred)	• 2-view off-SEL high signal-to-noise ratio (SNR) VIS imaging >80 $R_\odot$ + >67% long. coverage of B_{phot} + upstream in situ • >67% long. coverage of B_{phot} • distributed in situ P&F msrts 0.7–1 AU	3-view (120°) off-SEL coronagraphic imaging >20 $R_\odot$ + off-ecliptic (>60°) VISimaging to >80 $R_\odot$ + distributed in situ P&F msrts upstream + >67% long. coverage of B_{phot}
	Speed on Arrival	>30%	105 of arrival speed	same as above	same as above	same as above	same as above	same as above

Phenomenon	Parameter of Value to Models & SWx*-Casting Products	Forecasting Status (If Known)	Forecasting Requirement	Research Gaps	Maintain	Improve	Advance	Close (Actionable Forecasting)
	Mass Density	2–3× overestimate at 1 AU	none known	• small-scale density structure of CME/CIR front • IP evolution	off-SEL VIS imaging to 20 $R_\odot$	• off-SEL high SNR VIS imaging >80 $R_\odot$ • >50% long. coverage of B_{phot}	• 2-view off-SEL high SNR VIS imaging >80 $R_\odot$ • >67% long. coverage of B_{phot} • distributed in situ P&F msrts 0.7–1 AU	off-ecliptic (>60°) VIS imaging to >80 $R_\odot$ + distributed in situ P&F msrts upstream of Earth
	Impact Duration	~3× overestimate	none known	• IP propagation • Line-of-site (LOS) effects • CME/shock shape at L1	SEL EUV disk imaging + VIS coronagraph imaging to >20 $R_\odot$ with >95% duty cycle + L1 in situ (P&F)	• off-SEL high SNR VIS imaging >80 $R_\odot$ • off-SEL EUV imaging of the Earth-facing disk	off-SEL high SNR VIS imaging >80 $R_\odot$ + off-SEL EUV imaging of the Earth-facing disk + distributed in situ P&F msrts 0.7–1 AU	• multipoint in situ P&F msrt >0.1 AU from Earth • 2-view off-SEL + off-ecliptic (>60°) high SNR VIS imaging >80 $R_\odot$
	Magnetic Configuration (strength, orientation, duration)	~30 min	strength: 24 h orientation/duration: 2–3 h	• unknown at-birth CME magnetic properties • unknown sub-Alfvénic corona properties • remote sensing of CME magnetic field in corona/heliosphere • CME/shock IP propagation • Earth trajectory through magnetic structure	• SEL EUV disk imaging + VIS coronagraph imaging to >20 $R_\odot$ with >95% duty cycle + L1 in situ (P&F) • SEL vector B_{phot} • SEL SXR disk imaging	• 2-view stereoscopic EUV imaging of source regions • SEL vector B_{phot} + B_{chrom} in ARs • off-limb UV/NIR spectroscopy <5 $R_\odot$ • >50% long, coverage of B_{phot} • off-SEL high SNR VIS imaging >80 $R_\odot$	• >60% long. coverage of B_{phot} • multipoint in situ P&F msrt at ~0.3 AU from Earth • distributed in situ P&F msrts 0.7–1 AU • 2-view off-SEL high SNR VIS imaging >80 $R_\odot$	• multipoint in situ P&F measurement at ~0.3 AU from Earth + distributed in situ P&F msrts from Earth to 0.3 AU upstream (for CME B_z) + 67% long. coverage of B_{phot} (for shock B_z)
Flares	All Clear	little better than "no skill" in probabilistic forecasting; some skill but no robustness in binary forecasting	6-h and 24-h of flare occurrence	• non-potential energy buildup • energy release via reconnection • uncertainty over triggers as precursors	• SEL vector B_{phot} • SXR/EUV irradiance profiles	• SEL imaging of hot plasmas • multiwavelength EUV imaging • EUV/UV imaging spectropolarimetry • SEL vector B_{phot}+B_{chrom} in ARs • off-SEL SXR irradiance profiles	• off-SEL (EUV imaging + vector B_{phot}) • 2× off-SEL (EUV imaging + vector B_{phot})	• multi-height vector magnetic field msrts • multi-view local helioseismology & vector B_{pho}

Phenomenon	Parameter of Value to Models & SWx*-Casting Products	Forecasting Status (If Known)	Forecasting Requirement	Research Gaps	Maintain	Improve	Advance	Close (Actionable Forecasting)
	Peak SXR Flux	same as above	M1+, X1+ at 24-, 48-, and 72-h intervals	• energy release rate and amount before flare onset • 3D reconnection evolution and ambient loop systems • detailed energy budgets	same as above	same as above plus: • high-performance HXR imaging spectroscopy	same as above plus: • off-SEL HXR imaging spectroscopy of reconnection region (loop-top source)	multi-height vector magnetic field msrts
	SXR Duration/Fluence	same as above	M1+ and X1+ for 24-, 48-, and 72-h forecast intervals	• energy budgets • coronal current systems	same as above	same as all clear	same as all clear	same as all clear
	EUV Irradiance Enhancement	same as above	same as peak flux	• same as peak flux • Incomplete EUV spectrum coverage	same as above	same as all clear	same as all clear	same as all clear
Radio Bursts	Metric Wavelengths	mostly Type II and IV bursts as proxies for eruptive events; no current forecasting capability specifically for these burst types	not currently	• circular polarization • inadequate flux calibration	24-h dynamic spectral coverage from 25 to 200 MHz; requires distributed ground-based network, 1-s time resolution, <1 MHz spectral resolution	increase coverage to 15–600 MHz + add circular polarization	• increase coverage to 15–600 MHz + circular polarization • well-calibrated fluxes	• increase coverage to 15–600 MHz + circular polarization • well-calibrated fluxes
	Decimetric, GNSS Bands	bright coherent bursts interfere with GNSS, cell phone and radar signals; no current forecasting capability	not currently	same as above	single-frequency msrts spaced from 400 to 2.0 GHz with 1-s time resolution	dynamic spectra from 200 to 2000 MHz with polarization, 1-s time resolution, 24-h coverage	flux-calibrated circular polarization dynamic spectra up to at least 2.0 GHz	flux-calibrated circular polarization dynamic spectra up to at least 2.0 GHz
	Microwaves	can interfere with satellite signals, particularly for geosynchronous belt in spring and fall	for F10.7 (2.8 GHz) same as for irradiance below	current observations limited to ~5 fixed frequencies from 2.5 to 15 GHz	24-h monitoring of ~5 fixed frequencies from 2.5 to 15 GHz with 1-s cadence	monitoring of full frequency range 2–20 GHz with dense frequency coverage, circular polarization msrts	extend coverage to higher frequencies; important as K- W-, and V-band communications become more widely used	extend coverage to higher frequencies; important as K-, W-, and V-band communications become more widely used
	Decametric and Lower	mostly Type II/III bursts as proxies for eruptive events; reliance on research inner heliospheric satellites prevents robust use for operations	not currently	real-time data	24×7 dynamic spectra <10 MHz with <1-h latency	24×7 dynamic spectra <10 MHz with 95% duty cycle with ~15-min latency	24×7 dynamic spectra <10 MHz with 95% duty cycle with ~1-min latency	24×7 dynamic spectra <10 MHz with 95% duty cycle with ~1-min latency

Phenomenon	Parameter of Value to Models & SWx*-Casting Products	Forecasting Status (If Known)	Forecasting Requirement	Research Gaps	Maintain	Improve	Advance	Close (Actionable Forecasting)
Irradiance	UV/EUV Irradiance	<3 days	>7 days	• pointing flux from photosphere to corona • sources of irradiance • long timeseries • long-term calibration	limited msrts of SXR fluxes and EUV/UV spectral line data	• off-SEL UV/EUV spectra/bands • B_{phot} >50% surface	• complete coverage of Sun's <300 nm spectrum variable component • full-disk spatially resolved bolometric msrts	• full spectrum msrts (0.1–300 nm at 0.1 nm resolution) • robust network of systems providing uniform and assured data availability
	EUV Spectral Irradiance	<7 days using global magnetic field models to generate EUV spectral bands (e.g., "stan bands") or F10.7 as a proxy	>7 days	spectrally resolved irradiance msrts (e.g., EVE-like) at high cadence and spectral resolution to resolve major spectral lines	same as above	• more complete spectral coverage of the coronal EUV range • 1–6 nm SSI • off-SEL SSI • B_{phot} >50% surface	• complete coverage of Sun's short wavelength spectrum variable component • full-disk spatially resolved SSI msrts	• full spectrum SSI msrts (0.1–200 nm at 0.1 nm resolution) • robust network of systems providing uniform and assured data availability
	F10.7 (radio flux at 2.8 GHz)	<7 days using global magnetic field models	>7 days	24-h coverage	well-calibrated msrts 3×/day from single site	• well-calibrated msrts with 24-h coverage from multiple sites • uniform instrumentation	n/a	n/a
SEP	All Clear: Pre-eruption Forecast of **not** Crossing Thresholds	one method: probability of detection (POD) = 0.62, false alarm ratio (FAR) = 0.16 for >10 MeV protons; performance unknown for >100 MeV protons	• FAR as low as possible • prediction window requirements: ○ general: 24-h all-clear forecasts of >100 MeV protons not exceeding 1 pfu ○ EVA: 24- and 6-h all-clear forecasts of >10 MeV protons not exceeding 10 pfu	see Flares and Climate research gaps • role of "seed particle" populations	• SEL vector B_{phot} • SEL SXR irradiance • in situ (P&F): e-, p+, & heavy ion msrts (e-0.1–1 MeV; p+ 0.02–700 MeV)	• >50% long. coverage of B_{phot} • SEL imaging of hot plasmas • EL vector B_{phot} + B_{chrom} in ARs	• high SNR imaging spectroscopy of off-limb Ly-α emission • >67% long. coverage of B_{phot} • off-SEL: (SXR+EUV) imaging+vector B_{phot}	• 4π coverage of surface B and coronal structure • multi-height vector magnetic field msrts

Phenomenon	Parameter of Value to Models & SWx*-Casting Products	Forecasting Status (If Known)	Forecasting Requirement	Research Gaps	Maintain	Improve	Advance	Close (Actionable Forecasting)
	Post-eruption Forecast of Crossing Thresholds	one method: POD = 0.71, FAR = 0.41 for >10 MeV protons; POD = 0.81, FAR = 0.30 for >100 MeV protons	same as above	• role of "seed particle" populations • respective roles of flare and CME shocks/compressions in acceleration • particle acceleration and transport mechanisms • GLE particle acceleration • solar radio and solar wind research gaps	• SEL EUV disk imaging + VIS imaging to >20 $R_\odot$ with 95% duty cycle • H-alpha imaging • SEL SXR Imaging • in situ (P&F): e-, p+, & heavy ion msrts (e-0.1–1 MeV; p+ 0.02–700 MeV) • Type II and III SRB msrts • ground-based neutron msrts for GLEs	• same as above • same as CME ToA • same as solar radio (improve) • off-SEL VIS coronagraph imaging to >20 $R_\odot$ + EUV disk to >1.5 $R_\odot$ imaging • in situ (e-, 0.1–1 MeV, p+ 0.02–1000 MeV, composition up to 100s MeV/n) at distributed locations (L1, upstream-L1, L4, L5; Mars-L1, Earth-Mars space)	• same as above • same as CME ToA (advance) • same as solar radio (advance) • in situ (e-, 0.1–1 MeV, p+ 0.02–1000 MeV, composition up to 100s MeV/n) at 1 AU (±60° at 30° intervals)+radially distributed (0.3–0.9 AU)	• same as above • same as CME ToA (close) • same as solar radio (close) • in situ (e-, 0.1–1 MeV, p+ 0.02–1000 MeV, composition up to 100s MeV/n, at 1 AU and 0.3 AU (±90° at 20° intervals)
	Onset time forecast (>10, >30, >50, >100 MeV p+)	onset time: limited knowledge of forecasting status one method: forecast lead time of about 4 h for >10 MeV protons, 1 h for >100 MeV protons	onset time: desired onset time forecast accuracy should improve current accuracy, with a mean error as low as possible forecast lead time: 30 min for promptly-increasing events and 2 h for gradually-increasing events (decision to deploy and enter a storm shelter and EVA support) for both >10 MeV and >100 MeV protons	same as above	same as above	same as above	same as above	same as above
	Peak intensity forecast (>10, >30, >50, >100 MeV p+)	limited knowledge of forecasting status; one method shows underforecasting by over 1 order of magnitude, another shows overforecasting with most predictions within one order of magnitude	forecast accuracy of one order of magnitude (decision to deploy and enter a storm shelter and EVA support)	same as above	same as above	same as above	same as above	same as above

Phenomenon	Parameter of Value to Models & SWx*-Casting Products	Forecasting Status (If Known)	Forecasting Requirement	Research Gaps	Maintain	Improve	Advance	Close (Actionable Forecasting)
	Intensity profile forecast (>10, >30, >50, >100 MeV p+)	limited knowledge of forecasting status	requirement unknown but under investigation; related to general mission planning, launch support, and decision to leave shelter	same as above	same as above	same as above	same as above	same as above
Solar Wind	ToA and Duration of HSS, SIR/CIR	ToA: 24 h ±6 h duration: <±12 h	0 ±2 h (for actionable electric grid measures)	intra-stream structure (lon/lat) inputs to inner heliospheric models (global field coverage, coronal models)	• B_{phot} >50% of surface • SEL in situ P&F • SEL EUV img	• B_{phot} >50% of surface (east limb preferred) • off-SEL in situ P&F (<30° east of SEL preferred)	• off-ecliptic B_{phot} including poles • off-SEL high SNR VIS imaging >120 $R_{\odot}$ (L4 preferred)	• distributed P&F in situ msrts (east to SEL) • off-SEL EUV disk msrts • continuous 4π full-disk Doppler magnetograph
	Plasma and Magnetic Properties of HSS, SIR/CIR	mag. field strength: MSE ±30% mag. field orientation: poor density: MSE ±80% speed: MAE 80 km/s	undefined	• same as above • radial evolution • off-ecliptic compression effects on B_z	same as above	same as above	same as above	same as above
Long-Term SWx and Space Climate	Active Region Emergence and Evolution	farside detection is in research stage but promising for SWx; AR emergence in early research stage	no specific requirement exists; AR emergence forecast would increase irradiance (7+days) and eruption (24 h+) forecast horizons	- no farside B or imaging meas. - only single-point time-distance helioseismology	SEL vector B_{phot} + Doppler	B_{phot} + Doppler >50% of surface	B_{phot} + Doppler >67% of surface	4π B_{phot} + Doppler coverage
	AR Solar Cycle Properties	only rough global properties; AR lat vs time, waiting time distribution, mag. flux, tilt	desired: • extend solar-cycle predictive capability • use to infer SWx probability	- farside AR info - AR evolution beyond 13 days passage - long-term synoptic studies	same as above	same as above	same as above	same as above

Phenomenon	Parameter of Value to Models & SWx*-Casting Products	Forecasting Status (If Known)	Forecasting Requirement	Research Gaps	Maintain	Improve	Advance	Close (Actionable Forecasting)
	High-Latitude Flows-MC, DR, and CF	rates changes with depth, latitude, and solar cycle MC: poleward, peaks at ± ~20 m/s at ~45° DR: relative velocity ~200–250 m/s CF: spectrum of spatial, temporal, and velocity scales	desired: • MF: accuracy within ~1 m/s at ~45°, throughout the convection zone • DR: accuracy within ~10 m/s at ~45° throughout the convection zone • CF: agreement at low wave number (largest spatial scales)	High-Latitude Observations (MC, DC,CF) Depth Dependence	same as above	high-latitude (>60°) B_{phot} + Doppler (for at least 3 CR)	high-latitude (>60°) B_{phot} + Doppler (multiple CRs at different solar-cycle phases)	same as above
	Polar Fields	predictor of amplitude of next cycle able to predict ~3 years in advance	desired: • extend prediction window • need to know if this is fundamentally limited by stochastic processes	High-Latitude Observations	same as above	same as above	same as above	same as above

Legend			
existing NASA capability (short-term) critical gap existing NASA or NOAA capability (long-term) novel measurement (new tech, next-gen)	**B_{chrom}**–chromospheric mag. field	**ECOR**–wide-field EUV	**SPCTR**–spectroscopy
	B_{phot}–photospheric mag. field	**EUV**–EUV imaging	**SSI**–spectral solar irradiance; **SPCTR**–spectroscopy
	CORHI–coron/helio imaging 1->80 $R_{\odot}$	**HXR SPCTR**–hard X-ray imaging spectroscopy	**SXI**–soft X-ray imaging
	d_up_P&F–distributed in situ	**m_DpI**–multipoint helioseismology	**SXR-NUV BoI**–SXR-NUV bolometric imaging
	dcR–decametric radio spectra	**m_up_P&F**–multipoint (grid) in situ	**vBp**–vector phot. mag

5.1.1 Coronal Mass Ejections (CMEs)

5.1.1.1. "All Clear"

"All Clear" is a widely used parameter in forecasting. In operational settings, 'All Clear' signifies that the forecast of some threshold of interest (i.e., intensity, particle fluence, etc.) will not be crossed or is not exceeded currently. In the CME case, here, 'All Clear' signifies the likelihood of a CME occurrence directed toward a specific location (i.e., Earth, Mars).

Measurement Method: The occurrence of a CME is determined by its detection, as a bright, transient feature propagating away from the Sun, in visible (VIS) light coronagraph images. Other phenomena, such as waves or dimmings in visible, EUV or X-ray coronal images, sometimes occur in conjunction with CMEs and are used as indicators of their location and importance. Features that are observed to propagate beyond 10–15 $R_{\odot}$ are of most SWx relevance (Vourlidas et al, 2010; 2020). CMEs arrive at Earth (or, more generally, at 1 AU) within 3 days, on average, but those that cause the greatest SWx impacts are on the extreme end of the CME velocity distribution. Typical CME speeds are ~400 km/s, but a few are observed traveling outward at over 2000 km/s. The fastest Sun-to-1 AU crossing for SC24 was the event of July 23, 2012, which arrived at the STEREO-A spacecraft within 18 h (Baker et al., 2013). This crossing time is almost identical to the estimated 17 h 40 min crossing time of the Carrington event of 1859 (Green & Boardsen, 2006), which is regarded as the most extreme solar eruption in recorded history so far. We adopt, therefore, 18 h as the minimum crossing time for CMEs.

Forecasting Status: We cannot presently predict the occurrence of an eruption so a CME "all clear" can only be derived via (1) direct VIS coronagraph observations ("has a CME occurred?"); (2) a sequence of such observations (at least two) to roughly assess the CME direction ("is this a halo/partial-halo CME or not?") and speed (for ToA projections); and sometimes, (3) solar disk imaging in EUV ("is there a CME-associated dimming on the Earth-facing disk?").

The forecasting status is determined by the detection rate of CMEs and the minimum warning time. Namely, **97% of all CMEs**, and **100% of fast (>500 km/s) and/or wide (>30°) CMEs** can be detected by current spaceborne instruments (Vourlidas et al., 2020) because VIS and EUV solar observations are available around the clock by LASCO and SDO/AIA. The warning time is >**16 h to 2–3 days** because it takes 1–2 h to detect and assess the morphology of a CME within the coronagraph field of view (FOV).

Forecasting Requirement*:* No official requirement exists so we define one here: *All user-directed CMEs must be detected within 2 h of eruption*. The requirement is met for all fast/wide CMEs and for 97% of all CMEs.

Measurement Gap: CMEs are missed for three reasons: (1) "stealth" CMEs (Robbrecht et al., 2009), without easily detectable coronal or solar disk signatures, (2) overlapping events during periods of high activity, and (3) low observing duty cycle.

Required Measurements (maintain current status):

- **SEL EUV disk imaging + VIS coronagraph imaging to >20 $R_{\odot}$ with >95% duty cycle**. This maintains the current capability offered by LASCO + AIA. By 2025, it will be available

operationally by NOAA through SWFO + GOES/SUVI. These measurements are insufficient if an "all clear" capability is required for other places in the heliosphere besides the Earth location (see next paragraph).

Required Measurements (forecasting improvement):

- **Off-SEL VIS coronagraph imaging to > 20 $R_\odot$ + EUV disk to 1.5 $R_\odot$ imaging with 95% duty cycle.** EUV imaging provides constraints on propagation direction, width, and shock history. When combined with SEL capability, it improves detection of stealth CMEs and discrimination of overlapping events. Optimal location is **quadrature with Earth or L1**, for Earth-based '"all clear." It satisfies partially the requirement for other heliospheric locations and is therefore the threshold requirement for Mars exploration activities.

Required Measurements (forecasting advancement):

- **Two-view (90°) off-SEL VIS coronagraph imaging >20 $R_\odot$ + EUV disk to 1.5 $R_\odot$ imaging with 95% duty cycle.** This measurement set meets the "all clear" requirement for Earth, without the need of an SEL coronagraph measurement, and partially fulfills the requirement for other heliospheric locations if SEL coronagraph measurements are available. The off-SEL EUV imaging provides strong constraints on propagation direction, width, and shock history. It is therefore the baseline requirement for Mars exploration activities

Required Measurements (likely closure):

- **Three-view (120° apart) VIS coronagraph imaging >20 $R_\odot$ + EUV disk to 1.5 $R_\odot$ imaging with 95% duty cycle.** This measurement set ensures 100% detection of every CME, irrespective of solar activity levels or event speed. EUV imaging provides strong constraints on propagation direction, width, and shock history.
- **Off-ecliptic (>60°) VIS imaging to >0.3 AU with 95% duty cycle.** The measurement provides direct assessment of CME direction and ecliptic width and an estimate of the Earth (or other target) component speed. These quantities cannot be estimated reliably from the ecliptic-based measurement described above. This measurement will thus provide a transformative improvement to the "all clear" accuracy. When combined with SEL coronagraph imaging, it should result in closure.
- **Measurement of coronal currents in ARs.** None of the above measurements contribute to eruption prediction. For this, we need measurements of the existence, properties and evolution of currents of the AR corona (since ARs are the sources of the most SWx-relevant eruptions). See Section 5.3.1 for specific discussion. This measurement, if achievable, will provide the most robust improvement for "all clear" forecasts while enabling transformative research into eruption prediction (e.g., Patsourakos et al., 2020).

5.1.1.2. Hit/Miss

We define this parameter as the forecast of a CME impacting Earth or another location of interest in the heliosphere. It is a binary forecast (yes/no). It is also closely related to the event ToA, discussed in the next section.

Measurement Method: Once a CME has been detected in the coronagraph FOV, forecasting on whether the CME will impact Earth is performed via the following process: (1) is the source region close to SEL? (source region location from EUV or soft X-ray [SXR] images); (2) is the CME a halo/partial-halo? (VIS coronagraph images from the SEL); (3) if the CME is partial-halo, does the flank cross the SEL? (sequence of VIS coronagraph images from the SEL). To be useful for SWx, this methodology requires imaging information from both coronagraphs and solar disk imagers, if the measurements are made from the SEL (or Sun-target line, more generally). It also requires assumptions about the ejecta properties (size, shape, internal pressure and magnetic field orientation), evolution, and propagation through the ambient medium.

Forecasting Status: Although the procedure is straightforward, the hit/miss accuracy is only ~80% (e.g., Vourlidas et al., 2019). The number includes statistics from various heliospheric locations. The error is driven by both false positives (forecasted hit did not occur) and false negatives (forecasted miss but hit occurred). However, NOAA has a different requirement (see Forecasting Requirement below) for which the current status is 53.3%

Forecasting Requirement: The operational requirement is defined only for Earth-directed CMEs as the prediction of a G1+-level storm, at least 24 h in advance, 59% of the time. There are no official requirements for other locations in the heliosphere, where human exploration or sensitive spacecraft operations are taking place. We adopt, therefore, the 24h+ prediction of a CME hit at a given Heliospheric target (i.e., Earth, Mars) as the forecasting requirement.

Measurement Gaps: Accurate hit/miss forecasting requires knowledge of the CME direction angular (ecliptic) width and speed to provide an accurate ToA (0, in the case of miss). The errors arise from three issues:

1. CME propagation after it leaves the coronagraph FOV (after 20–30 $R_{\odot}$ or so) is not well understood. CMEs can undergo expansion, deflections, and rotation, and they can interact with other CMEs or solar wind structures (Manchester et al., 2017). We cannot yet reliably predict CME IP propagation.
2. The halo appearance of a CME, so key to observing Earth-directed events, is not well understood. It has been interpreted in a number of ways (Rollett et al., 2016; Millward et al., 2013), and may reflect the extent of the CME-driven shock rather than the width of the CME itself (Kwon et al., 2015). Since shocks can dissipate, particularly at locations further from the CME nose, hit/miss assessments based on the halo measurement may lead to false positives. This issue also affects partial-halo events
3. The occurrence of stealth CMEs, without detected coronagraph or Earth-facing disk signatures, remains problematic. Because these CMEs have no obvious low corona (i.e., no flaring, dimming, or filament motions from SXR to radio) or VIS coronagraph signatures (they are very faint when directed toward the observer because they propagate slowly and at large angular distance from the sky plane), they are easily missed leading to false negatives. Although stealth CMEs are usually of less SWx concern themselves because they are typically weak-to-moderate events, they can interact with other CMEs, altering their geo-effective characteristics.

In general, single-viewpoint observations (along SEL, for example) provide very little information on the 3D structure of the CME and its associated shock. Thus, they do not allow for the development of more sophisticated hit/miss forecasts such as a partial hit (hit by the shock/sheath but not the ejecta) or leg hit (hit by the lower-impact flanks of the magnetic ejecta), which could improve the assessment of the SWx-impact level for a given event.

Required Measurements (maintain)

- **SEL EUV disk imaging + VIS coronagraph imaging to >20 $R_\odot$ with > 95% duty cycle + L1 in situ (particles and fields [P&F]).** This maintains the current capability offered by SOHO/LASCO-SDO/AIA-DSCVR-ACE-Wind. By 2025, it will be available operationally by NOAA through SWFO + GOES/SUVI. EUV imaging is preferred to SXR because EUV exhibits more CME-associated signatures, including pre-eruptive structures, such as sigmoids. These measurements are insufficient to provide reliable hit/miss forecasts for other places in the heliosphere.

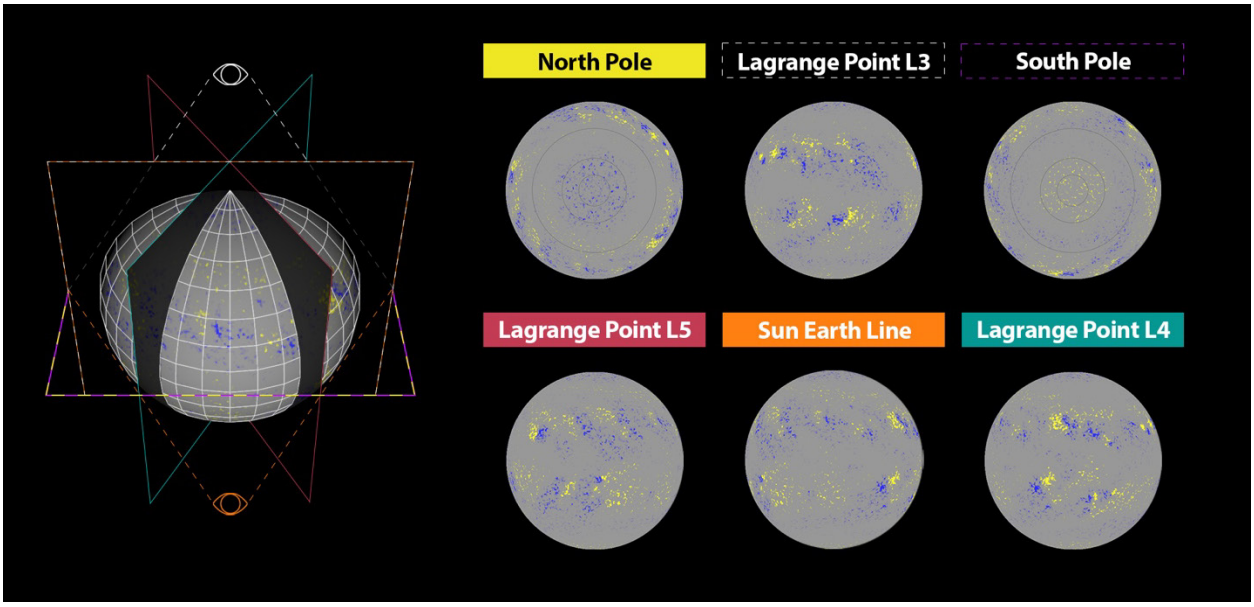

Figure 5-11. Simulated views of the magnetic field distribution on the solar photosphere from different locations within 1 AU, including polar viewpoints.

Required Measurements (improve):

- **Off-SEL VIS imaging to >80 $R_\odot$ + EUV disk to 1.5 $R_\odot$ imaging with 95% duty cycle.** EUV imaging provides constraints on CME propagation direction, width, and shock history. When combined with SEL capability, it improves detection of stealth CMEs and discrimination of overlapping events and enables 3D reconstruction of CME and shock (Thernisien, 2011). Heliospheric imaging of the CME's IP propagation enables limited adjustments to direction and orientation. Optimal locations are **at L4 or L5 (60° away from Earth)** to image low corona evolution over source regions at potential geo-effective heliolongitudes and to bring the trajectory of Earth-directed events close to the heliospheric imager's Thompson surface (Vourlidas

& Howard, 2006) for maximum detectability. This measurement set satisfies partially the requirement for other heliospheric locations and is therefore the threshold requirement for human exploration activities.

- **Line-of-sight (LOS) photospheric field (B_{phot}) measurements over >50% of the solar surface.** All existing heliospheric models use B_{phot} as their main input. Expanding the observation from the current ~⅓ to ½ of the visible solar surface will improve the fidelity of the models. This in turn will lead to more accurate description of the corona and solar wind and the interactions of solar transients with ambient structures. High priority should be given to **B_{phot} measurements over the eastern limb** because these longitudes are the most important for SWx forecasting: (1) magnetic field estimates from synoptic magnetograms are the least dependable for these longitudes and (2) information on flux emergence or AR evolution from these longitudes provides longer lead-time for forecasts.

Required Measurements (advance):

- **In situ P&F measurement sunward of L1**. Any measurement upstream of L1 validates hit/miss forecasts made with imaging and provides forecasting improvement proportional to distance from Earth. An obvious location is **at 0.3 AU upstream of Earth** because it provides hit/miss forecasting of 24 h for a 500 km/s CME/shock. Baseline requirement for cislunar exploration activities.
- **Two-view off-SEL VIS imaging to >80 $R_\odot$ + EUV disk to 1.5 $R_\odot$ imaging with 95% duty cycle.** Optimal locations at **L4 and L5**. In combination with SEL capability, they provide CME direction and ecliptic width via 3D reconstructions for all Earth-directed events, along with detection of stealth CMEs and event overlap disambiguation. It improves understanding of the changes in the corona/heliosphere and in the near-Earth heliosphere before impacting L1. Baseline requirement for cislunar and Mars (when Mars is within 60° of SEL) exploration activities.
- **Off-ecliptic (>60°) VIS imaging to >80 $R_\odot$.** Off-ecliptic imaging is the only way to measure directly the longitudinal extent and deflections in the ecliptic of the CME/shock. When combined with SEL or off-SEL VIS imaging, it further enables 3D reconstruction of CME/shock and can thus lead to the development of sophisticated hit/miss forecasts, as discussed in the measurement gaps paragraph. Baseline requirement for cislunar and Mars exploration activities.

Required Measurements (close):

- **Multipoint in situ P&F measurement >0.1 AU from Earth.** Closely spaced in situ measurement can provide the medium-scale structure of the incoming event which could affect hit/miss forecast for glancing hits. It thus enables sophisticated hit/miss forecast validation and update. The incident angle of disturbed solar wind conditions also affects detailed predictions of geospace responses.
- **Distributed in situ P&F measurements from Earth to 0.3 AU upstream.** This measurement set allows tracking of the incoming event, raising hit/miss forecast accuracy to 100% (with decreasing forecast horizon, however, and depending on the number and location of the measurements).
- **Three-view (120° apart) + off-ecliptic (>60°) VIS imaging to >80 $R_\odot$ + distributed in situ P&F measurements upstream of Earth.** This measurement set enables robust measurement of CME direction, angular ecliptic width, and 3D envelope of both CME and shock/sheath

with near-simultaneous validation of the estimates by the in situ measurements. It drives data assimilation and ensemble modeling of events throughout the inner heliosphere (depending on data latency). It provides the most robust improvement while enabling transformative research into IP propagation of transients.

5.1.1.3. Time of Arrival (ToA)

The ToA of the shock (typically) but could also refer to the magnetic ejecta (within the CME) at Earth (or other locations).

Measurement Method: ToA forecasting is performed via modeling (empirical or physics-based; see Vourlidas et al., 2019, for details). The primary input is the **CME speed** at some height (i.e., at 20 $R_\odot$ for input to heliospheric propagation models or average linear speed, more generally). The speed is derived from linear or second-order fits to height-time measurements of the CME front (usually the fastest point along the CME front) in VIS coronagraph images. The speeds are quantities projected on the sky plane and thus lower limits (on average) of the CME velocity, so the community has developed several approaches for projection corrections. These approaches use the location of **disk activity**, and/or the **CME width** to estimate the speed component toward the observer. The ambient solar wind properties (i.e., speed profile, density) are necessary for some ToA forecast methods and is provided either through physics-based modeling (which in turn requires the **photospheric magnetic field**) or direct measurements from L1 (or from another appropriate location).

Forecasting Status: Currently, the average mean-absolute-error (MAE) of ToA is 9.8 ±2 h (Vourlidas et al., 2019) based on studies which exploit off-SEL VIS imaging. The ToA MAE worsens to >17 h if only SEL VIS observations are used.

Forecasting Requirement: SWx users (GICs) require a MAE of 0 ± 2 h.

Measurement Gaps: Forecasting ToA requires knowledge of the **CME speed** throughout its IP propagation, **CME direction**, **angular ecliptic width and shape**, and the ability to discriminate between the shock and the driver CME. Modeling of the CME/shock propagation requires photospheric magnetic field for accurate representation of the background wind. All of these quantities are inadequately measured. The main gaps are as follows (see Vourlidas et al., 2019, for details):

1. **CME/shock evolution from about 30 $R_\odot$ to 1 AU**. We cannot adequately evaluate the complexities of the IP evolution of solar transients. In situ measurements are very sparse and infrequent (even with Parker Solar Probe, Solar Orbiter, and BepiColombo in operation) and, in any case, measure only a very small region of extended structures. Heliospheric imaging has been routinely deployed only since 2007 from STEREO. The present imagers do not have sufficient spatial resolution or signal-to-noise ratio (SNR) to image the internal structure or separate shock and CME beyond about 50–60 $R_\odot$, depending on the event. LOS integration complicates the measurements, even with two or three viewpoints available, at times
2. **CME size** and **front shape** at 1 AU. CMEs are much larger than the Earth. We do not have a direct measurement of the CME size at impact, but in situ reconstructions and magnetohydrodynamic (MHD) modeling suggest sizes at considerable fractions of 1 AU. Additionally, in-

teractions with ambient structures during the IP propagation can alter the front shape and affect the timing of CME or shock arrival at 1 AU (e.g., Scolini et al., 2018). Obviously, accurate predictions of ToA (and momentum or magnetic field) will require high precision modeling of the 3D shape of the transient that is beyond our current capabilities. Little is known about the intermediate-scale variations within CMEs and shocks (Koval & Szabo, 2010; Lugaz et al., 2018; Ala-Lathi et al., 2020). Understanding the nature and causes of such variations on scales of 0.01–0.2 AU are key for accurate prediction of the CME properties and for improving the modeling of the solar driver inputs to the magnetosphere.

Required Measurements (maintain):

- **SEL EUV disk imaging + off-SEL VIS imaging >30 $R_\odot$.** Combined with the NOAA-provided VIS coronagraphic and in situ P&F measurements at L1 (SWFO), this measurement set replaces the STEREO + LASCO capability that led to the existing ~10 h MAE. Without these two measurements, our ToA MAE will regress to the pre-STEREO levels of 17+ h, which is of the same order as the ToA of the fastest, most SWx-relevant CMEs. **Preferred location for VIS imaging is L4 or L5**. The above assumes that SEL B_{phot} field measurements are available from the ground or space.

Required Measurements (improve):

- **Two-view off-SEL VIS imaging to >80 $R_\odot$.** Optimal locations at **L4 and L5**. In combination with SEL capability, they provide CME direction and width in the ecliptic via 3D reconstructions for all Earth-directed events, along with detection of stealth CMEs and event overlap disambiguation. It improves understanding of the changes in the corona/heliosphere and in the near-Earth heliosphere before impacting L1, particularly with the addition of the B_{phot} measurements below. Baseline requirement for cislunar and Mars (when Mars is within 60° of SEL) exploration activities.
- **LOS B_{phot} measurements over >50% of the solar surface.** All existing heliospheric models use B_{phot} as their main input. Expanding the observation from the current ~⅓ to ½ of the solar surface will improve the fidelity of the models. This in turn will lead to more accurate description of the solar wind and the interactions of solar transients with ambient structures. High priority should be given to **B_{phot} measurements over the eastern limb** because these longitudes are the most important for SWx forecasting: (1) magnetic field estimates from synoptic magnetograms are the least dependable for these longitudes and (2) information on flux emergence or AR evolution from these longitudes provides longer lead-time for forecasts. Baseline requirement for cislunar and Mars (when Mars is within 60° of SEL) exploration activities.
- **Multipoint in situ P&F measurement >0.1 AU from Earth.** Closely spaced in situ measurements can provide the shape, medium-scale structure, and speed of incoming events several hours before L1 arrival and thus reduce ToA error (albeit at the expense of forecasting horizon). The optimum location to reach the forecasting requirement of a MAE of 0 ± 2 h of ToA is an area where further research is needed. A distance of >0.1 AU from Earth is necessary to obtain a 2-h advanced warning even for the fastest CMEs.

Required Measurements (definitive):

- **LOS B_{phot} fields for >67% of the solar surface.** To further improve the fidelity of the main inputs to heliospheric solar wind and CME propagation models. **Preferred locations are L4 and L5,** since these longitudes are the most responsible for the solar wind reaching Earth. It may be suboptimal for Mars-directed solar wind, when Mars is >60° away from Earth.
- **Two-view VIS imaging + upstream in situ + B_{phot} >67% of solar surface.** The measurement set leads to definitive improvement to heliospheric models, CME speeds, sizes, and interaction, and enables upstream validation and updates of the forecasts (Kay et al., 2020).
- **Distributed in situ P&F measurements from Earth to 0.3 AU upstream.** This measurement set allows tracking of the incoming event as it approaches L1, providing validation (and enabling data assimilation) to model forecasts (albeit with decreasing forecast horizon). Final accuracy depends on the number and location of the measurements).

Required Measurements (close):

- **Three-view (120° apart) + off-ecliptic (>60°) VIS imaging to >80 $R_{\odot}$ + distributed in situ P&F measurements upstream of Earth + LOS B_{phot} for >100% of solar surface.** This measurement set enables robust measurement of CME direction, angular ecliptic width, and 3D envelope of both CME and shock/sheath with near-simultaneous validation of the estimates by the in situ measurements. It drives data-assimilation and ensemble modeling of events throughout the inner heliosphere (depending on data latency). Off-ecliptic viewpoints directly image CME deflection and distortion in the ecliptic and measure CME ecliptic widths/shapes with minimum assumptions. Measurement of the magnetic field over the full photosphere increases the fidelity of MHD modeling of the background solar wind and hence improves the modeling of CME propagation through the inner heliosphere.

5.1.1.4. Speed on Arrival (SoA)

The SoA of a CME, is typically measured at the shock or in the sheath region but could also refer to the magnetic ejecta, at Earth (or other location). It is an important parameter used in the calculation of the coupling with the magnetosphere and for momentum/dynamic pressure evaluation.

Measurement Method: The SoA is derived with the same methodology as the ToA. See previous section.

Forecasting Status: There have been few statistical studies of the SoA MAE performance (see Table 1 in Vourlidas et al., 2019). The performance varies with event sample and forecasting methodology, but errors tend to be well above 30% of the actual velocity at arrival (e.g., Colaninno et al., 2013). We are currently unable to forecast SoA.

Forecasting Requirement: The NOAA requirement for the measurement accuracy of solar wind speed at L1 is 10%. Although this is not a forecast requirement, it expresses the level of accuracy that operational models may need. So, we adopt it as a forecast requirement here.

Measurement Gaps: The gaps for SoA are identical to the ToA gaps, discussed above.

Required Measurements (maintain):

- The required measurements are identical to the ToA ones, discussed above.

Required Measurements (improve):

- The required measurements are identical to the ToA ones, discussed above.

Required Measurements (definitive):

- The required measurements are identical to the ToA ones, discussed above.

Required Measurements (close):

- The required measurements are identical to the ToA ones, discussed above.

5.1.1.5. Mass Density

The CME mass density, ρ, although it is seldom discussed in the SWx context, is required for both momentum (ρv) and ram/dynamic pressure (ρv^2) estimates, which are key parameters in determining the geo-effectiveness of a CME impact.

Measurement Method: The CME **mass** is rather routinely derived in the coronagraph FOV using well-established techniques (Vourlidas et al, 2010) for the methodology and statistics on mass density). Reliable masses can generally be extracted only out to about 20–30 $R_\odot$. The **density** along the SEL can also be extracted from the measurements, but this approach is rarely used to forecast the mass flux at 1 AU directly (e.g., Savani et al., 2013, is the only attempt we are aware of). Instead, the magnetospheric response is modeled based on the output of heliospheric propagation models, which use the CME size and total mass (nominally at 20 $R_\odot$) as inputs.

Forecasting Status: Heliospheric magnetohydrodynamic models, such as ENLIL, typically produce 2–3 times higher densities in CME sheaths than are measured in situ (Mays et al., 2015). The reason is that the higher density is required to drive the CME simulation. Other MHD simulations with more self-consistent treatments of CMEs are under development but are only in the research rather than forecast model stage.

Forecasting Requirement: There is no forecasting requirement on CME density, momentum or ram pressure. The time series of these quantities are also important as their spatiotemporal variability and resulting modulation of the magnetospheric compression determine geospace SWx hazards such as GICs.

Measurement Gaps: Since the momentum and ram pressure are primarily magnetospheric drivers, only their terrestrial impact from CMEs is relevant for the present analysis. Therefore—with the exception of future Mars space weather forecasting needs—we are interested only in the CME/CIR component along the SEL. The measurement gaps that prevent reliable forecasting of this component are:

1. **The small-scale mass structure of the CME front**. Current coronagraphs can resolve arcmin scale density structures with signal-to-background ratio of >2 (Savani et al., 2013; Kwon & Vourlidas, 2018) up to 10–20 $R_\odot$. This includes the shock sheath for fast CMEs. However, it is exceedingly difficult to resolve the front structure beyond 20 $R_\odot$ because it becomes fainter and broader as it expands. CME fronts can be tracked beyond 30 $R_\odot$, sometimes all the way to 1 AU, but heliospheric imaging requires long integrations with larger pixels so the fine scale information is lost. Another contributing factor is the longer LOS through the structure with increasing elongation. Currently, there is no ability to resolve SIR or CIR fronts (only visible beyond 0.3 AU).
2. **IP evolution of the CME front**. Although some CME fronts can be tracked beyond 30 $R_\odot$, their mass is difficult to calculate. The method requires the subtraction of a suitable pre-event image to allow the measurement of the excess mass due to the CME. But the long integrations and large FOVs of heliospheric imagers require the use of pre-event images taken at significantly earlier times. In that case, the subtraction leaves many artifacts due to the rotation of coronal structures. Therefore, the mass estimation requires assumptions about the CME shape and its evolution. Although heliospheric propagation models and in situ measurements at 1 AU indicate plasma pileup ahead of the CME, we are unable to validate the models or examine how the CME front interacts with the ambient plasma. These issues affect our understanding (and thus forecasting) of other SWx-relevant components, such as ToA, SoA, and magnetic structure, as we discuss later.

The presence of dense, often trailing filament material and/or compression at the rear of CMEs by a following high speed stream (HSS) is also a consideration, apart from the "front" issues described here. These can significantly alter the course and geoeffectiveness (indirectly, by the compression of the CME magnetic field) of some events late in the CME passage.

Required Measurements (maintain):

- **Off-SEL VIS imaging >20 $R_\odot$.** By definition, the measurement of CME mass to forecast momentum or ram pressure at Earth must be made from outside the SEL. Optimal location is **in quadrature with Earth,** so that the structure of interest is imaged with maximum sensitivity as it lies close to the Thompson surface.

Required Measurements (improve):

- **Off-SEL VIS imaging >80 $R_\odot$ with high SNR**. To make progress, we need imaging of the initial stages of the CME IP propagation, and the formation of SIRs, with spatial resolution and exposure times comparable to coronagraphic imaging (i.e., <1 min exposure, 30 arcs resolution). Optimal location is **in quadrature with Earth.** Such measurements will allow tracking the fine-scale structure of the front further into the heliosphere, data assimilation and validation of heliospheric models, at least in the early phase of IP propagation when pileup and other interactions are more likely. These capabilities will work best for primarily bright and hence more SWx-relevant events.
- **LOS photospheric field (B_{phot}) measurements over >50% of the solar surface.** All existing heliospheric models use B_{phot} as their main input. Expanding the observation from the current ~⅓ to ½ of the Earth-facing solar surface will improve the fidelity of the models. This in turn

will lead to more accurate description of the solar wind and the interactions of solar transients with ambient structures. High priority should be given to **B_{phot} measurements over the eastern limb**, because these longitudes are the most important for SWx forecasting: (1) magnetic field estimates from synoptic magnetograms are the least dependable for these longitudes and (2) information on flux emergence or AR evolution from these longitudes provides longer lead time for forecasts.

Required Measurements (definitive):

- **Two-view Off-SEL VIS imaging >80 $R_\odot$ with high SNR.** Optimal locations are the L4 and L5 Lagrange points because slight brightness variations in the Earth-directed component of the front seen from the two vantage points provide information to mitigate to some extent LOS effects.
- **LOS B_{phot} fields for >67% of the solar surface.** To further improve the fidelity of the main inputs to heliospheric solar wind and CME propagation models. **Preferred locations are L4 and L5,** since these longitudes are the most responsible for the solar wind reaching Earth. It may be suboptimal for Mars-directed solar wind, when Mars is >60° away from Earth.
- **Distributed in situ P&F measurements from Earth to 0.3 AU upstream.** This measurement set allows tracking of the incoming event as it approaches L1, providing validation (and enabling data assimilation) to model forecasts (albeit with decreasing forecast horizon). Final accuracy depends on the number and location of the measurements).

Required Measurements (close):

- **Off-ecliptic (> 60°) VIS imaging to > 80 $R_\odot$ + distributed in situ P&F measurements upstream of Earth.** This measurement set enables robust measurement of CME direction, angular ecliptic width, and density profile along both CME and shock/sheath. It drives data assimilation and ensemble modeling of events throughout the inner heliosphere (depending on data latency).

5.1.1.6. Impact Duration

The duration of the CME/shock interaction with Earth (or other target) is an input parameter to forecasting D_{st} and assessing the IP magnetic flux transferred into the magnetosphere (along with the time profile of the southward magnetic field component, discussed in Section 5.1.1.7). Impact duration, Δt, is determined by a combination of the CME/sheath size and speed, along the Sun-observer vector.

Measurement Method: The CME shape, as observed in coronagraph images, is fitted with an appropriate model (i.e., a cone is a common choice for single-view observations, ellipses or the Graduated Cylindrical Shell model are employed in multi-view observations). Assuming a self-similar expansion, the model is propagated to 1 AU and the SEL vector is derived.

Forecasting Status: A recent study of 31 Earth-directed CMEs using the above methodology (Wood et al., 2017) found a discrepancy to a factor of three between predicted (average 54.8 h) and measured (average 18.5 h) durations.

Forecasting Requirement: No requirement is levied directly on Δt, but it is used in several models (mostly to forecast geomagnetic indices, such as D_{st} or K_p) that depend on the duration of the high dynamic pressure sheath and overall magnetic character of the CME (especially the duration of southward B), which we will discuss in the next section. The duration has a relatively weak effect on D_{st} ($\propto \Delta t^{\sim 0.3}$, Wang et al., 2003) but is nevertheless important for improved forecasts. The duration of the shock sheath and overall duration of the impact are also useful for forecasting sudden storm commencements and long-term K_p levels, respectively.

Measurement Gaps: Capturing the CME boundaries accurately, resolving (and understanding) the CME substructure (from the shock, through the sheath, magnetic flux rope (MFR), and trailing plasma structure), and deriving the CME ecliptic direction are essential components for forecasting the impact duration. There are significant gaps in all three components:

1. **Low-resolution imaging of CME in IP**. The only information on the global morphology of CMEs comes from heliospheric imaging observations. As we discussed in Section 5.1.1.5, these observations suffer from low spatial resolution which is aggravated by motion smearing due to the long exposures. For many events, it becomes difficult to delineate their outline beyond 90 $R_\odot$, let alone separate the contribution from the sheath or internal structures. We resort to 3D reconstructions of the CME within the coronagraph or, at best, the inner FOV of a heliospheric imager, which are then propagated self-similarly to 1 AU (with the discrepancies noted above).
2. **LOS integration.** The long LOSs are inevitable for imaging at large elongations. Structure overlap and Thompson scattering effects reduce our ability to resolve fine-scale magnetic structures within the CME, such as MFRs. The mitigation of this effect by shorter LOS is demonstrated by the close-by observations of CME flux ropes by WISPR (e.g., Rouillard et al., 2020).
3. **No in situ measurements upstream of L1.** Although the operations of Parker Solar Probe and Solar Orbiter in the inner heliosphere provide such measurements, neither of the two missions is capable of low latency or sustained observations along the SEL. The serendipitous CMEs detections by multiple spacecraft will be useful for research, but it is unclear whether they could contribute to the improvement of forecasting methods.

Required Measurements (maintain):

- Given the absence of quantified forecasting requirements, the minimum measurement necessary for a rudimentary constraint/model of CME size is the same as for hit/miss. Namely, **SEL EUV disk imaging + VIS coronagraph imaging to >20 $R_\odot$ with > 95% duty cycle + L1 in situ (P&F).** This maintains the current capability offered by LASCO-AIA-DSCVR-ACE. By 2025, it will be available operationally by NOAA through SWFO + GOES/SUVI (not SWxSA priority). EUV imaging is preferred to SXR because EUV exhibits more CME-associated signatures, including pre-eruptive structures, such as sigmoids. These measurements could be used to provide rudimentary duration forecasts for other places in the heliosphere.

Required Measurements (improve):

- **Off-SEL VIS imaging >80 $R_\odot$ with high SNR**. It is essential to reconstruct the CME envelope as far in the inner heliosphere as possible to provide reliable initial input to heliospheric

propagation models and data assimilation and validation capability as the CME evolves. Imaging requires spatial resolution and exposure times comparable to coronagraphic imaging (i.e., <1 min exposure, 30 arcs resolution). Optimal location is **in quadrature with Earth. It assumes SEL VIS and EUV imaging.** This capability will work best for primarily bright and hence more SWx-relevant events.

- **Off-SEL EUV imaging of the Earth-facing disk**. In combination with the off-SEL VIS imaging above and SEL VIS/EUV imaging, this measurement will allow 3D reconstruction of CIRs (as in Wood et al., 2010) and will further constrain the size of Earth-bound CMEs.

Required Measurements (definitive):

- Off-SEL VIS imaging >80 $R_{\odot}$ with high SNR + off-SEL EUV imaging of the Earth-facing disk + distributed in situ P&F upstream of L1. Combining this measurement set with similar measurements from SEL allows improved 3D reconstruction of the CME volume, possibly of CME substructures (e.g., sheath, flux rope) with validation and updated from the in situ measurements closer to 1 AU. Optimal location is in quadrature with Earth for VIS and L4/L5 for EUV.

Required Measurements (close):

- **Multipoint in situ P&F measurement >0.1 AU from Earth.** Closely spaced P&F measurements will uncover both the medium-scale structure of the incoming CME/shock and measure its duration directly. This approach should provide closure to Δt prediction, albeit for a short-term forecast horizon of several hours.
- **Two-view off-SEL + off-ecliptic (>60°) VIS imaging >80 $R_{\odot}$ with high SNR.** The combination of a third out-of-the-ecliptic viewpoint with two off-SEL viewpoints will enable robust 3D reconstructions of the CME and its substructures and is required to achieve closure to Δt forecasting for long-term horizons of days.

5.1.1.7. Magnetic Field (B_s)

The magnetic field geometry and strength of the incoming CME shock are the most important physical parameters for assessing the driver's SWx impact. In particular, the duration and magnitude of the southward (relative to Earth's dipole) component, B_s, determines the amount of magnetic reconnection driven magnetospheric convection and hence the amount of energy transferred to the magnetosphere from the transient. These effects are relevant to planetary magnetospheres only. However, the magnetic content of the CME or shock plays a role in producing and trapping energetic particles and as such is relevant to human space exploration activities.

Measurement Method: The magnetic field content of solar transients can be measured only by in situ spacecraft, almost exclusively from 1 AU. No remote sensing capability exists today to obtain directly the entrained magnetic field. Close to the Sun, estimates can be extracted from radio observations (Vourlidas et al., 2020 and references therein) or off-limb spectropolarimetry (e.g., Ko et al., 2016, and references therein). Further into the heliosphere, Faraday rotation remains the only method for magnetic field estimation (e.g., Jensen & Russell, 2008). Unfortunately, none of these measurements are available on a routine basis. Hence, all methods that attempt to forecast the magnetic field properties of CMEs rely either on empirical methods, based on proxies, such as reconnection flux in flare ribbons, the size of the dimming, coronal magnetic field extrapolations,

and 3D reconstructions of the CME (see Section 5 in Vourlidas et al., 2019 for details). The other approach is to use a combination of the observations above to construct a model of the CME at 20 $R_\odot$ and input that to heliospheric propagation models, such as EUFHORIA (Pomoell & Poedts, 2018) or SUSANOO-CME (Shiota & Kataoka, 2016). As it can be surmised by the large number of indirect observations and assumptions involved, forecasting of the CME structure at 1 AU is still in its infancy and generally unreliable.

The situation is similar for forecasting shock sheath magnetic structure. The magnetic profile is the result of the IMF draping around the CME, which simplifies its structure to 2D planar sheets. However, this structure is subject to reconnection both with the ambient IMF and within the sheath itself, which is extremely difficult to model, especially as it includes swept-up solar wind with its own complex B variations that cannot be predicted in a model.

Forecasting Status*:* Currently, in situ measurements at L1 are used to forecast at the B_s at the magnetospheric boundary, but that provides only a short forecast horizon (i.e., 30 min for a 500 km/s transient). The forecast of B_s from heliospheric propagation models is still in a research/exploratory stage, even for operationally deployed models, such as ENLIL or SUSANOO-CME.

Forecasting Requirement: The B_s strength needs to be forecasted 24 h in advance to be actionable. There is no specific requirement on the orientation or equivalently, the time series profile of B_s, but a 2- to 3-h forecast requirement flows from the 2-h requirement for GIC users.

Measurement Gaps: The quantification of the magnetic properties of solar transients is the most challenging, and likely most important, subject in SWx research and forecasting. Since all SWx-relevant solar activity is magnetic in origin, progress on this subject impacts a wide range of SWx issues, from long-term prediction to particle acceleration to energy input in the magnetosphere to radio blackouts. Here, we discuss only the most relevant gaps for improving the forecast of the magnetic properties of CMEs at the magnetospheric boundary or at another location in the inner heliosphere (see more discussion in Vourlidas et al., 2019).

1. **Unknown magnetic properties of the CME during its formation**. CME formation is a subject of intense research. The magnetic properties (magnitude, topology, helicity) of the ejected structure cannot be measured directly via remote methods in a comprehensive fashion, as discussed above. Radio or EUV off-limb imaging and spectroscopy provide occasional estimates for parts of the problem (e.g., magnetic field magnitude).
2. **The sub-Alfvénic corona properties (nominally below 20 $R_\odot$) are poorly measured.** This is the region where the solar wind heats and accelerates and where the lack of coronal density, temperature, and magnetic field measurements greatly reduces the reliability of MHD modeling in the region. This is also the region where the initial evolution of CMEs and their shocks occurs and where many of their physical properties are established (e.g., Vourlidas et al., 2013). We have a weak handle on how the ambient field responds to the generation of the shock and the propagating CME, how the CME magnetic energy transforms into heat and kinetic energy, and how (and when) the magnetic connection to the source region is severed.

3. **The CME evolution to 1 AU is uncertain**. This is the same problem that affects the ToA, SoA, hit/miss, and density forecasting. The B_s-specific issues are the evolution of the magnetic structure (rotation, compression, deflection), including erosion from reconnection with ambient fields (see Section 7.2 in Manchester et al., 2017), and the evolution of the sheath. These processes affect both the magnitude and geometry of the CME magnetic field at 1 AU (Nieves-Chinchilla et al., 2018). Again, we have no means to probe the actual magnetic structure of the interplanetary CME/sheath/CIR remotely. We can only infer it from observations of the density structure, which are uncertain as discussed in Vourlidas et al. (2019). Some progress regarding the magnetic content of the CME ejecta might be possible in the near future (e.g., Möstl et al., 2018; Palmerio et al., 2017; Jin et al., 2017), but the forecasting of the magnetic field strength and orientation inside CME sheaths is not yet captured by current numerical models. CME sheaths may result in moderate to intense geomagnetic storms, independently of the magnetic field content of the ejecta (Kilpua et al., 2017). Additionally, a significant proportion of extreme events are associated with the interaction of successive CMEs and the timing of the interaction is critical in the enhancement of the magnetic field, for example in the compression of the southward magnetic field inside a CME ejecta by an overtaking IP shock (Lugaz et al., 2017).

Required Measurements (maintain):

- **SEL EUV disk imaging + VIS coronagraph imaging to >20 $R_\odot$ with > 95% duty cycle + L1 in situ (P&F).** This maintains the current capability offered by LASCO-AIA-DSCVR-ACE. By 2025, it will be available operationally by NOAA through SWFO + GOES/SUVI. EUV images the extent of region participating in the eruption (i.e., through dimmings) and possibly an estimate of pre-eruptive magnetic topology (i.e., through analysis of sigmoids seen in hot channels). As we discussed, this measurement set is insufficient for actionable forecasting of the magnetic structure of fast CMEs.
- **SEL vector B_{phot} measurements**. These are currently provided by SDO/HMI 24×7 and by ground-based observatories. The magnetic field measurements are needed to extrapolate the coronal fields within the source regions and to initialize heliospheric propagations models.
- **SEL imaging of hot plasmas (~10 MK).** Imaging of coronal plasma at ~10 MK is a robust method to identify sigmoidal structures in ARs. These structures are considered as the loci of intense currents in the corona and may mark, therefore, the flaring sites (see Section 5.1.2), and by extension the MFR at the core of the eventual CME (Green et al., 2018). Nevertheless, these measurements do not provide a direct measurement of the magnetic field. They are provided by EUV imaging in hot channels, such as 94 Å or 131 Å.

Required Measurements (improve):

- **Two-view stereoscopic EUV imaging of source region**. Stereoscopic reconstructions of coronal loop systems, before and after an eruption, in combination with B-field extrapolations, will constrain the amount of ejected magnetic flux. They will help decipher the pre-eruptive topology (Patsourakos et al., 2020) leading to further constraints on the B-field strength and topology (Patsourakos & Geogoulis 2017) and possibly on the timing/conditions for an eruption. Such a measurement was advocated in the COSPAR SWx Roadmap (Schrijver et al., 2015) as well. Optimal **angular separation of 5°–15°** and **continuous viewing** of the Earth-facing solar hemisphere.

- **SEL vector B_{phot} + B_{chrom} measurements in ARs.** Increasing the height coverage of vector magnetic field measurements will increase the fidelity of the extrapolations and enable a more robust assessment of the pre-eruption magnetic topology and its evolution toward eruption. It will also improve the quantitative estimates of free magnetic energy and helicity in ARs, which will constrain both estimates of the erupted flux and the modeling of the magnetic field configuration (hence improving the 1 AU B_s forecasting). If combined with stereoscopic measurements, this measurement set could lead to a definitive improvement in medium-term forecasting of B_s. This measurement approach bypasses the challenges involved with the direct measurement of the coronal magnetic field due to the much fainter signals of the available magnetically-sensitive lines. It does, however, require some degree of extrapolation to estimate the coronal field. While the committee feels the trade is adequate for SWx improvement, a quantitive assessment of the SWx value of direct coronal measurements could be pursued through a focused study, such as an Observing System Simulation Experiment (OSSE).
- **Off-limb EUV/NIR spectroscopy <5 $R_\odot$.** Spectroscopic measurements of Doppler shifts and plasma temperatures in the CME or shock provide information on the 3D morphology of the erupting structure, further constraining the magnetic field configuration of the CME/shock within the sub-Alfvénic corona. The measurements will also greatly improve the quantitative characterization of the ambient sub-Alfvénic corona, increasing the fidelity of the coronal models and capturing in detail the initial evolution of the CME and shock within the region where most magnetically driven evolution takes place. Preferred location is **off-SEL** to observe Earth-directed events.
- **LOS B_{phot} measurements over >50% of the solar surface.** All existing heliospheric models use B_{phot} as their main input. Expanding the observation from the current ~⅓ to ½ of the solar surface will improve the fidelity of the models. This in turn will lead to more accurate description of the solar wind and the interactions of solar transients with ambient structures. High priority should be given to **B_{phot} measurements over the eastern limb** because these longitudes are the most important for SWx forecasting: (1) magnetic field estimates from synoptic magnetograms are the least dependable for these longitudes and (2) information on flux emergence or AR evolution from these longitudes provides longer lead time for forecasts. Baseline requirement for cislunar and Mars (when Mars is within 60° of SEL) exploration activities.
- **Off-SEL VIS imaging >80 $R_\odot$ with high SNR.** To make progress, we need imaging of the initial stages of the CME IP propagation, particularly the evolution of the entrained flux rope with exposure times comparable to coronagraphic imaging (i.e., <1 min exposure, 30 arcs resolution). Optimal location is **in quadrature with Earth.** Such measurements will allow: (1) tracking the fine-scale structure of the front and cavity further into the heliosphere, (2) separating effects of pileup and distortion at the front versus the evolution of the entrained magnetic structure, (3) data assimilation and validation of heliospheric models (kinematic and dynamic variables, indirectly for magnetic field) in the early phase of IP propagation when pileup and other interactions are more likely. These capabilities will work best for primarily bright and hence more SWx-relevant events.

Required Measurements (advance):

- **LOS B_{phot} fields for >67% of the solar surface** to further improve the fidelity of the main inputs to heliospheric solar wind and CME propagation models. **Preferred locations are L4**

and L5, to cover the heliolongitudes most relevant for the solar wind reaching Earth. It may be suboptimal for Mars-directed solar wind, when Mars is >60° away from Earth.

- **Multipoint in situ P&F measurement ~0.3 AU from Earth.** Closely spaced P&F measurements (~1°) will measure directly the magnetic properties of incoming CME/shock sheath and uncover their medium-scale structure with about 24 h forecasting horizon (depending on the final orbit). They will increase the fidelity of forecasts, assuming availability of similar in situ measurements from L1.
- **Distributed in situ P&F measurements from Earth to 0.3 AU upstream.** This measurement set allows tracking of the incoming event as it approaches L1, providing validation (and enabling data assimilation) to model forecasts (albeit with decreasing forecast horizon). Final accuracy depends on the number and location of the measurements.
- **Two-view off-SEL VIS imaging >80 $R_\odot$ with high SNR** to follow the 3D evolution of the CME flux rope as far into the heliosphere as possible. Optimal locations are the L4 and L5 Lagrange points to mitigate LOS effects, to some extent.

Required Measurements (close):

- **Multipoint in situ P&F measurement at ~0.3 AU from Earth + distributed in situ P&F measurements from Earth to 0.3 AU upstream.** These measurement sets should provide closure to B_s forecast for CMEs, depending on the deployed number of measurements and their locations. If combined with >67% B_{phot} coverage of the solar surface it may lead to closure on the sheath B_s forecast because of the higher-fidelity modeling of the ambient IMF.

5.1.2 Flares

Solar flares play a double role within the SWx forecasting framework. As a direct SWx driver, they cause radiation effects in the ionosphere–thermosphere–mesosphere system, particularly in the ionosphere. Since these effects propagate at the speed of light (within ~8 min to 1 AU), any related forecasting requires prediction of a flare occurrence. Flares are also often associated with major SWx phenomena, such as CMEs, SRBs, and SEPs, and hence are widely used as "markers" or "proxies" for these phenomena.

Therefore, flare-related SWx quantities fall under two measurement groups: (1) pre-flare measurements used to assess the likelihood of a flare such as magnetic energy buildup, magnetic instabilities, and magnetic reconnection and (2) flare measurements used as proxies to forecast other SWx drivers (i.e., SEP fluence or CME speed).

5.1.2.1. "All Clear"

"All Clear" represents the occurrence (presently) or the low likelihood of occurrence (in the future) of a flare on the solar hemisphere visible by a SWx user (i.e., Earth, Mars).

Measurement Method: Flare onset predictions require pre-event information through observation, modeling, or a combination of both. The most common observations are: (1) photospheric magnetic vector and LOS measurements to assess magnetic complexity in the photosphere and upward Poynting flux; (2) coronal topology through SXR, EUV, and UV imaging to assess magnetic complexity and energy built-up in the corona/chromosphere via detection of null points or sigmoids (in SXR

or EUV) and flux tube configuration and evolution (UV/EUV); (3) Doppler velocity mapping on the photosphere to identify concentrations of emerging flux below the surface via helioseismology.

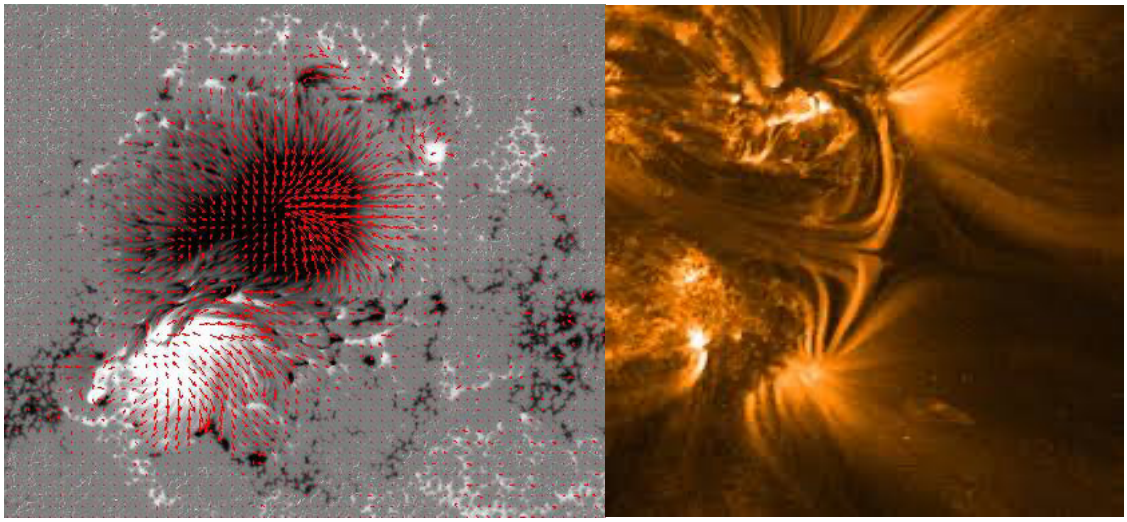

Figure 5-12. Photospheric vector field measurements and a coronal null image in EUV. Left: Photospheric vector field measurements are the main input in flare prediction schemes. The red arrows mark the magnetic field vectors (image credit: National Astronomy Observatory of Japan [NAOJ]/JAXA). Right: a coronal null imaged in EUV 171 Å. Coronal nulls are indicators of possible eruptive topologies (image credit: NASA/LMSAL).

Flare prediction schemes, such as the Flare Likelihood and Region Eruption foreCASTing (FLARECAST; Georgoulis et al., 2021), rely on large databases of flaring activity predictors, mostly from photospheric magnetic field measurements, for the development of their algorithms. So hindcasting is a very important component of these efforts. The European Space Agency (ESA) supported FORSPEF (Papaioannou et al., 2015) and SEPsFLAREs (Garcia-Rigo et al., 2016) systems have combined flare and SEP forecasting capabilities or pre-eruptive and post-eruptive forecasting capabilities. Both systems leverage empirical models to establish flare and SEP predictions.

Forecasting Status: Flare occurrence forecasting is a very active field encompassing models and development of approaches from both research and operational perspectives. However, no approach presently stands out as being more robust than others. Overall, forecasting accuracy stands currently at little above chance (TSS of 0.3–0.4; Leka et al., 2019).

Forecasting Requirement: A 6 h and 24 h forecast of a flare occurrence is required for human space exploration (as an SEP proxy) and HF communications users (as an SRB proxy, and to forecast short-wave fadeouts).

Measurement Gap: While we know that flares occur above polarity inversion (PIL) and are results of heating due to the release of magnetic energy accumulated in the corona, we do not know *when* the energy release will happen. There are several reasons for this:

1. We do not have the means to quantify pre-flare energy accumulation and distribution over the PIL. Thus, we generally have to rely on proxies (e.g., Poynting flux from photospheric magnetograms, presence of sigmoids, coronal magnetic field extrapolations).

2. We do not fully understand energy release via reconnection. Theory and models suggest that small-scale reconnection should be a common occurrence in the corona, yet a flare requires that a significant amount of energy must be accumulated and stored in the corona for hours or days and released within minutes.
3. The release can be initiated by any number of triggers (e.g., photospheric motions, flux emergence, coronal magnetic topology changes, either locally or at distant locations) complicating the search for reliable pre-cursors.

There is solid evidence that flare occurrence is stochastic and hence we should only strive for probabilistic approaches to this problem. The selection of the measurement requirements below was guided by this understanding.

Required Measurements (maintain):

- **SXR irradiance profiles (light curves).** The SXR light curves fulfill the general purpose of nowcasting solar flares, establishing and maintaining flare databases for further research, and providing triggers for non-flare models, including SEP and CME models. SXR emission profiles aid in predictions of SEP properties (e.g., Nunez, 2011) as well as event onset (short-term) predictions (e.g., Balch, 2008, and references therein). This measurement is covered operationally by NOAA through the GOES program until the mid-to-late 2030s, at least.
- **Vector photospheric field (B_{phot}) measurements of Earth-facing disk with >95% duty cycle.** Quantities derived from this dataset (i.e., magnetic flux, helicity, distribution, photospheric motions, location, extent) are used by almost every forecasting model and methodology both operationally and for research. HMI has provided such measurements since 2010. Continuity is necessary to extend the historical databases for nowcasting and algorithmic validations. These measurements could be performed from the ground if an appropriate world-wide network existed.
- **EUV irradiance profiles (light curves).** EUV irradiance profiles provide direct measurement of the EUV background and flare-related increases. They are used as input to mesosphere/thermosphere heating models and consequently for thermospheric drag and collision/avoidance forecasting. Flare-associated depletions in EUV light curves are also used as proxies for CME speed and/or extent before the CME can be measured in visible coronagraph FOVs (generally above 2 $R_{\odot}$). This measurement is covered operationally by NOAA through the GOES program until the mid-to-late 2030s, at least; further discussion is provided in Section 5.1.6.

Required Measurements (improve):

- **SEL imaging of hot plasmas (~ 10 MK).** Because coronal currents result in loop heating, images in lines forming at high temperatures (~10 MK) can capture non-potential AR loops. EUV channels at 94 Å are better suited than the more traditional SXR imaging because of the narrower spectral response and the reduced influence of plasmas at other temperatures. This is particularly true for sigmoids, which are a strong predictor for flares and CMEs (e.g., Green et al., 2018). This measurement is covered by the NOAA/SUVI for the foreseeable future.
- **Multiwavelength narrowband EUV disk imaging.** Plasmas from 0.1 to several million K emit within the EUV spectrum (~100–400 Å, in this case). High sensitivity, sub-arcsec resolution, and simultaneous, imaging within carefully selected bandpasses in the 100–400 Å range

to image plasmas from the upper chromosphere (to observe filamentary loops over polarity inversion lines) to flaring plasmas (to detect sigmoids and pre-existing MFRs, e.g., Nindos et al., 2020). In principle, only an AR-size (3–4 arcmin) FOV is required since the AR PILs are the sources of SWx-relevant flares, but full-disk imagers are preferred operationally since they require less commanding and simplify situations such as what occurred on October 31, 2003, when three regions were producing major flares simultaneously. Faster than 12 s cadence is required to image the formation of MFRs (e.g., Patsourakos et al., 2013).

- **UV/EUV imaging spectropolarimetry** of polarity inversion lines. Their forecasting purpose and use include calculating the polarity inversion and extracted metadata along the line to estimate free energy proxies for solar flares and eruptions. Non-potential energy build-up can also be more readily quantified with imaging spectropolarimetry, as can flux emergence and cancellation.
- **SEL vector B_{phot} + B_{chrom} measurements in ARs.** Increasing the height coverage of vector magnetic field measurements will increase the fidelity of the extrapolations and enable a more robust assessment of the pre-eruption magnetic topology and its evolution toward eruption (e.g., Korsos et al. 2020). It will also improve the quantitative estimates of free magnetic energy and helicity in ARs, which will constrain both estimates of the erupted flux and the modeling of the magnetic field configuration.
- **Off-SEL SXR irradiance profiles.** Expands SXR monitoring of the solar corona, resulting in larger flare property databases for training and validation of forecasting algorithms, and improving coverage of AR flaring history. Preferred location at L5 to monitor ARs rotating toward Earth-facing disk. Preferred bandpasses same as GOES to provide uniformity of measurements.

Required Measurements (advance):

- **Off-SEL EUV imaging + vector B_{phot}.** Extends coverage of AR flaring history and magnetic configuration over ~⅔ of the solar corona. It enables a longer time series of flux emergence and energy build-up across a larger portion of AR lifetime. Preferred location is L5 to provide information for ARs rotating onto the Earth-facing disk. However, L4 is preferable if SEP forecasting takes priority for reasons of human activity in space due to the better magnetic connection of ARs westward of the central meridian. This assumes that a similar set of measurements are available along the SEL. EUV imaging should include a hot line (e.g., 94 Å) for detection of pre-eruptive structure and strong currents within ARs.
- **2× off-SEL EUV imaging + vector B_{phot}.** Provides greater solar surface/corona coverage and thus captures an even longer portion of the AR flaring lifetime. Preferred locations are L5 and L4. This arrangement provides maximum SWx benefit both for human exploration activities and longer-term assessments.

Required Measurements (close):

- **Multi-height vector magnetic field measurements.** Mapping the 3D field through the $\beta = 1$ interface to the upper chromosphere and transition region may suffice to provide robust estimates of coronal currents in ARs (since ARs are the sources of the most SWx-relevant eruptions). SEL measurements are the baseline and required to validate this approach. L4 measurements would be preferable to support lunar exploration, because they would map the currents in magnetically connected ARs. This measurement provides the most robust improvement for "all clear" forecasts while enabling transformative research into eruption prediction.

- **Multi-viewpoint local helioseismology.** Doppler measurements of the solar surface over a wide range of heliolongitudes (e.g., ±60° from SEL) permit probing deeper layers of the convection zone, possibly all the way to the tachocline. This capability will allow studies of flux emergence rate and spatial structures, thus paving the way for long-term prediction of flares and related phenomena.

5.1.2.2. Peak SXR Flux

Measurement Method: The peak flux (or equivalently, GOES flare class) is obtained directly from SXR flux measurements. The GOES class is defined by the maximum flux measured in the 1–8 Å band by the GOES spectrometer. Flux measurements can also be obtained from the SDO/EVE spectrometer or derived by integrating spatially resolved SXR emission in images (e.g., from Hinode/XRT). The rise phase of a flare can be used to forecast the peak flux, but since this occurs within a few minutes (generally <10 min), the method is useful for nowcasting only.

Most, if not all, flare prediction schemes provide forecasts (usually probabilistic) for flares classes, e.g., C1+, M1+, X1+. As such, the measurement gap identified in the previous section also apply here.

Forecasting Status: The performance of flare class forecasting is comparable to "all clear" status. Different algorithms perform at different levels depending on the metric used. Overall, the majority performs a little better than the "no skill" forecast. Human-in-the-loop tends to increase scores. However, there is no clear winning approach at this moment (Leka et al., 2019).

Forecasting Requirement: There is no broadly accepted requirement across the various SWx entities. NOAA/SWPC requires M1+ and X1+ for 24-, 48-, and 72-h forecasting intervals. ESA requires a 24-h forecast of M1+, M5+, X1+, and X5+ with a 3-h update interval.

Measurement Gap: The measurement gaps are very similar to the flare occurrence gaps although the questions at hand are a bit different. We require the forecasting of the energy release rate and amount *before* flare onset. This is the energy component imparted on particle beams accelerated downward from the reconnection region. This requires mapping the magnetic topology of the reconnected systems, understanding the 3D evolution of the reconnection region and ambient loop systems, and quantifying the energy partition to the various constituents (particles, plasma motion, radiation, etc.).

Required Measurements (maintain):

- Same as Section 5.1.2.1.

Required Measurements (improve):

- Same as Section 5.1.2.1, plus **high-performance hard X-ray (HXR) imaging spectroscopy.** HXR imaging spectroscopy with high SNR, spatial resolution (1–2 arcs), and cadence (seconds) from SEL will provide a wealth of data to understand the initial stages of energy release and magnetic connectivities within the flaring region. HXR imaging spectroscopy currently have no operational use for forecasting flares but are relevant for understanding and observing physical processes that in turn may lead to better forecasts. An example is the possible link between 300 keV hard X-rays and 100-MeV γ-rays (e.g., Share et al, 2018).

Required Measurements (advance):

- Same as Section 5.1.2.1, plus **off-SEL HXR imaging spectroscopy of the reconnection region (loop-top source).** Yohkoh, RHESSI, and radio microwave observations have shown that the initial energy release occurs high in the corona, just above the flaring loops (hence, the name "loop-top" source). The emission is HXR arising from bremsstrahlung by nonthermal electrons colliding with the coronal plasma but is almost always much fainter than the HXR emission from the flare footpoints (caused by the electrons impacting the dense chromosphere), which occurs almost simultaneously. The best cases of loop-top imaging occur when the flare footpoints are behind the limb. Hence, the best measurements should be made from off-SEL, **preferably from L5** (because the flares from ARs magnetically connected to Earth will be occulted from L5).

Required Measurements (close):

- **Multi-height vector magnetic field measurements.** Mapping the 3D field through the $\beta = 1$ interface to the upper chromosphere and transition region may suffice to provide robust estimates of coronal currents in ARs (since ARs are the sources of the most SWx-relevant eruptions). This measurement provides the most robust improvement for "all clear" forecasts while enabling transformative research into eruption prediction.

5.1.2.3. SXR Duration/Fluence

Measurement Method: The total SXR fluence is derived by integrating the SXR light curve (e.g., from GOES) over the duration of the flare (defined as the time above the pre-flare background). The fluence can be predicted from the flare rise profile and can thus provide a few hours of forecasting horizon for long-duration (LD) flares (longer than 2 h). SXR fluence, rather than peak SXR flux, has been found to have a stronger association with the likelihood of SEP occurrence.

Forecasting Status: unknown

Forecasting Requirement: unknown

Measurement Gap: The fluence of a flare is primarily determined by the spatial extent of the post-flare loop systems (which correlates with event duration) and by the peak flux. Since LD flares are usually associated with CMEs, the forecast of flare fluence is connected to the CME eruption forecast and hence is subject to similar gaps (and the flare gaps discussed above). We do not have quantitative information on the coronal current systems (energy, extent, detailed topology) and we lack understanding of how the magnetic energy, released via reconnection, is partitioned among flares, CMEs, and particles.

Required Measurements (maintain):

- Same as Section 5.1.2.1.

Required Measurements (improve):

- Same as Section 5.1.2.1.

Required Measurements (advance):

- Same as Section 5.1.2.1.

Required Measurements (close):

- Same as Section 5.1.2.1.

5.1.2.4. EUV Flux Enhancement

Measurement Method: The EUV spectral irradiance enhancement is measured by EUV spectrometers (e.g., GOES/EUVS). It can also be obtained (in broader bandpasses) by integrating spatially resolved emission in EUV imagers (e.g., GOES/SUVI). It can also be forecasted using appropriate flare models (e.g., FISM) for a particular flare class.

Forecasting Status: The forecasting of the EUV flare output requires the peak flux and flare duration as inputs. So, the status is the same as for the previous flare quantities.

Forecasting Requirement: Solar EUV irradiance enhancements impact the ionosphere near instantaneously. The thermosphere responds with a 2-h time lag. Hence, the affected users require the same flare forecasting horizon as for peak flux above. Namely, NOAA/SWPC requires M1+ and X1+ for 24-, 48-, and 72-h forecasting intervals.

Measurement Gap: FISM requires the flare class as input, so the same measurement gaps that hinder peak flux or fluence apply here. In addition, the EUV variations may be affected by LOS effects due to plasma motions (e.g., from the outflowing CME plasma or absorption/emission by an erupting filament or interference from a homologous eruption). Both EUV imaging and spectroscopy are required to understand the importance of these effects on the forecasted EUV flux enhancements. Some measurements are operationally available from the current and future GOES series (EUVS and SUVI). However, EUVS includes only one clear coronal line (Fe XV at 284 Å,) and thus relies on a model (Thiemann et al., 2019) to forecast flare irradiances. Narrowband EUV imagers such as SUVI and AIA can help, but they are not calibrated for irradiance applications and thus cannot easily complement the EUVS model, particularly for flaring regions where the emission may saturate the detectors. Thus the desired temperature ranges for certain applications, such as “EUV dimmings” which require cool lines, may not be covered.

Required Measurements (maintain):

- Forecasting: Same as Section 5.1.2.1.
- Specification: Same as Section 5.1.6.1.

Required Measurements (improve):

- Forecasting: Same as Section 5.1.2.1.
- Specification: Same as Section 5.1.6.1.

Required Measurements (advance):

- Forecasting: Same as Section 5.1.2.1.
- Specification: Same as Section 5.1.6.1.

Required Measurements (close):

- Forecasting: Same as Section 5.1.2.1.
- Specification: Same as Section 5.1.6.1.

5.1.3 Solar Radio Emission

SRBs that can impact terrestrial conditions are closely related to solar flares. Just as technological use of the radio spectrum tends to confine applications into different frequency bands depending on the characteristics needed, it also happens that different physical emission mechanisms tend to dominate solar radio emission in different parts of the spectrum, providing different properties.

At frequencies below about 500 MHz, bursts produced by the plasma emission mechanism tend to dominate. This mechanism relies on the production of electrostatic Langmuir waves at the plasma frequency, $f_p = 9000\ \mathrm{sqrt}(n_e)$ where n_e is the electron density in the source, and their conversion to propagating electromagnetic waves at f_p and $2f_p$. Thermal absorption of plasma emission is proportional to f^4 where f is the frequency, so higher frequency plasma emission tends to be absorbed before it can escape the Sun's atmosphere. Langmuir waves are very efficiently produced by electron beams or other nonthermal electron velocity distributions, and their production is coherent so very bright bursts can result. The frequency range below 500 MHz is convenient for hand-held radio communication devices, including satellite-to-ground communications, as well as radar applications. Since hand-held devices generally have omnidirectional antennas, solar radio bursts can interfere with their operation at any time of day. Bright solar radio bursts in this frequency range are also often associated with major solar eruptions, so they have been used as a diagnostic of solar activity for forecasting purposes.

Plasma emission also dominates solar emission at frequencies below 10 MHz that cannot reach the ground due to the plasma frequency cut-off in the ionosphere. These frequencies can only be observed from above Earth's atmosphere and are sensitive to conditions in the outer solar atmosphere and solar wind. They have also been associated with other forms of solar activity: clusters of low frequency Type III bursts have been shown to have a strong association with SEP events (Cane et al., 2002; Laurenza et al., 2009), and hence have value for forecasting solar energetic particle events. Interplanetary Type II bursts are clear indicators of the presence of shocks driven by CMEs and thus may also convey information on the acceleration of energetic particles at shocks.

The brightest solar radio bursts in the critical frequency range from 500 to 2000 MHz (decimetric wavelengths) are believed to have a very different source: electron cyclotron maser emission. This frequency range encompasses GNSS such as GPS and Galileo, cell phone transmissions, and radar applications. GPS devices and cell phones also need to have omnidirectional antennas, so they can be affected any time of day, regardless of the Sun's position in the sky. The well-studied radio burst of December 6, 2006, was so bright at GPS frequencies that most GPS devices in the daylight hemisphere lost lock for ~20 min. Such bright bursts are rare, but given our increasing reliance on

satellite systems such as GPS, including control of passenger aircraft landing in the near future, their impact can be grave. Global navigation signals are circularly polarized, and the electron cyclotron maser mechanism produces highly circularly polarized emission, so it is critical to measure polarization properties to know if a burst will result in degraded operations. Furthermore, these bursts show a lot of spectral structure and the brightest features can be narrowband, so fixed-frequency observations may well miss the strongest emission.

Above 2000 MHz (microwave frequencies), solar radio bursts are generally dominated by gyrosynchrotron emission from the same nonthermal electrons that produce hard X-rays and γ-rays in solar flares. The resulting flux depends on the size of the flare, and the strength of the magnetic field in the radio source. At higher frequencies, most applications use focusing collecting areas that have a limited primary beam on the sky, so that the impact of the Sun is generally minor unless it is within the beam or its significant sidelobes. As an example, television services from geosynchronous satellites can suffer interference twice a year if the Sun is active when it passes through the geosynchronous belt in the sky. Microwave frequencies are used for satellite operations, communications and high-bandwidth applications.

5.1.3.1. Metric Radio Bursts

The frequency range from 10 to 500 MHz is the domain of the classic radio burst types (Types I–V). Types II, III, and IV are flare-related: Type II bursts, representing shocks in the corona, are instantaneously narrowband with fundamental and harmonic traces, drifting gradually to lower frequencies with time. Type III bursts, representing electron beams injected into the corona, are of short duration and rapidly drift to lower frequencies. Type IV bursts are broadband continua that tend to occur in the decay phase of a flare and also tend to drift gradually lower in frequency with time. Metric Type II and IV bursts are treated as proxies for the presence of CMEs, and are used in some SEP forecasting models (e.g., Balch, 2008).

Measurement Method: Dynamic spectra, i.e., full-disk receivers capable of high time resolution and HF resolution across a broad frequency band, are necessary to make burst identifications. An example is given in Figure 5-13. Flux calibration is often difficult at these low frequencies but is needed to provide robust assessments of impacts on, for example, communication and radar operations.

Current Status: The only operational 24-h monitoring of solar radio emission is currently provided by the U.S. Air Force's Radio Solar Telescope Network (RSTN) of four stations. RSTN provides dynamic spectra from 25 to 180 MHz, together with fixed frequency observations at 245, 410, and 610 MHz. The National Institute of Information and Communications Technology (NiCT) operates a spectrometer from 70 to 9000 MHz that is used for space weather monitoring in Japan (Iwai et al., 2017). The Royal Observatory of Belgium operates a spectrometer covering 45–1500 MHz. The Paris Observatory operates a decameter array observing from 10 to 80 MHz at Nançay. The Yunnan Observatory in China operates a spectrometer observing from 70 to 700 MHz. The Indian Institute of Astrophysics has a spectrograph at Gauribidanur Observatory covering 40–440 MHz (Kishore et al., 2014). The Space Weather Services in Australia continue to operate a spectrograph at Culgoora from 18 to 1800 MHz. Another valuable data source is the network of Callisto spectrometers, of order 50 individually operated systems spread around the

world and providing data in various frequency ranges between 2 and 1600 MHz to a central collecting site in Switzerland. Carley et al. (2020) provide a survey of current solar radio instrumentation used for space weather purposes.

Forecasting Requirement: Reporting radio burst types is needed, e.g., for SEP modeling, but forecasting their occurrence has little application. They are closely tied to solar flares, which are the major target of forecasting efforts. At low frequencies, Type III bursts in solar flares are fairly common and there is little incentive for forecasting them. Type II and IV bursts are much less common and are more often associated with eruptive events that are generally more SWx-effective, but forecasting the occurrence of these burst types is less important than forecasting CMEs themselves.

Measurement Gap: Two properties of metric radio bursts are not consistently measured at present. One is circular polarization, which contains information on the magnetic field in the source; the other is well-calibrated fluxes.

Required Measurements (maintain):

- **Monitoring of metric radio bursts.** It is expected that the current coverage from 25 to 180 MHz provided by RSTN will continue for the immediate future.

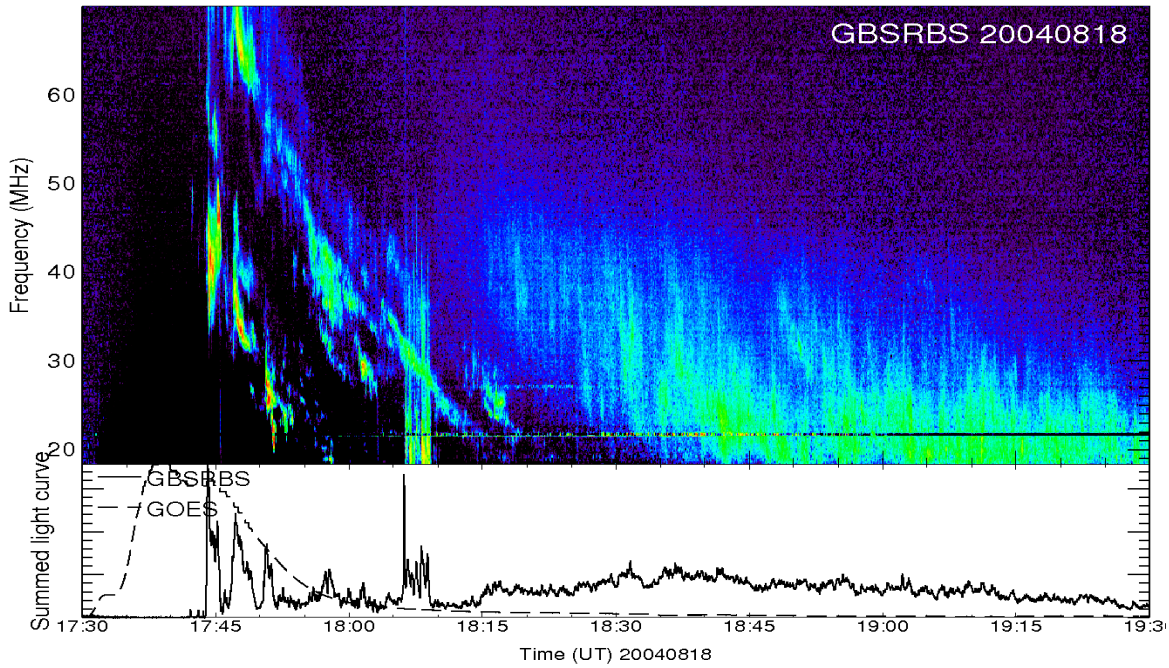

Figure 5-13. An example of radio burst types produced by a flare. A Type II burst consisting of split bands starts at 17:45 UT and drifts to lower frequency, ending at 18:20 UT. Nearly vertical features from 18:06 to 18:09 are Type III bursts, while the emission starting at about 18:15 UT around 40 MHz and continuing to 19:30 is a Type IV burst. Note that before 17:45 UT, the dark region in the spectrum indicates absorption in the ionospheric D-layer due to increased ionization there caused by the intense SXR from the flare penetrating to below 100-km altitude in the atmosphere. Data from the Green Bank Solar Radio Burst Spectrometer.

Required Measurements (improve):

- **Extending the frequency range of operational dynamic spectra.** As discussed below in the context of the GNSS frequency range, wider frequency coverage of the dynamic spectrum measurements is necessary.

Required Measurements (close):

- **Extended frequency range, polarization and calibration.** Together with wider frequency coverage, circular polarization and well-calibrated flux measurements are needed.

5.1.3.2. Decimetric Radio Bursts

The bright bursts that impact the frequency range from 500 to 2000 MHz, including GNSS frequencies, can be narrowband, highly polarized, and have complex temporal and spectral structure. Current single-frequency measurements cannot capture the properties of these bursts adequately.

Measurement Method: Modern radio spectrometers can readily handle 2 GHz of bandwidth.

Current Status: RSTN provides fixed frequency observations at 1415 MHz. The National Astronomy Observatory of Japan (NAOJ) operates fixed-frequency polarimeters at 1.0 and 2.0 GHz. The NiCT spectrometer operates from 70 to 9000 MHz. The Royal Observatory of Belgium operates a spectrometer covering 45–1500 MHz. The French Air Force together with the Paris Observatory operates the ORFEES spectrograph observing from 144 to 1000 MHz. The Ondrejov Observatory in the Czech Republic observes with a spectrometer at high time resolution from 0.8 to 5.0 GHz. In Italy, the Astronomical Observatory of Trieste is developing a system to observe from 1 to 19 GHz with good spectral resolution and circular polarization measurements (Jerse et al., 2020). Space Weather Services in Australia continue to operate a spectrograph at Culgoora from 18 to 1800 MHz. Callisto spectrometers provide data up to 1600 MHz. However, most of these instruments are intended for research use and are generally not suitable for real-time operational use at present.

Forecasting Requirements: Because of the complex nature of bursts in this frequency range, continuous frequency coverage, i.e., a dynamic spectrum, up to at least 2.0 GHz is needed. GNSS signals are circularly polarized: flux measurements in both senses of circular polarization across the entire frequency range are needed to assess whether a burst will affect GNSS operations.

The ability to forecast the bright decimetric bursts that can impact GNSS would be a significant advance, but little work has been done on this topic. The emission mechanism is coherent, and the necessary conditions for strong amplification are difficult to identify. The relatively small number of bright bursts observed means that there is no large sample of properties to study.

Measurement Gap: There is currently no uniform source of dynamic spectra with circular polarization measurements and appropriate flux calibration with full 24-h coverage in this frequency range. This is a glaring gap in current operational coverage, which was mostly designed before the advent of GNSS. Current real-time coverage of the frequency range 500–2000 MHz is inadequate to provide warnings of likely degradation of navigation capability.

Required Measurements (maintain):

- **Flux monitoring at decimetric wavelengths.** It is expected that RSTN will continue to provide the single-frequency measurements for the immediate future.

Required Measurements (improve):

- **Provision of operational dynamic spectra covering the decimetric range.** Expanded frequency coverage of the dynamic spectrum measurements up to at least 2.0 GHz is necessary if impacts to GNSS assets are to be identified.

Required Measurements (close):

- **Flux-calibrated circular polarization dynamic spectra up to at least 2.0 GHz.** Together with wider frequency coverage, circular polarization and well-calibrated flux measurements are essential if impacts to GNSS operations are to be monitored. This is particularly critical if commercial air traffic is to use GNSS to aid in landing aircraft.

5.1.3.3. Microwave Radio Bursts

Flare-related gyrosynchrotron bursts at frequencies above 2.0 GHz generally have a fairly well-behaved broadband spectrum peaking in the range 5–30 GHz. Single-frequency measurements with sufficient density in frequency space are able to characterize their properties, but broadband spectrometers with continuous frequency coverage are also an option.

Measurement Method: Standard radio astronomy measurements. Software-defined radio systems are increasingly being used for measurements such as this.

Current Status: Most of the systems are mentioned in the preceding subsection. RSTN provides fixed frequency observations at 2695, 4995, 8800 and 15400 MHz. NAOJ operates fixed frequency polarimeters at 3.75, 9.4, 17 and 35 GHz. The National Resource Council of Canada operates the critical monitoring at 2.8 GHz that provides the carefully calibrated F10.7 index widely used in atmospheric models (e.g., Tapping, 2013). The Korean Space Weather Center also monitors 2.8 GHz emission.

Forecasting Requirements: Sufficiently dense frequency coverage with well-calibrated flux measurements to characterize the typical gyrosynchrotron spectral shape. There has been significant work on forecasting F10.7 (the radio flux at 2800 MHz) because of its importance as a proxy for ionizing flux in atmospheric models. The method relies on the fact that the (non-flare) coronal material that produces F10.7 is closely tied to magnetic fields in the atmosphere, so global models of solar magnetic fields provide a robust estimation of F10.7 (e.g., Ulrich, 1991; Henney et al., 2012; Schonfeld et al., 2019).

Microwave bursts from gyrosynchrotron emission are in principle easier to forecast, since they are produced by an incoherent mechanism and generally linked to flare size, but the strong dependence on the magnetic field strength in the source (typically flux $\propto$ B3-4) makes it difficult to forecast fluxes to better than an order of magnitude. In fact, burst flux spectra (particularly the frequency at which the flux peaks) can be used to infer the magnetic field strength in the source.

Measurement Gap: Circular polarization measurements provide information on magnetic fields in the source and thus are valuable for research that may lead to better prediction of burst fluxes. RSTN does not provide such measurements; denser frequency coverage for such polarization measurements would be valuable for this purpose.

Required Measurements (maintain):

- **Flux monitoring at microwave frequencies.** It is expected that RSTN will continue to provide the single-frequency measurements for the immediate future.

Required Measurements (improve):

- **Expand frequency coverage.** Denser frequency coverage would be valuable.

Required Measurements (close):

- **Continuous frequency coverage with calibrated flux measurements in both circular polarizations.** Receiver systems capable of complete sampling of frequencies up to 35 GHz will be feasible. Such systems would offer the flexibility of selecting particular frequencies or frequency ranges of interest for specific applications, without necessarily generating high-data volume complete dynamic spectra for the full frequency range. The data need to be flux-calibrated in order to assess impacts, and circular polarization measurements will add information on magnetic fields that may be valuable for other areas of forecasting, such as flare occurrence.
- **Coverage of higher frequency bands.** Another long-term goal should be extending coverage to higher frequencies: V-band (40–75 GHz) and W-band (75–110 GHz) are drawing more interest for wide bandwidth applications, including satellite communications, but there is no real-time monitoring in these bands at present. Dense spectral coverage in these bands is not needed since gyrosynchrotron spectra are generally smooth, so fixed-frequency observations should suffice.

5.1.3.4. Coronal Magnetic Field Measurements at Radio Wavelengths

A strength of non-flare radio observations at microwave frequencies is that they are sensitive to coronal magnetic fields in the range 200–2000 G, and measurements on the solar disk are straightforward provided one has broad frequency coverage (e.g., White & Kundu, 1997). Coronal magnetic fields are assumed to be the source of the free energy that drives solar flares and CMEs, but there is currently no source of routine daily measurements of coronal fields in the ARs likely to produce space weather impacts. It is highly likely that forecasting such impacts could be greatly enhanced were routine measurements of the evolution of coronal fields available. However, since no routine measurements have been available to this point, their value as a forecasting tool remains a research topic awaiting suitable data.

Coronal magnetic fields can also be measured from the ground at optical and near-IR wavelengths by exploiting the Hanle and Zeeman effects in spectral lines (e.g., Casini et al., 2017), but the brightness of the solar disk at these wavelengths currently limits their use to off-limb observations. The ratio of magnetic-induced transitions in EUV lines is also being explored as a means to measure field strength (e.g., Si et al., 2020). These techniques will not be discussed further here, but

they will need to be included in any future efforts at comprehensive measurements of coronal magnetic fields (see Gibson et al., 2020).

Measurement Method: Spatially resolved measurements at arcsecond resolution with good time cadence, ideally from 2 to 20 GHz, are needed to measure the spatial structure of magnetic fields in the corona at field strengths from 200 to 2000 G and to follow their evolution. This requires a radio interferometer consisting of many tens of elements with maximum dimension of several kilometers, in order to map the full solar disk at the spatial resolution required.

Current status: Major radio telescopes such as the VLA can make the required measurements but are not solar-dedicated and hence not useful for space weather applications, other than the important role of demonstrating the technique. In the United States, the EOVSA is a solar-dedicated interferometer covering the required frequency range. EOVSA has sufficient receivers to image microwave solar radio bursts, which are generally confined to small areas of the disk, but too few to map the full solar disk instantaneously at arcsecond resolution, although it can provide valuable data if a single AR dominates the microwave emission. The FASR is an instrument proposed in the United States that is designed to make routine measurements of coronal magnetic fields, among other applications. In China, the MUSER has capabilities similar to those planned for FASR, and suitable data analysis methods are under development (Mei et al., 2018).

Forecasting Requirements: The use of coronal magnetic field measurements for forecasting has not been developed due to the lack of suitable data, i.e., many cases of flaring ARs where the association between changes in coronal fields and the occurrence of flares can be assessed. This requires long time sequences of high spatial resolution images of solar ARs in both senses of circular polarization from ~2 to ~-20 GHz.

Measurement Gap: The data required to assess the value of coronal magnetic field measurements for forecasting flares and eruptions, described in the previous paragraph, are not currently available.

Required Measurements (maintain):

- There is currently no capability to be maintained.

Required Measurements (improve):

- Expanding EOVSA by adding more elements to improve instantaneous snapshot imaging across large regions; construction in the United States of a solar-dedicated radio interferometer with many elements designed to measure corona magnetic fields, such as FASR; successful development of MUSER imaging across the full microwave frequency range.

Required Measurements (close):

- 24-h coverage of coronal magnetic field measurements via three radio interferometers such as FASR and MUSER.

5.1.3.5. Decametric and Lower Frequencies

This is the area of solar radio emission where NASA resources are directly relevant, since frequencies below the ionospheric cutoff, typically around 10 MHz in daytime, cannot be observed from the ground. Emission at these low frequencies is characteristic of erupting material since it has to originate above the 10 MHz plasma level in the corona, typically of order 2 solar radii above the surface.

Measurement Method: Requires satellites outside Earth's atmosphere. Usually log-periodic dipole antennas are connected to receivers sampling both electric and magnetic fields directly to measure both electromagnetic waves from remote sources and plasma waves local to the spacecraft in the solar wind.

Current Status: Observations of solar radio emission below 10 MHz are limited to scientific satellites such as WIND, STEREO, Parker Solar Probe, and Solar Orbiter. Telemetry limitations for satellites that are not orbiting Earth or at L1 make it difficult to robustly provide such data for operational use in real time.

Forecasting Requirements: Return of dynamic spectra covering frequencies below 10 MHz in real time. The presence of different burst types would be identified in these data and may be used by operational SWx models, particularly for forecasting SEP events.

Measurement Gap: Real-time data; none of the current data sources can reliably satisfy this need.

Required Measurements (maintain):

- **Provision of dynamic spectra below 10 MHz.** Currently satisfied by scientific payloads but not available fast enough for operational use.

Required Measurements (improve):

- **Faster return of data.** Any improvement in data latency will enhance the use of such data.

Required Measurements (close):

- **Real-time dynamic spectra below 10 MHz suitable for operational use.** This will require new payloads orbiting Earth or at L1. It is possible that CubeSats can play a role; this is being tested with NASA missions such as Sunrise. For continuity purposes, the frequency coverage should extend at least up to 20 MHz since ground-based systems increasingly suffer from RFI in this range. The latency of data provision to operational sites needs to be of order minutes or less if the data are to be of use in forecasting tools.

5.1.4 Solar Wind Structure

We have identified six parameters related to solar wind stream structure which are of importance to SWx operations and models: ToA, duration, speed, density/momentum, magnetic field, and presence/absence of a shock.

The speed, density/momentum, and magnetic field in the solar wind are significant drivers of geo-effects. Speeds of up to 800 km/s, proton densities of >80/cc, dynamic pressures of >25 nPa and magnetic fields >25 nT can be attained at Earth during corotating solar wind streams (i.e., excluding CMEs and CME-driven shocks). The highest speeds (not associated with CMEs) are found in HSSs that are typically associated with large, low latitude coronal holes and the extensions of polar coronal holes toward the solar equator. However, the other enhanced parameters occur during the passage of SIRs, where higher speed streams running into slower wind produce compressions of the plasma and field (Jian et al., 2019). About 25% of SIRs are found to drive a fast magnetosonic shock, or a forward/reverse shock pair, at 1 AU (Jian et al., 2006), while almost all SIRs drive shocks by 5 AU. As such, SIRs are the main source of shocks during solar minimum conditions and the main drivers of changes in Earth's radiation belts. Additionally, the "background" solar wind structure has been found to affect CME ToA and SoA (see Section 5.1.1); therefore, accurately forecasting the solar wind stream structure is critical for accurate SWx forecasting of CME ToA and properties, and SEP onset forecasting. Work in the past decade regarding the forecasting of solar wind streams has focused on using STEREO in situ measurements near L5 or other locations near 1 AU and east of the SEL to forecast solar wind stream arrival and properties at L1 (Turner & Li, 2011; Thomas et al., 2018; Allen et al., 2020; Bailey et al., 2020), the further development, validation, and testing of numerical models (Jian et al., 2015; Reiss et al., 2016; Hinterreiter et al., 2019), using heliospheric imagers to forecast SIRs (Davis et al., 2012) and directly using solar images to forecast HSS properties near 1 AU (Vrsnak et al., 2007; Bu et al., 2019; Garton et al., 2018; Hofmeister et al., 2018).

5.1.4.1. ToA and Duration of HSSs and SIRs/CIRs

The ToA of the solar wind stream and/or its associated shock at Earth (or other locations). The duration of the solar wind stream structures.

Measurement Method: ToA forecasting is performed via modeling (physics-based models) or assuming 27-day recurrence. The primary input is the **photospheric magnetic field** for models or in situ **measurements of a solar wind stream** during the previous CR. Coronal hole images in the EUV from the solar disk are also often used to perform empirical forecast of the ToA.

Forecasting Status: Jian et al. (2015) quantified the skills of the combinations of various numerical models and photospheric magnetic field maps to forecast HSSs and SIR arrival. Typical MAE for ToA was found to be ~1 day ± 6 h. Similar ToA error can be obtained with direct EUV images of the coronal holes from the solar disk (Bu et al., 2019). Single-day persistence and 27-day corotation models were found to outperform the majority of numerical simulations in forecasting the presence and arrival of SIRs, indicating the limits of numerical modeling (Jian et al., 2015). A tomography model using Interplanetary Scintillation (IPS) was found to be one of the best models in forecasting ToA and SoA but cannot currently forecast the magnetic field. Numerical models using daily updated maps of the photospheric field for inner boundary conditions capture the SIR duration with errors of < ±12 h (Jian et al., 2015). Direct forecast of HSS arrival can be made using solar images (Garton et al., 2018) with the duration depending on the coronal hole longitudinal width. Recently, Allen et al. (2020) used measurements by STEREO to forecast the arrival of stream interaction region at L1 using measurements from L5. Only ~75% of SIRs arrived at L1 within ±3 days of corotation (and ~45% within ±1 day of corotation). For a window size of ±12 h, ~45% of SIRs are correctly forecasted with measurements from 10° away from the SEL. Davis et

al. (2012) demonstrated the possibility of using off-SEL HI images to forecast the arrival of HSSs using STEREO-A with higher accuracy than assuming 27-day corotation.

Forecasting Requirement: SWx users (GICs) require a MAE of 0 ±2 h for actionable forecast.

Measurement Gaps: The main gaps are mainly related to solar wind forecast model inputs or lack of available data to assimilate into the models and/or validate the models. Specifically, these are due to short-term (<1 day) or undetected (e.g., farside, polar) variations in the solar magnetic field properties (for example, emergence of new ARs or changes in the area or shape of a coronal hole); and radial, latitudinal, and longitudinal variations (Jian et al., 2019) in the stream properties. These are not reproduced in the models due to poorly known inner boundary conditions on the speed and density (including in slow wind), the lack of required physics to measure the small and moderate-scale features and the inadequate spatial resolutions (see MacNeice et al., 2018). These measurement gaps produce differences in the modeled arrival times and plasma parameters of HSSs and their related compression regions. In addition, a forecasting gap relates to the difference in arrival times obtained from using, as boundary conditions, photospheric field measurements from different spacecraft and/or observatories (Jian et al., 2015) and the influence of numerical resolution (Hinterreiter et al., 2019).

Required Measurements (maintain):

- **LOS photospheric field (B_{phot}) measurements over >50% of the solar surface**. Combined with numerical modeling, this allows for the simulations of solar wind streams via empirical or physics-based models.
- **In situ P&F measurements at L1** to ascertain the arrival of a stream near Earth.
- **SEL EUV disk imaging** to image the change in the area of equatorial coronal holes, the source of the fast solar wind at Earth.

Required Measurements (improve):

- **LOS photospheric field (B_{phot}) measurements over >50% of the solar surface**. Combined with numerical modeling, this allows for the simulations of solar wind streams via empirical (Wang-Sheeley-Arge [WSA]) or physics-based models. The additional photospheric field measurements should occur ***beyond the east limb of the Sun seen from Earth*** to image coronal holes and regions that are ready to corotate toward Earth. Currently, the part of the solar disk just beyond the east limb is the one for which photospheric measurements are the oldest (3–4 weeks old) and for which there is most value in obtaining more recent measurements.
- **In situ P&F measurements east of the SEL near 1 AU**. Recent studies (e.g., Bailey et al., 2020) indicate that measurements within ~10–20° from the SEL are necessary for high accuracy. This would provide an 18–36 h advanced warning. Further research is needed to determine the improvement from various separations from the SEL, including L5. The latitudinal separation with Earth and radial separation from 1 AU should be kept as minimal to minimize propagation and variation effects.

Required Measurements (advance):

- **LOS photospheric field (B_{phot}) measurements from off-the-ecliptic**. Equatorial extension of polar coronal holes significantly contribute to HSSs and SIRs at L1.
- **Off-SEL VIS imaging >120 $R_{\odot}$ with high SNR**. SIRs and their associated compression regions can be imaged by heliospheric imagers (Rouillard et al., 2008; Davis et al., 2012). An ideal location has not been determined, but this type of measurement might be more appropriate from locations west of the SEL and relatively close to it, for example L4 (Davis et al., 2012).

Required Measurements (close):

- **Distributed in situ P&F measurements from Earth to east of the SEL.** This measurement set allows data assimilation of solar wind structures in numerical models as well as direct forecasting using measurements of streams before they impact Earth.
- **Off-SEL disk EUV measurements**. The additional photospheric field measurements should occur east of the SEL to image coronal holes and regions that are ready to corotate toward Earth.
- **4π LOS photospheric field (B_{phot}) measurements.**

5.1.4.2. Plasma and Magnetic Field Properties of Streams and Presence and Absence of Shocks

Measurement Method: The speed, density/momentum, and magnetic field in the solar wind that impacts Earth needs to be measured outside Earth's magnetosphere; the L1 point is a convenient location for in situ plasma and magnetometer measurements. This can also be also used to determine whether a shock (or a pair of shocks) will occur during the passage of a SIR.

Forecasting Status: Forecasting the properties of the solar wind is primarily done through a combination of empirical models (such as the WSA model, Wang & Sheeley, 1990; Arge & Pizzo, 2003) and MHD models (such as ENLIL, see Odstrcil, 2003). As mentioned above, these models require knowledge of the photospheric magnetic field to specify the inner boundary conditions. Recent efforts have also been undertaken to directly forecast HSS speed from coronal hole areas or other parameters (Rotter et al., 2015; Hofmeister et al., 2018; Bu et al., 2019). The accuracy of peak magnetic field strength forecasts is relatively poor (MSE of ±30% for the best models), the accuracy in forecasting the density (MSE ~ ±80%) and magnetic field orientation are very poor, while the accuracy in forecasting the peak speed has been quantified to be MAE ~ 80 km/s from coronal hole images (Bu et al., 2019) or RMS errors of ±90–120 km/s from numerical models (Jian et al., 2015).

Forecasting Requirements: The required forecasting accuracies for the dynamic pressure, speed and B_{south} have not yet been quantified. The current inability to forecast the southward component of the field, B_{south}, is of particular importance because of its impacts on magnetospheric coupling and effects.

Gaps: Like the ToA forecasts described above, current limitations of the solar wind property forecasts are due to the following factors:

1. Coronal hole boundaries that are constantly evolving due in part to unobservable photospheric magnetic fields on the farside hemisphere and near the limb—including the polar regions—therefore limiting what is used in the models;
2. Small-and moderate-scale spatial variations in stream properties associated with deviations from radial flows, especially associated with latitudinal variations, and complex sources in the streamer belt;
3. Time-dependent/radial evolution, including SIR compression and shock formation;
4. Orientation of the magnetic field during the off-the-ecliptic compression associated with SIRs (the major source of southward IMF outside of CMEs). Critical for forecasting, the properties of solar wind streams can change drastically in ~1 day (during which corotation is ~13°).

For example, Bailey et al. (2020) found that the correlation between the magnetic field in solar wind streams measured 20° east of the SEL and that measured at L1 is only ~0.5, while the speed remains correlated to much larger separations (~0.65 at 60° separation). In addition, near 1 AU, SIRs are still in the process of forming, which strongly affects our forecasting capabilities. For example, the two STEREO spacecraft longitudinally separated by <10° measured the same SIR with and without a shock (Jian et al., 2019).

Required Measurements (maintain):

- Same as Section 5.1.1.3.

Required Measurements (improve):

- Same as Section 5.1.1.3.

Required Measurements (advance):

- Same as Section 5.1.1.3.

Required Measurements (close):

- Same as Section 5.1.1.3.

5.1.5 Solar Energetic Particles

While the most important site of SEP acceleration is the vicinity of a CME-driven shock as it travels outward, flare-accelerated particles may play a role, as either seed particles or as a component of the overall SEP population. Resolving their contribution is therefore important for the success of future SEP event forecast models. The details of SEP transport that lead to their diverse and often broad spatial distributions are also outstanding subjects of research.

Some SEP models are coupled with coronal, heliosphere, and magnetic connectivity models. Similarly, solar radio, CME, and X-ray observations have been used in scientific studies of SEPs and as inputs to forecasting models. As such, addressing the science, forecasting, and observational gaps in these areas will also lead to improvements in SEP forecasting. These gaps are discussed in

detail in Sections 5.1.1, 5.1.2, and 5.1.3. A different set of science and forecasting gaps related to SEP forecasting *before* event or eruption (flare or CME) occurrence on the Sun are largely covered by the gaps discussed in Sections 5.1.1, 5.1.2, and 5.1.3. Questions specific to SEP forecasting include: *Will an SEP event be observed at the location of interest? How strong will the SEP event be? How long will the SEP event last? Will SEPs accelerated at a flare site or CME shock have access to a particular location (e.g., Earth or Mars) in the heliosphere?*

The majority of SEP forecasting is performed following the eruption of a flare or CME since certain precursors (e.g., X-ray flux, energetic electrons, magnetic connectivity to source, CME speed) are correlated to SEPs and the pre-eruption prediction of SEPs is extremely challenging. Post-eruption forecasts, however, provide little lead time—especially for prompt, energetic events which are a main concern for human exploration missions. Pre-eruption SEP models suffer from very low skill scores due to our incomplete understanding of energy release process (see also Section 5.1.2), in addition to the low number of historical SEP events usable for model training and validation. Also, the potential precursors (flares, CMEs) far outnumber SEP events, so prediction of these precursors is not directly related to SEP prediction. Instead, pre-eruption SEP forecasting currently relies heavily on human-in-the-loop forecasts.

We have identified five areas needing further improvement in the field of SEP forecasting, all of which are highly dependent on validation methodology and event set:

5.1.5.1. Pre-eruption "All Clear"

"All Clear" is defined as a pre-eruption forecast that >10 MeV protons WILL NOT exceed the specific threshold of 10 pfu or that >100 MeV protons WILL NOT exceed 1 pfu in the next 24 or 6 h. These thresholds are the NOAA definitions and apply to the peak intensity during SEP events, which may occur shortly after event onset or associated with an ICME shock arrival at the crewed vehicle. This forecast must be made before an eruption, flare or CME. It is generally expected that it will be a probabilistic forecast, although it could be a deterministic forecast that indicates predicted peak flux will not exceed threshold values.

Forecasting Status: Forecasts are currently made by a handful of models and human-in-the-loop forecasts. One forecasting method reports a probability of detection (POD) of 0.62, FAR of 0.16, and Brier skill score (BSS) of 0.46 for >10 MeV protons (Bain et al., 2021). Forecasting performance status is currently unknown for >100 MeV protons.

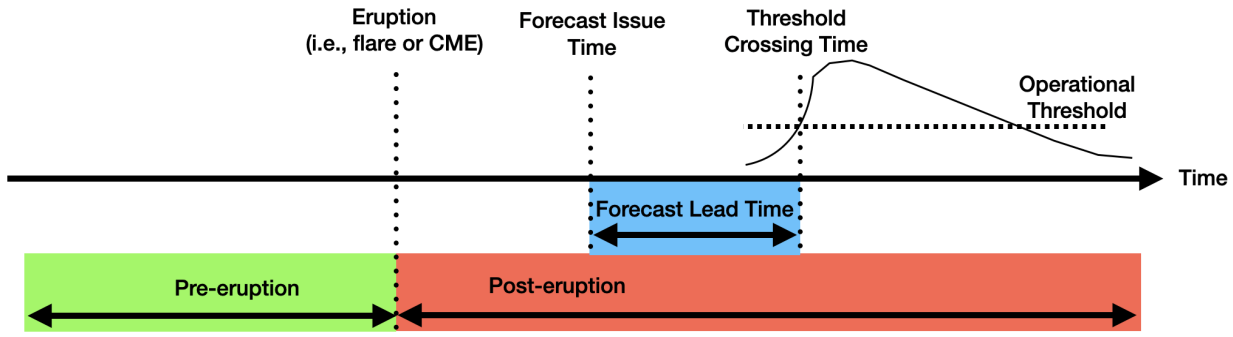

Figure 5-14. Schematic describing terms relevant to SEP forecasts.

Forecasting Requirement: Prediction window requirements include 24-h all-clear forecasts of >100 MeV protons not exceeding 1 pfu for general mission planning and situational awareness (SRAG requirement). For EVAs, 24- and 6-h all-clear forecasts of >10 MeV protons not exceeding 10 pfu are needed. The FAR is required to be as low as possible. We note that 6–12 h prediction windows have not been explored much by models and forecasting techniques, but they are needed for launch and pre-EVA support.

Measurement Gaps: Pre-eruption forecasts depend heavily on whether an eruption will occur or not, therefore measurement gaps are similar to those listed for flare and CME "all clear" (see Section 5.1.1.1 and 5.1.2.1).

Required Measurements (maintain): The following measurements are currently used to generate forecasts:

- **Solar SXR flux measurements with flare location detection, in situ e-, p+, and heavy ion measurements (e- 0.02–0.6 MeV; p+ 0.02–6 MeV, heavies 40 MeV/n).** The SXR and in situ measurements are covered by NOAA GOES, DSCVR, and IMAP and SWFO-L1 from 2024 onward. However, only the NOAA GOES detector will measure energetic protons above 40 MeV. It is important to have measurements of high energy protons from at least two simultaneous experiments, both for verification and calibration purposes, as many prior studies have shown (Sandberg et al., 2014; Bruno, 2017). Thus, a measurement gap for a second measurement of protons at energies above 100 MeV is identified for the near future.
- **Vector photospheric field (B_{phot}) measurements of Earth-facing disk with >95% duty cycle.** Quantities derived from this dataset (i.e., magnetic flux, helicity, distribution, photospheric motions, location, extent) are used by almost every forecasting model and methodology both operationally and for research. HMI has provided such measurements since 2010. Continuity is necessary to extend the historical databases for nowcasting and algorithmic validations. These measurements could be performed from the ground if an appropriate world-wide network existed.

Required Measurements (improve):

- **LOS photospheric field (B_{phot}) measurements over >50% of the solar surface.** All existing heliospheric models use B_{phot} as their main input. Expanding the observation from the current ~⅓ to ½ of the solar surface will improve the fidelity of the models. This in turn will lead to more accurate description of the corona and solar wind and the interactions of solar transients with ambient structures. High priority should be given to **B_{phot} measurements over the western limb** because these longitudes are the most important for SEP forecasting: (1) eruptions over these longitudes are much more likely to be magnetically connected to Earth/cislunar space and (2) the magnetic evolution of a magnetic connected AR is captured more accurately from off-SEL viewpoints. In fact around a quarter of >25 MeV proton events at Earth originate behind the west limb (Richardson et al., 2014).
- **SEL imaging of hot plasmas (~ 10 MK).** Because coronal currents result in loop heating, images in lines forming at high temperatures (~10 MK) can capture non-potential AR loops. EUV channels at 94 Å are better suited than the more traditional SXR imaging because of the narrower spectral response and the reduced influence of plasmas at other temperatures. This is particularly true for sigmoids, which are a strong predictor for flares and CMEs (e.g., Green et al., 2018). This measurement is covered by NOAA/SUVI for the foreseeable future.

- **SEL vector B_{phot} + B_{chrom} measurements in ARs.** Increasing the height coverage of vector magnetic field measurements will increase the fidelity of the extrapolations and enable a more robust assessment of the pre-eruption magnetic topology and its evolution toward eruption. It will also improve the quantitative estimates of free magnetic energy and helicity in ARs, which will constrain both estimates of the erupted flux and the modeling of the magnetic field configuration.

Required Measurements (definitive):

- **High-SNR imaging spectroscopy of off-limb Ly-α emission.** Currently, the only method to measure suprathermal populations (the "seed" populations) is directly in situ at 1 AU (or intermittently by inner heliospheric probes, such as Parker Solar Probe or Solar Orbiter). Unfortunately, the important "seed" populations are those in the near-Sun space where regular in situ measurements are impossible. There is, however, a potential remote sensing method for measuring the "seed" populations (Laming et al., 2013). It requires a precise measurement of the Ly-α off-limb spectral profile for detecting and quantifying departures from Gaussian (i.e., Maxwellian particle distributions). Because the quantity and location of these populations is needed for forecasting, **imaging the Earth-facing limb from off-SEL viewpoints would be the optimal location.**
- **LOS B_{phot} fields for >67% of the solar surface** to further improve the fidelity of the main inputs to heliospheric solar wind and CME propagation models. **Preferred locations are L4 and L5** since these longitudes are the most responsible for the solar wind reaching Earth. It may be suboptimal for Mars-directed solar wind, when Mars is >60° away from Earth.
- **Off-SEL EUV imaging + vector B_{phot}.** Extends coverage of AR flaring history and magnetic configuration over ~⅔ of the solar corona. It enables a longer time series of flux emergence, and energy buildup across a larger portion of AR lifetime. Preferred location is L5 to provide information for ARs rotating onto the Earth-facing disk. However, L4 is preferable if SEP forecasting takes priority for reasons of human activity in space due to the better magnetic connection of ARs westward of the central meridian. This assumes that a similar set of measurements are available along the SEL. EUV imaging should include a hot line (e.g., 94 Å) for detection of pre-eruptive structure and strong currents within ARs.
- **2× off-SEL EUV imaging + vector B_{phot}.** Provides greater solar surface/corona coverage and thus captures an even longer portion of the AR flaring lifetime. Preferred locations are L5 and L4. This arrangement provides maximum SWx benefit both for human exploration activities and longer-term assessments.

Required Measurements (close):

- **4π coverage of surface magnetic field and coronal structure.** To improve SEP transport models, we need a robust description of the magnetic structure of the inner heliosphere. This requires, in turn, the specification of the photospheric magnetic field all around the Sun to increase the fidelity of MHD models, particularly in their treatment of the open flux. Coronal information will help validate the modeling and constrain the density/temperature specification. This information will improve modeling of the Alfvénic background and thus provide constraints on shock development and their particle acceleration efficiency.

- **Multi-height vector magnetic field measurements.** Mapping the 3D field through the $\beta = 1$ interface to the upper chromosphere and transition region may suffice to provide robust estimates of coronal currents in ARs (since ARs are the sources of the most SWx-relevant eruptions). SEL measurements are the baseline and required to validate this approach. L4 measurements would be preferable to support lunar exploration, because they would map the currents in magnetically connected ARs. This measurement provides the most robust improvement for "all clear" forecasts while enabling transformative research into eruption prediction.

5.1.5.2. Post-eruption Forecast of Crossing Thresholds

The post-eruption forecast of >10 MeV protons exceeding 10 pfu or >100 MeV protons exceeding 1 pfu can be deterministic or probabilistic. This also includes post-eruption "all clear" forecasts that predict that thresholds will not be crossed.

Forecasting Status: Forecasts are currently made by a handful of models and human-in-the-loop forecasts. One forecasting method reports a POD = 0.71 and FAR = 0.41 for >10 MeV protons and POD = 0.81 and FAR = 0.30 for >100 MeV protons (Núñez, 2015). The forecast lead time status discussed in Section 5.1.5.3 also applies to deterministic forecasts of threshold crossings.

Forecasting Requirement: Same as the previous Section 5.1.5.1. The forecast lead time requirement discussed in the following subsection also applies to deterministic forecasts of threshold crossings.

Measurement Gaps: Post-eruption forecasts are currently hindered by limited imaging of the solar disk and corona, lack of in situ measurements distributed in space, uncertainty in magnetic connectivity to the Sun, and no public availability of space-based radio and CME measurements in real time.

EUV and X-ray imaging of the solar disk provide important inputs to a variety of SEP models that make predictions derived from flare X-ray peak flux, fluence, and location (Laurenza et al., 2018; Kahler et al., 2007; Dierckxsens et al., 2015). Imaging of the solar disk from an Earth-based vantage point is not optimal for a relatively large portion of the solar surface (60°-90°+ from central meridian) that may host flares and CMEs that send SEP particles to Earth, particularly regions at/close to the western limb that are sometimes the source of GLEs (e.g., as on September 10, 2017). Models dependent on this information cannot make accurate predictions when flares occur over the limb.

Multiple coronagraph viewing angles are required to better-determine CME speed, width, and direction, which are key components of current forecasting models (e.g., Richardson et al., 2014; Luhmann et al., 2018; Papaioannou et al., 2018; Richardson et al., 2018). Measurement gaps are the same as those stated in Section 5.1.1.2.

Continuous in situ measurements of particles at SEP energies are generally available from a single point in space (L1, GOES spacecraft at Earth) with limited historical measurements from other locations in the heliosphere. Previous missions, including the recent STEREO and Ulysses missions, have demonstrated that SEP events can spread widely in three-dimensional space, including throughout the inner heliosphere. Simultaneous measurements from multiple locations have been

used to develop a deeper understanding of how particles are transported from the acceleration region and predict the resulting event severity at the location of interest.

The suprathermal particle population near the Sun is posited to provide the seed particles that are accelerated by solar eruptions to SEP energies. The origin and energy distribution of these seed particles are not well understood due to sparse measurements (Desai et al., 2016). New measurements from Parker Solar Probe and Solar Orbiter will increase understanding of this population, however this suprathermal population is known to change dynamically with solar activity. This implies that continuous monitoring of particle populations near the Sun is needed to fully characterize an SEP event that will reach Earth or a vehicle location.

Magnetic connectivity plays an extremely important role in particle access to a location of interest, particularly for the highest energy particles. Knowledge of the magnetic connection between the observer and eruption region can aid in whether an SEP event onset occurs promptly or the intensity rises more slowly. Magnetic connection models range from simple "ballistic" models that assume ideal Parker spiral fields down to the photosphere, to those based on global solar wind models such as ENLIL that in principle can allow for solar wind structures. Model coronal fields can also be incorporated to map changes in the connectivity close to the Sun. However, these are model-dependent and also influenced by the magnetograms used to construct the field. In addition to uncertainties in their predictions, it is also difficult to assess which type of model provides the most reliable estimates of the connectivity since the true connection point is unknown. Measurement gaps are similar to those reported in Section 5.1.4.

Radio measurements have been demonstrated to have forecasting value in predicting the intensity and likelihood of SEP events (Laurenza et al., 2018; Richardson et al., 2014). The lack of real-time space-based radio measurements precludes the use of such tools that have already been developed and could easily be transitioned to operations.

Required Measurements (maintain): Currently the following measurements are used to generate forecasts:

- **SEL SXR light curves** to provide flare onset timing, peak and duration.
- **SEL EUV disk imaging + VIS imaging >20 $R_\odot$ + Hα disk imaging.** Used to provide flare location in combination with SXR irradiance measurements from GOES.
- **SEL metric-decimetric radio spectra.** To detect Type II/III emission as proxies for eruptive activity.
- **In situ e- (0.1–1 MeV), p+ (0.02–700 MeV) and heavy ion measurements.** Electrons are used as a precursor of an ensuing heavier particle event. Proton intensity profiles are used for nowcasting and alerts (i.e., when 10+ MeV protons exceed a threshold). Composition is used to assess the coronal origin and seed population of the SEP.
- **Ground-based neutron measurements.** Used for detecting GLEs. As the most energetic and thus earliest arriving particles, GLEs can be used to inform nowcasts for intensity/fluence of the trailing particles, in association with the other measurements in this section.

Required Measurements (improve):

- **Distributed in situ P&F measurements at key locations to support cislunar (e.g., L1 + upstream, L4, L5), and Mars exploration (e.g., Sun–Mars L1, Earth-Mars space).** Consistent, co-temporal multipoint in situ observations within the inner heliosphere but tailored to cislunar and Mars exploration needs will lead to improved predictions from physics-based models thanks to more comprehensive constraints on their output. These measurements enable the mapping of the (large-scale) longitudinal distribution of SEPs at 1 AU with a finer-scale mapping of the cislunar-directed component from 0.2 AU upstream to provide both longer forecast horizon and improved intensity forecasts, as follows:
  - In situ measurements at Sun–Earth L1, with additional measurements from off-SEL locations, primarily west 20° to ~60° (L4) to map the magnetic connection to cislunar space, and east 20° to ~60° (L5) to characterize the SEP productivity of source regions rotating toward Earth. Past research of SEP events measured from multiple spacecraft indicate that SEP events on average have a 1σ Gaussian width of about +-45° around the ideal connection point (90° spread) (Lario et al., 2013). Continuous in situ measurements located at ±60° and at L1 will sample the full array of SEP events that affect Earth. Also, multi-spacecraft observations of STEREO, L1, and other spacecraft show a delay in particle arrival with increasing connection angle (Lario et al., 2017). These measurements indicate that a well-connected SEP event at L4 or L5 could give 30 min to a few hours warning of particle arrival at Earth.
  - Based on the results above, it is expected that additional in situ particle measurements significantly upstream of L1 (0.1- 0.3 AU from Earth), along or close to the nominal Parker spiral connection to cislunar space, could provide in clear improvements in forecasting horizon.
  - Mars-vicinity particle measurements. Human exploration needs will be covered by a measurement system similar to the one for the cislunar space described above. For example, techniques and models to forecast SEP fluxes using Sun–Earth L1 measurements may be adapted and retrained to provide forecasts specific to Mars, after a sufficient baseline of measurements has been accumulated at the Sun–Mars L1 point. These measurements can be supported by additional measurements on Mars-directed missions, crewed or uncrewed, to develop the scientific understanding of particle distributions/properties beyond 1 AU. Since this is a largely unexplored space, *specific measurement requirements, including optimal locations should be provided by a focused study on this issue*.
  - A focused study derived from the Parker Solar Probe and Solar Orbiter missions should be carried out to evaluate how measurements near the Sun and out of the ecliptic may benefit SWx prediction at Earth and Mars. Near-Sun measurements may improve the understanding of the role of particle seed populations and magnetic connectivity and particle transport processes near the Sun and in the solar wind in the SEP variability observed at Earth and elsewhere in the heliosphere.
  - Specific measurement requirements:
    - At Earth, expand the proton energy range to 1000 MeV.
    - e- (0.1–1 MeV), p+ (0.02–1000 MeV), ion composition up to 100s MeV/n including anisotropy, and suprathermal energies. *The latter to be deployed at a subset of the above locations, defined with targeted study.* To resolve the high-energy spectra, it is

necessary to have approximately 20 energy bins equally spaced in log space between 1 and 1000 MeV.
    - For Mars-focused payloads, the minimum requirements become e- (0.1–1 MeV), p+ (10–700 MeV); heavy ions are optional.
    - The measurements should be well calibrated, have limited contamination, not saturate at high intensities, and have low instrument backgrounds at high energies.
- **VIS coronagraph imaging to >20 $R_\odot$ + EUV disk to >1.5 $R_\odot$ imaging.** This measurement combination enables the tracking of the early CME/flare and shock development (kinematics, size, direction). The measurements can be used as inputs to shock/particle models and thus provide increased forecast horizon, particularly for high-energy particles (thought to originate when CME front is within 4–10 $R_\odot$). **Uninterrupted EUV-VIS FOV** required. **Off-SEL viewing** preferred for terrestrial *and* Mars SWx forecasts. The latter require large off-SEL angular separation (e.g., L4/5) because the magnetically connected footpoints for Mars lie generally behind the solar limbs, as viewed from Earth. A world-wide network of ground-based coronagraphs could potentially fill the gap between EUV and space-based coronagraphs (~1.5 to 2.5 $R_\odot$) and used as an early warning system for CMEs and SEPs (St. Cyr et al., 2017) but such an effort lies outside NASA's remit.
- **Measurements listed under the "improve" paragraph in Section 5.1.5.1.**
- **Measurements listed under the "improve" paragraph in Section 5.1.1.3.**
- **Same as the "improve" paragraph in Section 5.1.3.5.**

Required Measurements (advance):

- In situ P&F measurements angularly distributed at 1 AU (120° at ≤30° intervals), and radially distributed in the inner heliosphere (~0.3 –0.9 AU). Similar reasoning to the measurement set under the "improve" paragraph above with additional in situ particle coverage to probe the angular and radial distribution of SEPs.
    - In situ measurements within ±60° from SEL with ≤30° angular separation at 1 AU in the ecliptic (5+ locations). These measurements focus on understanding the longitudinal profile of SEP intensities and magnetic connectivity and finer scales that currently possible leading to definitive advances in physics-based models. They focus on cislunar space primarily with secondary support for Mars exploration when the planet is magnetically connected to these locations.
    - In situ particle measurements sunward from Earth to probe the radial evolution of SEP events. For obvious science return, the measurements should be distributed along or close to the nominal Parker spiral connection to cislunar with radial heliocentric coverage from ~0.3 to 0.9 AU. However, a focused feasibility study is required for deriving the optimal distribution, including the need, if any, for off-ecliptic locations, for these measurements. The study should take into account the findings from the Parker Solar Probe and Solar Orbiter missions on this aspect.
    - For support to Mars exploration SWx needs, particle measurements can be obtained from Mars-bound spacecraft, as discussed in the "improve" paragraph above, with details to be derived from targeted studies.
    - In situ P&F measurements should be included whenever possible on all satellites and spacecraft deployed throughout the heliosphere.
- **Measurements listed under the "advance" paragraph in Section 5.1.5.1.**

- **Measurements listed under the "advance" paragraph in Section 5.1.1.3.** VIS and EUV observations of the farside are especially relevant to Mars SWx needs, as discussed above.
- **Same as the "advance" paragraph in Section 5.1.3.5.**

Required Measurements (close):

- **In situ P&F measurements angularly distributed at 1 AU (180° at ≤20° intervals), and at the Mercury orbit (~0.3 AU).** Similar to the measurement set under the "advance" paragraph above but with higher angular resolution:
  - In situ measurements within ±90° from SEL with ≤20° angular separation at 1 AU in the ecliptic for a total of 8+ in situ locations. These measurements will clarify the fine-scale profile of SEP intensities while also measuring the medium-scale of transients such as CMEs and CIRs, thus filling in the gaps discussed in Sections 5.1.1and 5.1.4.
  - In situ particle measurements equally spaced in longitude along the orbit of Mercury will provide long-term measurements of "seed" particle populations and of the angular spread of SEP events near the Sun and will be able to measure without confusion SEP events closely space in time (more common during solar maximum). In combination with the 1 AU measurements, they will provide robust constraints for disentangling transport effects from injection effects—a long-standing issue in particle acceleration research.
- **Measurements listed under the "close" paragraph in Section 5.1.5.1.**
- **Measurements listed under the "close" paragraph in Section 5.1.1.3.**
- **Same as the "close" paragraph in Section 5.1.3.5.**

5.1.5.3. Onset Time Forecast

The SEP onset time forecast for protons with energies >10, >30, >50, >100 MeV are generally made post-eruption but pre-SEP. This also includes the threshold crossing time forecasts, which is generally used in operations.

Forecasting Status: For *onset time*, there are not many methods predicting the onset/crossing time and there has been limited validation work; therefore, there is limited knowledge on the status of onset time forecast accuracy.

Forecast lead time is defined as the time difference between the observed SEP onset/threshold crossing time and the forecast issue time. One forecasting method reports a forecast lead time for threshold crossings of about 4 h for >10 MeV protons and 1 h for >100 MeV protons (Núñez, 2015). Another method reports an average forecast lead time for threshold crossing of 88 min and 10 min for >10 and >100 MeV protons respectively (Bain et al., 2021).

Forecasting Requirement: As there are not many models predicting the SEP onset/threshold crossing time, there is not a clear requirement for the onset time and the main requirement is focused on the forecast lead time requirement described below. The desired onset time forecast accuracy should be an improvement for the current accuracy, with a mean error as low as possible.

An onset time forecast lead time of 30 min for prompt SEP events and 2 h for slower rising events is required for the decision to deploy and enter a storm shelter and EVA support; however, any

non-zero forecast lead time is beneficial. This requirement needs to be met for >10 MeV protons and >100 MeV protons.

Measurement Gaps: Measurement gaps are the same as those outlined in Section 5.1.5.2.

Required Measurements (maintain):

- Measurements listed under the "maintain" paragraph in Section 5.1.5.2.

Required Measurements (improve):

- Measurements listed under the "improve" paragraph in Section 5.1.5.2.

Required Measurements (definitive):

- Measurements listed under the "definitive" paragraph in Section 5.1.5.2.

Required Measurements (close):

- Measurements listed under the "close" paragraph in Section 5.1.5.2.

5.1.5.4. Peak Intensity Forecast

The SEP peak intensity forecast for protons with energies >10, >30, >50, >100 MeV provides an estimate of SEP event intensity and implicitly is also a post-eruption forecast of crossing thresholds (parameter 2 above).

Forecasting Status: There are currently only a few methods predicting the peak intensity and there has been limited validation work; therefore, there is limited knowledge on the status of peak intensity forecasts. One preliminary study reports a Mean Log Error (MLE) of -1.05 for >10 MeV protons and MLE = 2212−1.10 for >100 MeV (underforecasting) (NASA ISEP internal report AES-CHP-SW-001). Another method reports that over 80% of their peak intensity forecasts (for ~25 MeV protons) were within one order of magnitude of the observed intensity (Richardson et al., 2018).

Forecasting Requirement: A forecast accuracy of one order of magnitude (MLE between 0 and 1) for the peak intensity is required for the decision to deploy and enter a storm shelter and EVA support. The peak intensity forecast and time of the peak intensity are the most important forecast quantities needed in human space exploration.

Measurement Gaps: Measurement gaps are the same as those outlined in Section 5.1.5.2.

Required Measurements (maintain):

- Measurements listed under the "maintain" paragraph in Section 5.1.5.2.

Required Measurements (improve):

- Measurements listed under the "improve" paragraph in Section 5.1.5.2.

Required Measurements (definitive):

- Measurements listed under the "definitive" paragraph in Section 5.1.5.2.

Required Measurements (close):

- Measurements listed under the "close" paragraph in Section 5.1.5.2.

5.1.5.5. Intensity Profile Forecast

An SEP intensity time profile forecast for protons with energies >10, >30, >50, >100 MeV necessarily also incorporates forecasts for onset time, threshold crossing, peak intensity discussed in Sections 5.1.5.4, 5.1.5.3, and 5.1.5.2, event duration, fluence, and spectra.

Forecasting Status: The few methods that exist to predict SEPs intensity profiles focus on the > 10MeV and >100 MeV protons. Validation efforts are also few and rather incomplete given the small number of actual events in the last two cycles. SEPMOD, used operationally by NOAA, has a lead time of less than an hour with a Critical Success Index (True Positive / (True Positive + False Positive + False Negative)) of 0.70. Intensity profiles are also produced by physics-based models developed for scientific purposes but those require long computation times and may not yet be useful for operations.

Forecasting Requirement: The intensity time profile is the most important forecast overall, since all other forecast quantities can be derived from it. The forecasting requirement for intensity profile forecasts is not currently defined but is under investigation. The forecast requirement is related to general mission planning, launch support, and decision to leave shelter.

Measurement Gaps: Measurement gaps are the same as those outlined in Section 5.1.5.2.

Required Measurements (maintain):

- Measurements listed under the "maintain" paragraph in Section 5.1.5.2.

Required Measurements (improve):

- Measurements listed under the "improve" paragraph in Section 5.1.5.2.

Required Measurements (advance):

- Measurements listed under the "advance" paragraph in Section 5.1.5.2.

Required Measurements (close):

- Measurements listed under the "close" paragraph in Section 5.1.5.2.

5.1.6 Solar Irradiance

5.1.6.1. Solar Spectral Irradiance

The critical role played by short-wavelength solar irradiance in driving the upper atmosphere makes it an essential component of atmospheric models used to forecast radio propagation conditions, radar response, thermospheric drag, TEC, short-wave fadeouts and other space weather impacts.

Since these wavelengths are absorbed in the atmosphere, early modeling efforts came to rely on proxies for the solar short-wave flux that could be observed from the ground, such as sunspot number and F10.7 (the solar radio flux at 10.7 cm wavelength). Satellite measurements showed that the core-to-wing ratio of the 280 nm UV line of Mg II was a good proxy for solar EUV (Viereck et al., 2001). These proxies as well as the coronal plasma responsible for the short wavelength flux are associated with the magnetic fields driving solar activity. Hence, the use of photospheric magnetograms or selected EUV images to forecast these proxies and the EUV irradiance has shown considerable success (e.g., Henney et al., 2015; Fontenla et al., 2016).

Using a single proxy in complex atmospheric models to represent the impact of a highly variable spectrum covering 0.1–120 nm, produced by a wide range of disparate features in the solar atmosphere, will clearly be of limited efficacy. Reliable time-resolved measurements of the full spectrum would be preferable, but they must be uniform and guaranteed to be available over a long period of time if they are to be attractive to modelers. Thus, F10.7 has a daily history of over 60 years (e.g., Tapping, 2013), which enables modelers to tune their models to work well with F10.7 over a wide range of conditions. If a particular irradiance instrument is only going to be available for a few years, modelers may not deem it to be worth the substantial investment needed for a model to be "tuned" for a completely different data source.

The current operational resources providing 24-h coverage at high cadence are on NOAA's GOES-R series satellites (currently GOES 16 and 17). The GOES-R EXIS instrument has SXR bands for 0.05–0.4 and 0.1–0.8 nm and three grating spectrographs covering the wavelength ranges 25–31 and 117–141 nm at 0.6 nm resolution that are used to measure irradiances in seven spectral lines, and 275–285 nm that provides the Mg II index (Eparvier et al., 2009). One of the lines, Fe XV at 28.4 nm, is coronal.

NASA satellites provide additional resources. The EVE instrument on SDO covers 33–106 nm with a grating spectrograph at 0.1 nm resolution and 1-min cadence; unfortunately, another grating covering the corona-dominated range 5–37 nm failed in 2014. The SEE instrument on TIMED covers 27–194 nm at 0.4 nm resolution but is limited to 3% time coverage. The LYRA instrument on ESA's Proba-2 satellite incorporates diamond detectors with four broad channels covering 6–20, 17–80, 120–123 (Ly-α), and 190–222 nm. ESA also operated the SolACES instrument on the ISS until 2017, providing four bands at 16–58, 32–100, 40–150, and 115–226 nm.

Forecasting Status: <7 days forecast horizon.

Forecasting Requirements: There are both specification and forecasting requirements. The specification requirement is to provide enough information such that (the wide range of ionospheric and thermospheric) models can calculate the effects on the atmosphere. Calculation of thermospheric expansion requires specification of the heat input to the thermosphere over a period of time. There

are short-term forecasting needs, e.g., to plan for long-range VHF aviation communications and radar operations on a timescale of days, as well as longer-term needs such as satellite drag forecasts needed to plan station-keeping maneuvers weeks or months ahead.

EUV spectral irradiance: Minimum requirement is the EUV spectrum (5–120 nm) with 5 nm resolution, at 30 s cadence, with 30 s latency, and accuracy of 20% maintained for over 10 years of satellite life. *EUV irradiance horizon:* 72 h to 10 days (the requirement encompasses the thermospheric density forecast requirements from LEO [7-day] to GEO [10-day] and collision avoidance [72 h]).

Measurement Gaps: With the current resources listed above which do not measure the full 0.1- to 125-nm spectrum, specification relies on modeling effectively to reproduce the full spectrum using the limited measurements available (e.g., Thiemann et al., 2017; Thiemann et al., 2019). Measurement of the full spectrum is lacking. One of the obvious gaps in observational coverage has been the range from 1 to 6 nm containing many hot lines; this range can be modeled if there is coverage in the 6–36 nm range with sufficient wavelength resolution, but actual data would be preferable.

For forecasting purposes, one needs to be able to understand the relationship between levels of solar activity and the content of the irradiance spectrum, and use this relationship together with short- and long-term forecasts of activity to predict the time variation of the irradiance. There has been work on understanding this relationship, but not with the full spectral range available. Solar activity forecasts are addressed elsewhere in this report.

The question of what spectral resolution is needed for EUV irradiance has been addressed several times. Solomon & Qian (2005) used 22 spectral bands to cover the range from 0.05 to 105 nm, and 5-nm bands are often used from 105 to 175 nm (e.g., Torr et al., 1979). Ly-α at 121.6 nm is bright enough to be singled out for its own band (Woods et al., 2000). Spectral breakdown similar to this pattern is common for modeled irradiance used in atmospheric models, but the spectral resolution is inadequate for use in scientific research that can improve understanding of atmospheric driving since it is not adequate to resolve individual spectral lines.

Required Measurements (maintain):

- **Limited measurements of SXR fluxes and EUV/UV spectral line data.** The EUVS measurements of seven spectral lines (He II 25.6 and 30.4 nm, Fe XV 28.4 nm, C III 117.5 nm, H I 121.6 nm, C II/Si IV/O IV blend at 140.5 nm, and Mg II at 280 nm) and SXR measurements made by the GOES-R weather satellites are expected to continue until 2035. Other instruments currently in space are getting old, e.g., it is not clear how much longer the 27–194 nm spectra at 0.4 nm resolution from TIMED/SEE will continue to be available from the 20-year-old satellite.
- Degradation is a major issue for EUV instruments in the harsh environment of space, and calibrated irradiance measurements have to take this into account: regular rocket underflights carrying identical instrumentation are one method to achieve this.

Required Measurements (improve):

- **More complete spectral coverage of the coronal EUV range.** Restoration of the full spectral coverage initially provided by the SDO/EVE instrument (5–106 nm at 0.1-nm resolution).

- **1-to 6-nm SSI measurements.** The wavelength range covers the hot corona variations that impact the D-layer and radio communications. This part of the spectrum is largely unexplored with significant research and SWx discovery potential.
- **Off-SEL SSI measurements**. Measurements of spectral irradiance in key bands, such as MgII, Ly-α, and 27–35 nm, from vantage points eastward of the SEL will extend the forecast horizon from 3 days to 7 days (for L5 observations) or longer.
- **LOS photospheric field (B_{phot}) measurements over >50% of the solar surface.** Expanding the coverage from the current ~⅓ to ½ of the solar surface will improve the fidelity of the irradiance models that use magnetic field inputs and provide a reliable alternative to direct SSI measurements, if those are unavailable. High priority should be given to **B_{phot} measurements over the eastern limb** because (1) information on farside flux emergence and AR evolution is the only way to significantly improve forecast skill and (2) magnetic field measurements from these locations are currently the least dependable.

Required Measurements (advance):

- **Complete coverage of the variable component of the Sun's short-wavelength spectrum.** Provision of full spectral coverage: 0.1–125 nm at 0.1-nm resolution, 125–200 nm at 1-nm resolution. The shorter wavelengths need higher spectral resolution at least to Ly-α at 122 nm because there is much more variability with solar activity at the wavelengths dominated by coronal lines, whereas the spectrum at wavelengths longer than 125 nm have less variability over the solar cycle and can be specified adequately at lower resolution.
- **Full-disk spatially resolved SSI measurements.** Understanding the sources of SSI has been a long-sought objective in heliophysics. Acquiring precisely calibrated images of the Earth-facing disk in multiple wavelengths between 5 and 200 nm, will provide important validation and fine-tuning information to all atmospheric models while simultaneously making inroads in measuring the energy flux through the solar atmospheric layers.

Required Measurements (close):

- **Full spectrum SSI measurements (0.1–200 nm at 0.1 nm resolution).** The measurements should be taken with the required accuracy (<20%) over solar-cycle time scales. These dataset will take atmospheric modeling to the next level by providing a detailed description of the solar inputs across most SWx-relevant ionosphere–thermosphere–mesosphere heights, with sufficiently long duration and quality to fine-tune and validate the models.
- **Robust network of systems providing uniform and assured data availability.** Guaranteed long-term provision of full spectral coverage with identical instruments on multiple platforms with a quasi-regular launch sequence to avoid the possibility of a single-point failure. This is necessary to persuade modelers to make the research investment needed to adapt their models to make use of the full spectral information.

5.2 Geospace Observables

5.2.1 Solar Energetic Particles (SEPs)

In general, SEPs pose a threat to spacecraft via ETD and SEE hazards. For crewed missions, SEPs pose a radiation threat to astronauts on stations and vehicles throughout the heliosphere (including

the lunar and Martian surfaces). Specific to geospace, SEPs also represent a significant energy input to the D-region ionosphere and a radiation hazard to passengers and crew on aircraft in flight on polar routes. SEP access to Earth's magnetosphere and ionosphere is complicated by the state of the geomagnetic field at the time of SEP arrival (e.g., O'Brien et al., 2018; Chen et al., 2020). SEPs have access to different magnetic latitudes (and thus L-shells in the inner magnetosphere) dependent on the level of geomagnetic activity; in general, more active geomagnetic conditions correspond to SEP accessibility to lower magnetic latitudes and L-shells in the magnetosphere-ionosphere system.

Measurement Method: SEPs in geospace and on crewed stations, vehicles, and extravehicular suits can be monitored using dosimeters, which provide a crude yet effective measure of SEP intensity as a function of energy (integral only) and an accurate measure of contribution to ETD. They can also be measured by solid-state detectors (e.g., in a telescope configuration), which provide details of SEP composition (differentiating electrons, protons, and various heavy ion species) and differential intensity energy spectra. These are in situ measurements made from satellite observatories.

Current Status: Currently, the following provide knowledge of SEPs in Geospace: REACH dosimeters in LEO, POES/MetOp environmental sensors in LEO, GPS dosimeters in MEO, GOES Space Environmental Monitors-Energetic Particle Sensors (SEM/EPS) in GEO, TWINS environmental sensors in molniya-HEO, dosimeters on crewed vehicles (e.g., ISS, Orion capsule). Of those, only a subset are available for use in real time: GOES. GPS, TWINS, and REACH data are restricted access, but NASA and NOAA may negotiate with the respective owners of those data for access, including some available for near-real-time use. POES/MetOp have been discontinued, so when those existing spacecraft are no longer operational, we will lose that valuable source of SEP data at LEO.

Forecasting Requirements: See Section 5.1 for SEP event forecasting in general (in particular, the benefit to forecasting SEP events of a solar monitor at the Sun–Earth L4 Lagrange point). For nowcasting and forecasting accessibility of SEPs throughout the inner magnetosphere, a combination of SEP-capable observatories in polar LEO plus higher altitude orbits (e.g., MEO-GPS, GEO) are required. Specific to forecasting, observations contributing to forecasts of the state and evolution of the global magnetospheric B-field are required, since the magnetic field configuration (including open-closed field boundary) ultimately dictates SEP accessibility. To advance the science of space weather concerning SEP access to the inner magnetosphere, the composition and differential intensity energy spectra of SEP events are critical details for better understanding and quantifying the threat posed by SEP events. Considering astronaut health: *all* crewed vehicles, stations, and extravehicular suits should be equipped with radiation monitors (at least dosimeters) to characterize the radiation threat to astronauts, including that from SEPs.

Measurement Gaps:

Partial gaps: TWINS and REACH data are potentially available, though NASA would need to negotiate with the owners of those datasets for access to them.

Partial gap for ionospheric D-region absorption: Atmospheric EPP losses of SEPs represents a partial measurement gap of medium priority.

Full gap: Composition and differential intensity energy spectra of SEPs around all MLT from polar LEO.

Critical full gaps: SEP monitors on all crewed stations and vehicles (including polar aircraft, though not within the scope of this analysis) and EVA equipment.

Required Measurements (maintain): Coverage like that from the following SEP observatories in the inner magnetosphere should be maintained:

- **GOES SEM/EPS at GEO**
- **GPS dosimeters at MEO**
- **REACH dosimeters at LEO**

Required Measurements (improve):

- **Improved LEO and MEO coverage**, particularly composition and differential energy spectra to complement the dosimeter networks and GOES data. LEO observations with better composition and differential energy spectra will also be beneficial to modeling and quantification of SEP impact on the D-region ionosphere and contribution to D-region absorption.

Required Measurements (definitive):

- **Any subset of one or more of the "close" requirements identified below.**

Required Measurements (close): Coupled with the closure requirements for SEPs defined in Section 5.1, to close the requirements for nowcasting/forecasting of SEP accessibility throughout the inner magnetosphere and their impacts on the D-region ionosphere, the following observations would be necessary:

- **Solar and SEP monitor at the Earth-Sun L4 point**
- **Comprehensive network of SEP monitoring observatories at all MLT in polar LEO**
- **Comprehensive network of SEP monitoring observatories around all MLT at GEO**
- **Maintained network of SEP monitors on GPS constellation in MEO**
- **In addition to a broader network of distributed dosimeters (e.g., GPS, REACH), a subset of observatories with knowledge of SEP composition and differential intensity energy spectra (e.g., GOES SEM/EPS) distributed throughout the LEO, MEO, GEO network would bolster the science and understanding of SEPs contributing to space weather hazards throughout the inner magnetosphere and ionosphere (and polar atmosphere).**

5.2.2 Radiation Hazards in the Lunar Environment

With NASA's intentions to return astronauts to the Moon within the next several years, it is important here to also include the observational gaps relevant to space weather unique to the lunar environment. As a body without an atmosphere or strong, internally driven magnetic field in an orbit that spends most of the time (~25 days per lunar month, or ~85% of time) in the solar wind and the additional time transiting Earth's magnetotail at ~60 R_E geocentric distance, the lunar space weather environment represents a special case. Of highest significance to space weather in the lunar environment are solar hazards such as SEPs (including CME-SEPs; see Section 5.1.5), flares, and SRBs plus additional radiation hazards from cosmic rays and the secondary radiation produced

from cosmic rays interacting with lunar materials (e.g., spallation nuclei, albedo neutrons and albedo neutron decay products: high-energy electrons and protons). Also of noteworthy interest are bursts of energetic (several keV to several MeV) electrons in Earth's magnetotail, but those are not considered a high priority due to frequency of occurrence and relatively low impact as a radiation hazard (i.e., surface charging, internal charging, and ETD).

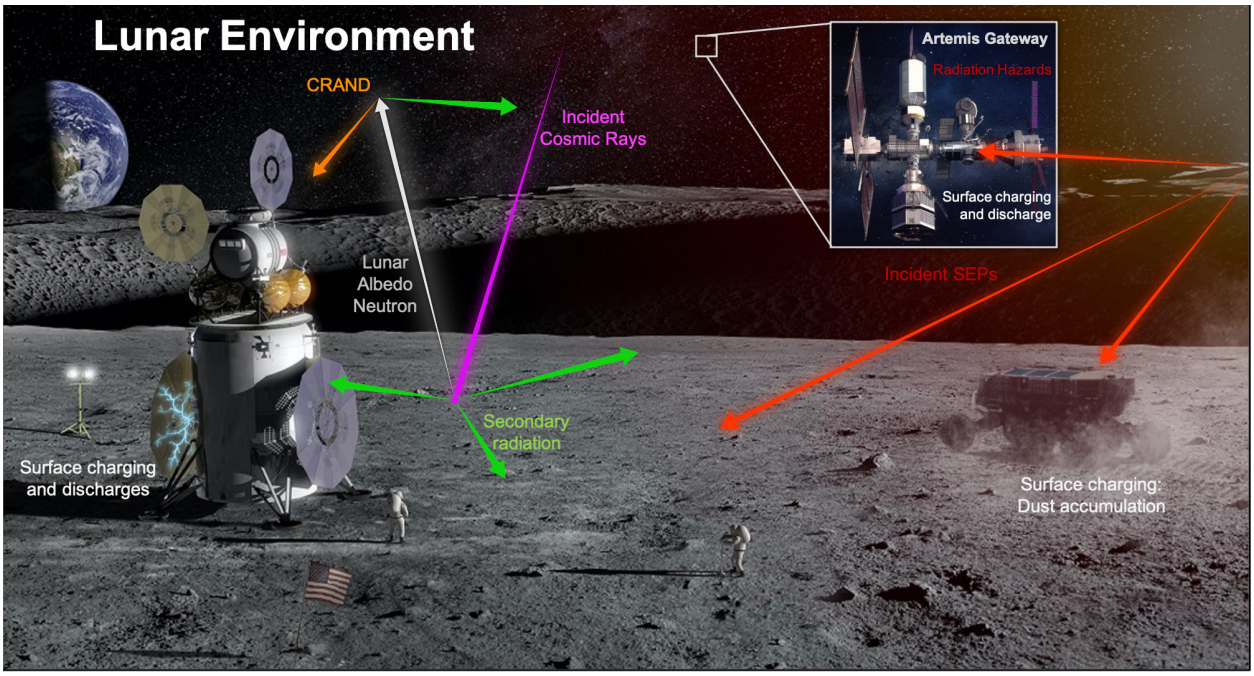

Figure 5-15. The lunar space weather environment.

Measurement Method: These are in situ measurements made from satellite observatories or monitors on the lunar surface. For solar observations, see sections above concerning SEPs, CMEs, solar flares, and SRBs.

Current Status: Cosmic rays at the Moon are currently being observed by NASA's CRaTER instrument suite on the Lunar Reconnaissance Orbiter (LRO). Lunar albedo neutrons are observed by China's CHANG-E-4 lander and were also observed by NASA's Apollo missions. Thus, access to current neutron data would involve negotiations with the relevant authorities in China, while historical Apollo data may be used as a baseline. TWINS observations in HEO provide some knowledge of SEP access to vehicles in transit to the Moon (lunar transfer orbit [LTO]), though those data are not openly available.

Forecasting Requirements: For solar hazards (SEPs, CMEs, flares, SRBs), see the corresponding details in Section 5.1. With commitment to return astronauts to the Moon this decade, knowledge of the radiation environment (now/forecasting SEP, CME, and flare events; now/forecasting of communication loss/disruption from SRBs; and climatology models of cosmic ray neutron and secondary environment around low lunar orbit [LLO] and the lunar surface) are of very high priority.

The intensity, spectra, and time variability of cosmic rays and cosmic ray secondaries are relatively well understood and predictable on long-term timescales (excluding Forbush decreases associated with solar wind transient events), but there are gaps (see next paragraph) in the datasets needed for

development of good climatological datasets for use in crewed operations in the lunar environment and mission design and planning.

Measurement Gaps: See Section 5.1 for gaps pertaining to operational hazards of solar origin in the lunar environment, including SEPs (highest priority considering astronaut health), CMEs, flares, and SRBs. The Cosmic Ray Isotope Spectrometer onboard the Advanced Composition Explorer (ACE/CRIS) measures GCR nuclei from ~100 to 500 MeV/nucleon, covering the peak of the energy spectrum for most isotopes. This data set has been used to calibrate GCR models and to determine the level of solar modulation of cosmic rays throughout the solar cycle (Slaba & Whitman, 2020; Matthiä et al., 2013). ACE/CRIS has been operating since 1997 and its replacement, IMAP, will measure ions up to 40 MeV/nucleon. This energy is too low to accurately track GCR modulation; therefore, there will be a gap for GCR measurements after ACE/CRIS is retired.

The current status of observations of lunar albedo neutrons and other secondary radiation renders those observations as a *partial gap of medium priority considering their significance to astronaut health and ETD*. It is important to note that the cosmic ray albedo neutrons and secondaries have a spatial- and energy-dependence in intensity relative to the lunar surface. Any successful model to quantify these radiation hazards (ETD) should recognize those dependencies and quantify them using observations from throughout a range of affected LLO altitudes and on the lunar surface.

Required Measurements (maintain):

- **Cosmic ray and radiation monitoring in the lunar environment from NASA's LRO/CRaTER**
- **Measurement of ions from 100 to500 MeV/nuc, similar to those provided by ACE/CRIS**
- **Radiation monitors on all crewed spacecraft, vehicles (including surface rovers), and stations**

Required Measurements (improve):

- Any one or more of the requirements in "close" below.

Required Measurements (definitive):

- Any one or more of the requirements in "close" below.

Required Measurements (close):

- **Solar measurements at Earth-Sun L4 point enabling more accurate now/forecast of SEPs, CMEs, solar flares, and SRBs (see Section 5.1.5)**
- **Cosmic ray albedo neutron and secondary radiation monitors around LLO and on the lunar surface**
- **Measurement of energetic electrons (~keV to ~MeV) around LLO and on the lunar surface; these electrons can pose a risk to spacecraft charging (surface, hybrid, and internal).**

5.2.3 Solar Wind in Peri-geospace

Awareness of the state of the solar wind at the magnetopause is of the utmost criticality for quantifying the driving conditions acting upon Earth's magnetosphere-ionosphere-thermosphere system, where the overwhelming majority of space weather hazards occur. Monitors of the Sun and solar wind at the Sun–Earth L1 point are of immense value, particularly as early warning systems and monitors of near-side solar conditions, but there are significant errors in propagation of solar wind quantities from observations at L1 to the subsolar bow shock and magnetopause. In particular, there is non-trivial error in the arrival time of solar wind structures (e.g., pressure pulses, velocity ramps, IMF rotations) and most critically in the IMF orientation using propagated data from L1. Those errors propagate through the various magnetosphere, ionosphere, and thermosphere models that rely on solar wind data at Earth's subsolar magnetopause as inputs and contribute nonlinearly to error on those models' output quantities.

Here, we refer to the space environment in the immediate vicinity of Earth's dayside magnetopause and bow shock (i.e., within a few tens of R_E; much closer to Earth than L1 and inside of lunar orbit) as peri-geospace (meaning around geospace). This is important to distinguish since there is a coherency scale of around 20–40 R_E in the solar wind, above which the average size of coherent solar wind flux tubes (~50–70 R_E) plus the spatiotemporal evolution in the turbulent medium begins to result in significant differences in observations of the plasma made at two different points (e.g., at the Sun–Earth L1 point versus just upstream of the subsolar bow shock). For examples of this, see Borovsky, 2017; Walsh et al., 2019; Burkholder et al., 2020, and references therein. While large-scale structures (e.g., CMEs) may be accurately captured, at other times the solar wind observed at L1 and closer to Earth can be completely different for up to hours at a time (e.g., see Figures 3–6 in Ashour-Abdalla et al., 2008) However, one must be careful with such observations in peri-geospace, particularly as inputs in solar wind driven models, since the nonlinear kinetic processes in the ion foreshock region must be considered and accounted for.

Measurement Method: These are in situ measurements made from satellite observatories; see Section 5.1.4.

Current Status: Considering that NASA's THEMIS/ARTEMIS and MMS missions each provide some knowledge of the solar wind conditions immediately upstream of the bow shock for only part of each month (ARTEMIS at 60 R_E) and year (~½ year from THEMIS and MMS), this is currently a partial observational gap. None of those missions' data are available in near real time; each mission has at least ~1-day delay in data availability.

Forecasting Requirements: The following quantities are required as inputs for models producing both nowcasts (within the last 5 min, including space situational awareness) and forecasts of the magnetosphere-ionosphere-thermosphere systems and all of the space weather hazards excluding SRBs. Required input quantities: solar wind plasma density, ion composition (at least protons and alphas), velocity, temperature (at least protons), pressure (thermal and dynamic pressures can be derived from other quantities listed here), plus energetic particle intensities, and IMF vector. These required observations and measurements are essentially the same as those described in Section 5.1.4 above for the solar wind structure, only within ~20 R_E of Earth's subsolar bow shock, there will be little to no error from propagation delay and spatiotemporal evolution of the turbulent solar wind.

Measurement Gaps: Due to the criticality of knowledge of the solar wind conditions (most importantly, Vx, density, proton temperature, and IMF components and magnitude) to all modeling of the magnetosphere-ionosphere-thermosphere system, *this is classified as a high-priority, partial observational gap*.

Required Measurements (maintain):

- **Solar wind observations from NASA's THEMIS/ARTEMIS and MMS missions**

Required Measurements (improve):

- **Reduced latency in availability of data from NASA's THEMIS/ARTEMIS and MMS missions**

Required Measurements (definitive):

- Same as "close" below

Required Measurements (close):

- **A constellation of spacecraft in orbits enabling continuous, real-time observations of critical solar wind quantities (i.e., plasma density, composition, velocity, temperature, pressure, plus energetic particle intensities, and IMF vector) in the solar wind within 10 R_E of the bow shock.**

5.2.4 Plasma Sheet Electrons and Injections into the Inner Magnetosphere

Energetic (~keV to ~MeV) electrons in Earth's magnetospheric plasma sheet that makes up the near-equatorial magnetotail and higher L-shells (L > ~6 to ~8) around the inner magnetosphere pose a threat to spacecraft via surface, subsurface/hybrid, and internal charging and destructive discharge. Auroral precipitation from the plasma sheet also contributes to F-region ionospheric density variability and gradients (see Section 5.2.8). Intensities of plasma sheet electrons are highly variable over a range of time scales down to seconds. Also, the plasma sheet boundaries move suddenly and dynamically with changes in solar wind and magnetospheric conditions. Of particular interest concerning space weather are sudden injections of plasma sheet electrons into GEO and MEO orbital ranges. Currently, there are no good systems in place to forecast such injections or plasma sheet variability, and there is an insufficient number of observatories around the magnetospheric system for nowcasting and space situational awareness of this environmental hazard.

Measurement Method: Energetic electrons in the keV to MeV range can be measured using electrostatic analyzers and instruments incorporating solid-state detectors. Charge-discharge sensors can also be used to measure the consequences of these electrons on and within spacecraft systems. These are all in situ measurements made from satellite observatories.

Current Status: Observations of plasma sheet electrons and energetic electron injections are currently available from the GPS constellation (dosimeters), GOES and LANL satellites around GEO, and NASA's THEMIS and MMS spacecraft. Of those, only GOES are available in near real time. GPS and LANL-GEO data are not openly available in real time. There is at least ~1-day latency

on the availability of MMS and THEMIS data, and the availability of those missions for plasma sheet and injected electrons are also dependent on the orbital motion of those spacecraft.

Forecasting Requirements: The following are required: (1) an accurate nowcast (within the last 5~10 min) of the magnetosphere system detailing the current, 3D state and extent of the plasma sheet and dipolarizations, fast flows, and energetic particle injections throughout the system; (2) an accurate forecast out to at least 2 h of the same system behavior, and in particular the probability of occurrence of a sudden increase or decrease in keV to 100s keV electron flux at any particular location due to plasma sheet motion or injections.

Solar wind conditions at the bow shock (see Section 5.2.3) and real-time geomagnetic index data (particularly AL; not in scope for this analysis) are critical for nowcast and forecast models of plasma sheet electrons. Nowcasting and forecasting may be achieved using data assimilative and/or ingestive models using near-real-time observations of plasma sheet electrons and other relevant quantities (e.g., B-field) throughout the magnetosphere. Crude forecasting (e.g., probability of event occurrence) may also be achieved using climatological models of energetic particle injections as a function of electron energy and location (L-shell, MLT).

Measurement Gaps:

For internal charging hazard: Plasma sheet electrons >100 keV: partial gap, medium priority. Localized injections of >100 keV plasma sheet electrons at GEO and MEO: partial gap (because of the partial coverage from GPS, LANL-GEO, GOES, THEMIS, and MMS) of medium priority.

For surface and subsurface/hybrid charging hazard: Plasma sheet electrons >100 keV: partial gap, high priority. Localized injections of >100 keV plasma sheet electrons at GEO and MEO: partial gap (because of the partial coverage from GPS, LANL-GEO, GOES, THEMIS, and MMS) of high priority.

Required Measurements (maintain):

- **~keV to ~MeV electron differential intensity observations from GOES, THEMIS, and MMS data**

Required Measurements (improve):

- **Accessibility to GPS and LANL-GEO observations in near real time**
- **Reduced latency on observations from THEMIS and MMS**
- **Additional observations measuring ~keV to ~100s keV electrons and protons around more MLT at GEO**

Required Measurements (definitive):

- **The above "improved" requirements plus any one or more of the following "close" requirements**

Required Measurements (close):

- **At least one observatory measuring ~keV to ~MeV electrons per MLT-hour around GEO**
- **~keV to ~MeV electron differential intensity observations from a high-inclination MEO constellation like GPS**
- **~keV to ~MeV electron differential intensity observations from a network of near-equatorial HEO spacecraft (like THEMIS and MMS but with apogees inside of ~10 R_E geocentric distance) spaced around several MLT**

5.2.5 Ring Current

Observational knowledge of the real-time state of Earth's ring current is of value concerning GICs and surface/subsurface/hybrid charging and destructive discharge hazards. EPP of ring current particles also affect the E-region ionosphere and can contribute to transient E-region disturbances (see Section 5.2.8). Like the plasma sheet, the intensities of electrons, protons, and heavier ions comprising Earth's ring current vary suddenly and dynamically, responding nonlinearly to changes in solar wind and geomagnetic conditions. The radiation environment in LEO is complicated by temporal variation as well as latitudinal (L-shell), longitudinal, and altitude dependencies within the atmospheric loss cones at <~1300-km altitude.

Measurement Method: Ring current electrons, protons, and heavier ions (~keV to ~100 keV) are measured using electrostatic analyzers and energetic particle detectors that can be combined with time-of-flight systems for species identification for composition. These are in situ measurements made from satellite observatories.

The ring current can also be monitored using remote sensing instruments such as energetic neutral atom (ENA) imagers (e.g., McComas et al., 2009). Such ENA imaging are also satellite-based observations.

Current Status: Currently, there are no in situ or remote sensing observatories providing measurements of Earth's ring current electrons, protons, or heavier ions. Previously, NASA's Van Allen Probes provided the full set of relevant observations from two spacecraft in GTO-like orbits, but those left a partial gap considering a lack of simultaneous knowledge over all MLT. GOES MAGED/MAGPD at GEO provide very limited partial coverage of only the highest energies, but it is not considered as partial gap coverage considering the extent of the ring current across a range of L-shells and distribution of the ring current around MLT (e.g., partial ring current). At LEO, POES, MetOp and several CubeSats (FIREBIRD-II, AC10, ELFIN, and soon CIRBE and REAL) currently offer some knowledge of the precipitation environment around LEO with varying levels of coverage and latency.

Forecasting Requirements: The following are required: an accurate nowcast (within the last 5~10 min) of the inner magnetosphere system detailing the current, 3D state, intensity, and extent of the ring current; and an accurate forecast out to at least 2 days' time of the same system behavior, particularly ring current intensification and the probability of occurrence of a geomagnetic storm.

Solar wind conditions at the bow shock (see Section 5.2.3) and real-time geomagnetic index data (particularly SymH or D_{st}; not in scope for this analysis) are critical for nowcast and forecast models of Earth's ring current. Nowcasting and forecasting may be achieved using data assimilative and/or ingestive models using near-real-time observations of ring current plasma and other relevant quantities (e.g., B-field) throughout the inner magnetosphere; considering the importance of the ring current for global magnetospheric dynamics and in magnetosphere-ionosphere coupling, such a data-informed modeling capability should likely prove to be of high value. Crude forecasting (e.g., probability of event occurrence of ring current enhancements above critical thresholds, for example) may also be achieved using climatological models of ring current populations as a function of particle energy and location (L-shell, MLT, MLat).

Measurement Gaps:

For GICs: Full gap, low priority (this can be monitored remotely from ground-based magnetometers)

For surface and subsurface/hybrid charging: Full gap, high priority

For ionospheric E-region EPP: Partial gap (some partial coverage from POES, MetOp, and CubeSats around LEO), medium priority

Required Measurements (maintain):

- Maintain GOES MAGED/MAGPD at GEO.

Required Measurements (improve):

- **Additional observations measuring ~keV to ~100s keV electrons and protons around more MLT at GEO**

Required Measurements (definitive):

- **The above "improved" requirements plus any one or more of the following "close" requirements**

Required Measurements (close):

- **In situ ring current observations (differential intensities of ~10 eV to ~100 keV electrons, protons, and heavier ions) from multiple, near-equatorial GTO spaced around several MLT and from several MLT at GEO**
- **Global imaging and pitch angle and energy distributions of the ring current with high resolution (pixel resolution of <1000 km projected onto the equatorial or meridional planes) from remote sensing**

5.2.6 Radiation Belts

5.2.6.1. Outer Radiation Belt

Earth's outer radiation belt electrons (100s keV to ~10 MeV) pose a threat to spacecraft via radiation ETD and subsurface/hybrid and internal charging and destructive discharge hazards. Outer belt electrons also contribute to EPP that affects the ionosphere via increased conductivity (contributing factor in GICs), D-region absorption and transient E-region disturbances (see Section 5.2.8). EPP of radiation belt electrons into Earth's atmosphere also affects thermospheric heating and cooling (see Section 5.2.9) via production of HOx and NOx (odd-reactive hydrogen and nitrogen, respectively). Intensities of outer belt electrons vary suddenly and dynamically, responding nonlinearly to changes in solar wind and geomagnetic conditions; intensities throughout the outer belt can change by over three orders of magnitude over periods ranging from tens of minutes to a few hours in both sudden enhancement and depletion events. The radiation environment in LEO is complicated by temporal variation as well as latitudinal (L-shell), longitudinal, and altitude dependencies within the atmospheric loss cones at <~1300-km altitude.

Measurement Method: Energetic electrons in the 100s of keV to ~10 MeV range can be measured using instruments incorporating solid-state detectors and dosimeters. Dosimeters provide crude proxies for electron intensities and only integral spectral information, but they provide a direct measurement for ETD and electron penetration of spacecraft shielding and materials. Solid-state detectors provide individual electron counts used to derive differential intensity energy spectra required for higher-fidelity models of the system and adverse effects. Charge-discharge sensors can also be used to measure the consequences of these electrons on and within spacecraft systems. These are all in situ measurements made from satellite observatories.

Current Status: Currently, there are no in situ observatories providing comprehensive measurements of Earth's outer radiation belt electrons throughout the full system. Previously, NASA's Van Allen Probes provided the full set of relevant observations from two spacecraft in GTO-like orbits, but those left a partial gap considering a lack of simultaneous knowledge over all MLT. GOES at GEO provide very limited partial coverage of only the highest energies at the outer edge of the outer belt, but it is not considered as partial gap coverage considering the extent of the outer belt across a range of L-shells (~$2.7 \leq L \leq 7$), peak intensities located well inside of GEO, and distribution of relevant wave environments around MLT. GTOSat is a 6U CubeSat pathfinder mission in development (launch expected ~2022) that might provide some partial coverage for this gap. At LEO, POES, MetOp and several CubeSats (FIREBIRD-II, AC10, ELFIN, and soon CIRBE and REAL) currently offer some knowledge of the radiation environment around LEO with varying levels of coverage and latency.

Forecasting Requirements: The following are required: an accurate nowcast (within the last 5~10 min) of the inner magnetosphere system detailing the current, 3D state, intensity, and extent of the electron radiation belts; and an accurate forecast out to at least 2 days' time of the same system behavior, particularly sudden intensifications and depletions of radiation belt electrons throughout the outer belt and slot region.

Solar wind conditions at the bow shock (see Section 5.2.3) and real-time geomagnetic index data (particularly AE, AL, D_{st}, and K_p; not in scope for this analysis) are critical for nowcast and forecast models of the outer radiation belt electrons. Nowcasting and forecasting may be achieved using data assimilative and/or ingestive models using comprehensive, near-real-time observations of outer belt electron populations and other relevant quantities (e.g., B-field, chorus waves, electromagnetic ion cyclotron [EMIC] waves, and hiss waves) at L-shells throughout the outer belt and distributions around MLT. Climatological models of outer belt electron populations as a function of energy and location (L-shell, MLT, MLat) and conditions (e.g., indices) already exist and are used routinely for spacecraft design.

Measurement Gaps: In general for nowcasting and forecasting, observations of full energy (100 keV ≤ E ≤ 10 MeV) and pitch angle distributions of electrons plus critical wave modes (at least EMIC, plasmaspheric hiss, and whistler-mode chorus) from a system of observatories distributed around all MLT are needed to accurately now/forecast the electron radiation belts. However, since the decommissioning of NASA's Van Allen Probes in 2019, no such system is even partially available. GOES provides information at the outermost edge of the outer belt, which is of value primarily for the GEO environment only. CubeSats in LEO provide only details within the atmospheric loss cones. NASA's GTOSat is a pathfinder CubeSat mission that may partially fill this observational gap by 2024, but only with a single-point and partial energy and waves coverage.

For GICs: EPP observations at LEO is a partial gap (POES, MetOp, CubeSats) of high priority.

For ETD: Full gap, low priority (effective climatological models exist).

For internal charging: Full gap, high priority.

For subsurface/hybrid charging: Full gap, high priority.

For thermospheric expansion: Partial gap (some partial coverage from Swarm and GRACE-FO), medium priority.

For ionospheric E-region transient disturbances: EPP of radiation belt electrons represents a partial measurement gap (some partial coverage from POES, MetOp, and CubeSats around LEO) of medium priority.

For ionospheric D-region absorption: EPP of radiation belt electrons represents a partial measurement gap (some partial coverage from POES, MetOp, and CubeSats around LEO) of medium priority.

Required Measurements (maintain):

- **GOES 10s keV to several MeV electron observations at GEO.**

Required Measurements (improve):

- **Additional observatories measuring the radiation belt EPP in the LEO environment at a range of altitudes (~300 km ≤ alt ≤ 1300 km), all geographic longitudes, and geographic latitudes up to at least ~75°.**

Required Measurements (definitive):

- **Additional observatories measuring differential intensity energy spectra and angular distributions of 10s of keV to multiple MeV electrons and chorus, EMIC, and hiss waves near the magnetic equator ranging from 2.5 ≤ L < 8.**

Required Measurements (close):

- **Continuous ≤100 km spatial resolution, real-time data transmission monitoring ring current and radiation belt EPP in the LEO environment at a range of altitudes (~300 km ≤ alt ≤ 1300 km), all geographic longitudes, and geographic latitudes up to at least ~75°.**
- **Multipoint observatories simultaneously measuring differential intensity energy spectra and angular distributions of 10s of keV to multiple MeV electrons and chorus, EMIC, and hiss waves near the magnetic equator ranging from 2.5 ≤ L < 8 spaced in at least 6 MLT sectors spanning 24-h MLT and phased to enable full radial distributions of the outer belt electrons at least once per hour.**

5.2.6.2. Inner Radiation Belt

Earth's inner radiation belt consists of 100s of keV to >1 MeV electrons and 10s of MeV to >GeV protons and heavier ions that pose a threat to spacecraft via radiation ETD, SEE, and internal and subsurface/hybrid charging and destructive discharge hazards. Inner radiation belt protons and heavy ions with energies >10 MeV can penetrate spacecraft shielding and result in SEE. Transient electron populations of 100s of keV to >1 MeV electrons may also suddenly flood the slot region between the inner and outer belts and then decay over several days during active geomagnetic conditions. These radiation populations also contribute to EPP that affects the ionosphere via increased conductivity (contributing factor in GICs), D-region absorption and transient E-region disturbances (see Section 5.2.8). Precipitation of radiation belt electrons and protons affects thermospheric heating and cooling (see Section 5.2.9) via production of HOx and NOx (odd-reactive hydrogen and nitrogen, respectively). The radiation environment in LEO is complicated by temporal variation as well as latitudinal (L-shell), longitudinal, and altitude dependencies within the atmospheric loss cones at < ~1300-km altitude.

Measurement Method: Energetic electrons in the 100s of keV to ~1 MeV and protons and heavier ions in the 10s of MeV to ~GeV range can be measured using instruments incorporating solid-state detectors, scintillators, and dosimeters. Dosimeters provide crude proxies for electron intensities and only integral spectral information, but they provide a direct measurement for ETD and particle penetration of spacecraft shielding and materials. Solid-state detectors and scintillators provide individual particle counts used to derive differential intensity energy spectra required for higher-fidelity models of the system and adverse effects. Charge-discharge sensors can also be used to measure the consequences of inner belt and slot electrons on and within spacecraft systems. These are all in situ measurements made from satellite observatories.

Current Status: Currently, there are no in situ observatories providing comprehensive measurements of Earth's inner radiation belt particles throughout the full system. Previously, NASA's Van Allen Probes provided the full set of relevant observations from two spacecraft in GTO-like orbits,

but those left a partial gap considering a lack of simultaneous knowledge over all MLT and critically throughout all relevant latitudes, all longitudes, and altitudes in LEO. GTOSat is a 6U CubeSat pathfinder mission in development (launch expected ~2022) that might provide some partial coverage for this gap. At LEO, POES, MetOp and several CubeSats (FIREBIRD-II, AC10, ELFIN, and soon CIRBE and REAL) currently offer some knowledge of the radiation environment around LEO with varying levels of coverage and latency.

Forecasting Requirements: The following are required: an accurate nowcast (within the last 5~10 min) of the inner magnetosphere system detailing the current, 3D state, intensity, and extent of the electron radiation belts; and an accurate forecast out to at least 2 days' time of the same system behavior, particularly sudden intensifications and depletions of radiation belt electrons throughout the inner belt and slot region.

Solar wind conditions at the bow shock (see Section 5.2.3) and real-time geomagnetic index data (particularly AE, AL, D_{st}, and K_p; not in scope for this analysis) are critical for nowcast and forecast models of the transient belts of electrons in the slot region. Nowcasting and forecasting may be achieved using data assimilative and/or ingestive models using comprehensive, near-real-time observations of inner belt and slot region electron populations and other relevant quantities (e.g., B-field). Climatological models of inner belt electron, proton, and ion populations as a function of energy and location (L-shell, MLT, MLat) and conditions (e.g., indices) already exist and are used routinely for spacecraft design. The proton and heavy ion radiation belt is relatively long-term stable (over decades); climatological models are sufficient for that population other than transient enhancements related to SEP events (see Section 5.2.1).

Measurement Gaps: In general for nowcasting and forecasting, observations of full energy (electrons: 100 keV ≤ E ≤ 10 MeV; protons and heavier ions: 10 MeV ≤ E < 2 GeV) and pitch angle distributions of electrons and ions plus critical wave modes (at least plasmaspheric hiss and lightning-generated whistlers) from a system of observatories distributed around all MLT are needed to accurately now/forecast the electron radiation belts. However, since the decommissioning of NASA's Van Allen Probes in 2019, no such system is even partially available. CubeSats in LEO provide only details within the atmospheric loss cones. NASA's GTOSat is a pathfinder CubeSat mission that may partially fill this observational gap by 2024, but only with a single-point and partial energy and waves coverage.

For GICs: EPP observations at LEO is a partial gap (POES, MetOp, CubeSats) of high priority.

For ETD: Protons: full gap, high priority; Electrons: full gap, medium priority.

For SEE: This is a partial gap (TWINS-HEO) of high priority.

For internal charging: Full gap, high priority.

For ionospheric D-region absorption and E-region transient disturbances: Partial gap of medium priority.

For thermospheric expansion: EPP of inner radiation belt particles represents a partial measurement gap (some partial coverage from POES, MetOp, and CubeSats around LEO) of medium priority.

Required Measurements (maintain): N/A

Required Measurements (improve):

- **Additional observatories measuring the radiation belt EPP in the LEO environment at a range of altitudes (~300 km ≤ alt ≤ 1300 km), all geographic longitudes, and geographic latitudes up to at least ~75°.**

Required Measurements (definitive):

- **Additional observatories measuring differential intensity energy spectra and angular distributions of 100s of keV to multiple MeV electrons and 1 MeV to GeV protons and heavy ions near the magnetic equator ranging from 1.1 ≤ L < 3.**

Required Measurements (close):

- **Continuous ≤100-km spatial resolution, real-time data transmission monitoring ring current and radiation belt EPP in the LEO environment at a range of altitudes (~300 km ≤ alt ≤ 1300 km), all geographic longitudes, and geographic latitudes up to at least ~65°.**
- **The equatorial monitor(s) described above in this section under "Required Measurements (definitive)."**

5.2.7 Plasmasphere

Earth's plasmasphere is an important region for space weather considering its dynamic nature and its roles in magnetosphere-ionosphere coupling, contributing to radiation belt electron variability, and affecting spacecraft surface charging. Real-time and forecast knowledge of the 3D plasmapause location is of particular importance to understanding and mitigating risk from surface charging and destructive discharge.

Measurement Method: Plasma density can be measured directly in situ using Langmuir probes, Faraday cups, electrostatic analyzers, or electric field (derived from spacecraft potential or upper hybrid frequency line) instruments. The plasmasphere can also be imaged using EUV remote sensing, as was done with NASA's IMAGE mission.

Current Status: Currently, there are no in situ observatories providing comprehensive measurements of Earth's plasmaspheric density content or 3D structure.

Forecasting Requirements: The following are required: an accurate nowcast (within the last 5~10 min) of the inner magnetosphere system detailing the current, 3D state, density content, and extent of the plasmasphere, or as a bare minimum requirement, the plasmapause; and an accurate forecast out to at least 2 days' time of the same system, particularly sudden plasmapause motion, plasmaspheric erosion and drainage plumes, or refilling.

Solar wind conditions at the bow shock (see Section 5.2.3) and real-time geomagnetic index data (particularly D_{st} and K_p; not in scope for this analysis) are critical for nowcast and forecast models of the plasmasphere and its evolution under different driving conditions. Nowcasting and forecasting may be achieved using data assimilative and/or ingestive models using comprehensive,

near-real-time observations of plasmaspheric density and other relevant quantities (e.g., E-fields, ionospheric outflow).

Measurement Gaps:

For surface and subsurface/hybrid charging: Plasmaspheric density as a function of time, L-shell, MLT, and MLat is a full gap of medium priority, and the current state of the 3D plasmapause location is a full gap of high priority.

Required Measurements (maintain): N/A

Required Measurements (improve): N/A

Required Measurements (definitive):

- **Continuous, near-real-time imaging of the plasmasphere**
- **At least one spacecraft traversing the near-equatorial plasmasphere and across the plasmapause (requires elliptical orbit with apogee out to ~7 R_E) and providing density measurements throughout it**

Required Measurements (close):

- **Multipoint (at least two, near-perpendicular vantage points), continuous, near-real-time imaging of the plasmasphere combined with multiple (number to be determined through a focused study or OSSE) spacecraft measuring the density content, radial distributions, and plasmapause location in situ enabling near-real-time and forecasts of the 3D plasmaspheric density structure updated on at least an hourly cadence**

5.2.8 Ionosphere

5.2.8.1. F-Region

Measurement Methods: The F-region and topside ionospheric electron density can be measured in situ by satellites or through remote sensing using both ground and space-based instruments.

Current Status: Currently, sparse in situ measurements of electron density are made by the trio of Swarm satellites at 450 and 520 km, and by the Defense Meteorological Satellite Program (DMSP) satellites that are in a near polar, Sun synchronous orbit at about 830 km. DMSP orbits were designed to be fixed in local time with equatorial crossing times near either 06:00 local time and 18:00 local time or near 09:00 local time and 21:00 local time.

Electron density profiles are also obtained from radio occultations by COSMIC and COSMIC2 satellites. ICON provides both daytime and nighttime O+ density as a function of altitude. The daytime O+ density profiles are remotely sensed by EUV and the nighttime density profiles by FUV. In addition, in situ measurements of precipitating particles are made by DMSP, NOAA-POES, and MetOp satellites in the topside ionosphere. Ion drifts are measured in situ by the DMSP and ICON satellites, and magnetic field perturbations (from which FACs can be derived) by DMSP and the AMPERE/Iridium satellite constellation.

Forecasting Requirements: The following are required: an accurate nowcast (within the last 60 min) of the large- (100s to 1000s km) and small- (<100 km) scale density structure of the F-region ionosphere at all geographic latitudes and longitudes; and an accurate forecast out to at least 1 h of the same quantities, particularly the TEC, NmF2, HmF2, bottomside structure (density profile below HmF2), at all geographic latitudes and longitudes; and current state and predicted evolution of GNSS loss-of-lock and position errors, highest affected frequency, maximum usable frequency, and phase and amplitude scintillation indices at all geographic latitudes and longitudes.

Measurement Gaps: The panel identified the following observational gaps relevant to ionospheric F-region density gradients and variability:

Solar irradiance spanning UV through X-ray wavelengths: partial coverage (see Section 5.1.6.1), reliable robust coverage is required.

Solar wind input (IMF vector, speed, density, temperature) at the bow shock: partial gap (THEMIS/ARTEMIS, MMS cover this partially but not at all times) at high priority.

In situ and remote sensing of F-region plasma density: partial gap (see Figure 5-5) at high priority.

Electric fields and ion velocities: partial gap (see Figure 5-5) at high priority.

Neutral winds: partial gap (covered in part by ICON and some ground-based instruments) at high priority.

Ion and neutral composition: partial gap at medium priority.

Cusp and auroral particle precipitation: partial gap at medium priority.

In situ and remote sensing of F-region plasma temperature: partial gap at low priority.

The global monitoring of the key F-region observables listed above using in situ probes offers an opportunity to fill the measurement gap only with high density networks of satellites. Impossible to achieve in years past, communications networks have recently been deployed with a dense coverage that approaches what could be seen as a feasible concept for coverage with in situ scientific measurements. The IRIDIUM-2 constellation with more 70 spacecraft should be seen as a minimum baseline for measurements that could be ingested and/or assimilated into a dynamic F-region ionospheric model.

Required Measurements (maintain):

- **Maintaining continuous measurements by DMSP, NOAA-POES, and MetOp are critically important.**
- **AMPERE/Iridium constellation is the only means of monitoring global FACs.**

Required Measurements (improve):

- **Currently the DMSP and NOAA satellites are confined to limited local time sectors; an expansion of local time coverage is critically needed.**

- **To better understand EPP, it is important to measure pitch angle resolved, differential energy spectra of the precipitating particles, which are currently not available from DMSP and NOAA-POES.**
- **Continue to enhance the network of single-point LEO observations through CubeSats, smallsats, and other means to characterize key observables of the F-region ionosphere (in situ and/or remote sensing), including at least plasma density, E-fields and ion velocities, neutral winds, particle precipitation, and ion and/or neutral composition.**
- **Any one or more of the "close" observations described below added to existing observatories.**

Required Measurements (definitive):

- **Multiple of the "close" observations described below distributed over all latitudes and multiple local times added to existing observatories**

Required Measurements (close):

- **F-region plasma density (in situ plus remote sensing profiles), electric fields, plasma velocities, neutral winds, ion and neutral composition, and cusp and auroral electron and proton precipitation from a network of observatories enabling regular (daily or less), full globe observations at ≤100-km spatial resolution and real-time data transmission**

5.2.8.2. E-Region

Magnetospheric currents driven into the ionosphere flow through the E-region, where the conductivity tensor allows FACs in the magnetosphere to flow perpendicular to the field and to heat the lower thermosphere. The conductivity enhancements produced in the cusp and auroral oval are unique to high latitudes. The plasma density in the E-region at high latitudes is strongly influenced by cusp, auroral, and EPP, the dominant sources of E-region plasma in the winter. Knowledge of the E-region conductivity is essential to characterizing the current flowing in the polar ionosphere and the heating associated with geomagnetic disturbances.

Away from the poles, the interaction of neutral winds in the E-region with the solar-produced plasma environment in the 100- to 200-km range produces a series of effects including the equatorial wind dynamo that generates dense F-region plasma.

Measurement Methods: Although ionospheric conductivity is a very important physical parameter that governs ionospheric electrodynamics, it cannot be directly measured. Instead, ionospheric conductivity is derived from electron and ion momentum equations via measurements of electron density, electron and ion temperature, and neutral composition. Particle precipitation is measured by in situ particle instruments, such as electrostatic analyzers and energetic particle detectors. Auroral imagers can be used for near-real-time and post facto information of conductivity and activity in the auroral region.

Current Status: The auroral E-region is currently measured mainly via remote sensing observations from DMSP using SSUSI/SSULI, provided by measuring the spectrally separated ratio of N2 Lyman-Birge-Hopfield band system at two wavelengths in downward viewing images of Earth in

the ultraviolet. This is possible for the fact that the aurora is the dominant production source when it is active. These observations provide information of the mean energy and energy flux of auroral energetic electron precipitation within a swath along the orbit track with ~100-min revisit times and 20~30% coverage of the polar ionosphere with each pass. Various CubeSats measuring in track particle electron precipitation in the 1- to 40-keV and 50-keV to >1-MeV range *may exist*. NOAA-POES, DMSP, and REACH measure relevant particle precipitation.

Forecasting Requirements: The following are required: an accurate nowcast (within the last 60 min) of transient disturbances, sporadic E-layers, and scintillation in the E-region ionosphere at all geographic latitudes and longitudes; an accurate forecast out to at least 1 h of the same quantities at all geographic latitudes and longitudes; and current state and predicted evolution of GNSS loss-of-lock and position errors, highest affected frequency, maximum usable frequency, and phase and amplitude scintillation indices at all geographic latitudes and longitudes.

The requirement to forecast the auroral and EPP intensity and pattern that will adequately capture the E-region conductivity to the degree necessary to calculate the intensity of atmospheric heating is notoriously difficult, for the fact that substorms and other nonlinear behaviors like multiple arc formation are formed in processes that are difficult to model at the necessary spatial scales. The significance of nowcasting the auroral conductance along with other key inputs is high because it provides for forecasts of the magnitude of atmospheric heating events whose effects last for 24+ h. The measurement of auroral conductance informs a key prediction of thermospheric density throughout periods of geomagnetic activity.

Measurement Gaps: The last global images of the aurora, providing information to adequately capture the full conductivity pattern in the auroral zone, were obtained in 2005 by NASA IMAGE. Those images had a capability for conductivity retrievals with simultaneous multispectral imaging at 2-minute timescales. It was rivaled only by the specific LBHL/LBHH measurements of POLAR ultraviolet imager (UVI), though that imager operated with a filter wheel and never obtained simultaneous images, a problem for any dynamical auroral environment. Each of these missions in highly elliptical orbits provided images with a duty cycle of up to ~ 50% in one hemisphere or the other, depending on the apsidal precession of the orbits. To make continuous monitoring of auroral activity, it is highly desirable to have a pair of conjugate high-altitude imaging satellites.

The global monitoring of cusp, auroral, and energetic particle (electron/ion) precipitation into the auroral E-region through in situ probes offers an opportunity to fill the measurement gap only with high density networks of satellites. Impossible to achieve in years past, communications networks have recently been deployed with a dense coverage that approaches what could be seen as a feasible concept for coverage with in situ scientific measurements. The IRIDIUM-2 constellation with more 70 spacecraft should be seen as a minimum baseline for measurements that could be ingested and/or assimilated into a dynamic auroral model.

In addition to global auroral imaging, the panel identified the following observational gaps relevant to ionospheric E-region disturbances and EM-signals scintillation:

Solar irradiance spanning UV through X-ray wavelengths: see Section 5.1.6.1.

Solar wind input (IMF vector, speed, density, temperature) at the bow shock: partial gap (THEMIS/ARTEMIS, MMS cover this partially but not at all times) at high priority.

In situ and remote sensing of E-region plasma density: partial gap (see Figure 5-4) at high priority.

Electric fields and ion velocities: partial gap (see Figure 5-4) at high priority.

Neutral winds at 100- to 150-km altitude: partial gap (ICON provides single-point coverage on this) at high priority.

Auroral and energetic precipitation: partial gap (DMSP, POES/MetOp, CubeSats) at high (auroral precipitation) and medium (EPP) priorities.

In situ and remote sensing of plasma temperature: partial gap (provided only by ISRs) at low priority.

Ion composition: partial gap (provided by LIDAR) at low priority.

Required Measurements (maintain):

- **Maintain NOAA-POES and DMSP observations and continue to develop capability to incorporate data from SSUSI/SSULI on an as-soon-as-available basis into E-region ionosphere and thermospheric models to simulate heating and verify with drag analyses.**

Required Measurements (improve):

- **Continue to enhance the network of single-point LEO observations through CubeSats, smallsats, and other means to characterize the precipitation of auroral and energetic particles (in situ measurements) or retrieve the resultant conductivity enhancements in the auroral zone (remote sensing), including at least auroral imaging, plasma density, E-fields and ion velocities, neutral winds, and/or EPP.**
- **Improve UV imaging platforms at MEO altitudes to demonstrate capabilities to predict thermospheric heating and density enhancements.**

Required Measurements (definitive):

- **Develop ≤100-km spatial resolution, 1- to 5-min temporal resolution auroral E-region characterization, including relevant auroral and EPP, in each hemisphere to verify capability, with real-time access through orbital communications networks.**

Required Measurements (close):

- **Continuous auroral imaging of both hemispheres from observatories in MEO/HEO dedicated to providing continuity in measurements (spatial and temporal). Full coverage in both hemispheres at ≤100-km spatial resolution and real-time data transmission would allow immediate nowcast of auroral activity and, with the build-up of modeling capability, an hour advance before the arrival of auroral effects (e.g., heating and EPP) and neutral density perturbations at middle and low latitudes, after which all satellite orbits will be affected.**

- **Continuous ≤100-km spatial resolution, real-time data transmission from cusp, auroral, ring current, and radiation belt EPP monitors distributed around MLT and spanning polar latitudes.**

5.2.8.3. D-Region

Measurement Method: The D-region ionosphere is measured mainly using ground-based remote sensing since the altitude of the region is too low for satellite in situ measurements. Riometers that measure the changes in large-scale radio flux at low frequencies due to absorption in the D-region are one approach. The electron density in the D-region is typically not very high, so ionosondes cannot always reliably measure it. EPP into the D-region can be measured by satellites at higher altitudes using energetic particle detectors.

Current Status: The D-region electron density profiles are measured by MF radars and ionosondes, and can also be inferred from observations by radiometers as well as very-low-frequency (VLF) interferometers. Incoherent scatter radars using specific processing modes can also sense higher levels in the D-region. The D-region ionosphere is directly subject to EPP, such as SEP and scattering of radiation belt particles. The EPP measurements are currently made by NOAA-POES and MetOp polar orbiting satellites at ~830 km as well as several operational CubeSats.

Forecasting Requirements: The following are required: an accurate nowcast (within the last 60 min) of plasma density and signal absorption in the D-region ionosphere at all geographic latitudes and longitudes; and an accurate forecast out to at least 1 h of the same quantities at all geographic latitudes and longitudes.

Measurement Gaps: The panel identified the following observational gaps relevant to ionospheric absorption of EM signals in the D-region:

Solar irradiance spanning UV through X-ray wavelengths: see Section 5.1.6.1. Soft X-ray irradiance is particularly important for the D-region: orders of magnitude increases in the X-ray flux during flares produce strongly enhanced absorption and short-wave fadeouts.

Solar wind input (IMF vector, speed, density, temperature) at the bow shock: partial gap (THEMIS/ARTEMIS, MMS cover this partially but not at all times) at high priority.

SEP forecast and real-time monitoring of inputs at LEO: full gap at low priority.

In situ and remote sensing of D-region plasma density: partial gap (see Figure 5-3) at high priority.

EPP from the radiation belts and SEPs: Full (SEPs) and partial (radiation belt EPP from POES/MetOp and CubeSats) gaps at low to medium priority.

Required Measurements (maintain):

- **Maintain NOAA-POES and DMSP observations**

Required Measurements (improve):

- **Continue to enhance the network of single-point LEO observations through CubeSats, smallsats, and other means to characterize the precipitation of SEPs and energetic particles (in situ measurements), including at least plasma density and EPP**
- **Any one or more of the "definitive" or "close" requirements listed below**

Required Measurements (definitive):

- **SEP forecast from a solar AR monitor**
- **Develop ≤100-km spatial resolution, 1- to 5-min temporal resolution SEP and radiation belt EPP monitors distributed around MLT and spanning polar latitudes**

Required Measurements (close):

- **SEP forecast from solar AR monitors spanning beyond the eastern and western limbs**
- **Continuous ≤100 km spatial resolution, real-time data transmission from SEP and radiation belt EPP monitors distributed around MLT and spanning polar latitudes**

5.2.9 Thermospheric Dynamics

Earth's upper atmosphere is subject to large changes in density on timescales of years to minutes and predicting changes in its density is a key requirement for satellite operation, orbit determination, and collision avoidance. Energy and momentum are deposited in this region through solar radiative input, Joule heating and EPP from the magnetosphere, and the breaking of waves from the lower atmosphere. Thermospheric temperature is determined by the net balance between the heating from the Sun and the magnetosphere and cooling through IR radiation by molecular species in the lower thermosphere, particularly by CO_2 and NO. Thermospheric density at a given height is influenced by thermospheric temperatures. The hotter the temperature is, the larger the thermospheric scale height becomes. Accurate prediction and nowcast of thermospheric neutral composition is of critical importance to predicting neutral density. During significant auroral disturbances, hydrostatic equilibrium can no longer be assumed, and dynamical models that simulate the redistribution of constituents and wind transport are required to capture the state of the thermospheric density at orbital altitudes. Satellite operators and debris catalog maintainers need both real-time measurements of the thermosphere to run models of the effects of drag and longer-term forecasting to plan for station keeping to compensate for altitude loss and collision avoidance.

Measurement Method: Thermospheric neutral mass density and winds are inferred from measurements by spaceborne accelerometers, and they are also measured through remote sensing (using stellar occultations for O_2 density retrievals, Doppler shift of visible emissions for winds). Long-term variations in density can be retrieved from satellite orbit decay, with variable precision and accuracy depending on the configuration and number of satellites used. Neutral composition can be measured directly using mass spectrometers and/or through remote sensing of UV emissions.

Current Status: Swarm and GRACE-FO are currently providing in situ neutral mass density measurements. ICON measures the neutral winds at altitudes from 90 to 300 km at low to middle latitudes through remote sensing, and temperatures in the 90- to 110-km range (mesopause). GOLD

also measures the thermospheric temperature at ~150-km altitude and composition through remote sensing. Other remote sensing of neutral composition is provided by TIMED-SABER, TIMED-GUVI, and DMSP-SSUSI and SSULI.

Currently, the only satellite observations of the neutral winds are from ICON and TIMED; the wind observations from the latter coming from the similar 90- to 110-km-altitude range as ICON temperatures.

Forecasting Requirements: The following are required: an accurate nowcast (within the last 5~10 min) of thermospheric density and temperature disturbances and transient structures (including traveling atmospheric disturbances) at large (~1000 km to global) and small (a few to hundreds of kilometers) scales; and an accurate forecast out to at least 3 days' time of the same quantities at all geographic latitudes and longitudes and altitudes from 100 km to 2000 km.

Measurement Gaps: The panel identified the following observational gaps relevant to thermospheric expansion and corresponding satellite drag and uncertainty in orbit prediction and collision avoidance:

Solar irradiance spanning UV through X-ray wavelengths: there is coverage in some spectral ranges with limited temporal sampling currently, but with mostly aging satellites. This is addressed in more detail in Section 5.1.6.1.

Solar wind input (IMF vector, speed, density, temperature) at the bow shock: partial gap (THEMIS/ARTEMIS, MMS cover this partially but not at all times) at medium priority. Coverage further out at L1 is more substantial.

In situ, remote sensing, and inferred/derived observations of thermospheric neutral density: partial gap (see Figure 5-2) at high priority.

In situ and remote sensing observations of thermospheric neutral temperature: partial gap (covered only partially by ground-based Fabry-Perot Interferometers [FPIs]) at high priority.

Remote sensing and derived observations of thermospheric neutral composition: partial gap (see Figure 5-2) at high priority.

EPP and nitric oxide concentrations: partial gap (see Figure 5-2) at medium priority

High-latitude neutral winds: partial gap (covered only partially by ground-based FPIs) at medium priority.

Required Measurements (maintain): N/A

Required Measurements (improve):

- **Continue to enhance the network of single-point LEO observations through CubeSats, smallsats, and other means to characterize key observables of the thermosphere (in situ and/or remote sensing), including at least neutral density, temperature, composition and wind, ionospheric E-field, velocity, and current, and/or EPP**

- **Dedicate simple missions to characterize orbital effects and atmospheric drag to support model verification/validation**

Required Measurements (definitive):

- **Progress toward populating the network of observatories defined in the "close" requirements listed below**

Required Measurements (close):

- **Continuous ≤100-km spatial resolution, real-time data transmission from neutral density, temperature, composition and wind, ionospheric E-field, velocity, and current, and EPP monitors distributed around MLT and spanning polar latitudes**

5.3 Long-Term Space Weather and Space Climate Prediction

We identified the following sets of parameters related to the space climate that are of value to SWx operations and models: AR emergence and evolution, AR solar-cycle properties, high-latitude flows, and polar fields. We also recognize the importance of long-term investigations of SWx drivers (both solar/heliospheric and geospace) for identifying data cycles on space climate time scales. For each parameter we briefly describe how they are calculated, provide the CBE (if known), and identify the research issues or measurement gaps that hold progress back.

5.3.1 AR Emergence and Evolution

AR emergence and evolution data are parameters associated with specific AR complexes and include size, complexity, local flows, bipolar polarity inversion lines, probability of additional emergence, nearby AR interactions, and many others (van Driel-Gesztelyi & Green, 2015; Toriumi & Wang, 2019). As described in previous sections, these parameters are used to determine the probability of flaring and eruption in specific AR complexes for the purpose of solar activity predictions (e.g., Tziotziou et al. 2012; Georgoulis et al. 2019). These parameters are used by dynamo and surface flux transport models to produce near term (days to weeks) predictions of the magnetic field evolution, which are used as an inner boundary for atmospheric and coronal models. Furthermore, these parameters are critical to these models to aid in predicting the long-term solar-cycle (months to years) variability.

Measurement Method: The spatial and magnetic properties of ARs are derived from full-disk synoptic magnetograms (vector or LOS) taken from the SEL. Local helioseismology (Gizon & Birch, 2005) has been used to measure the local horizontal flows within and surrounding ARs. In addition, Doppler measurements of the visible disk are used to probe the interior (down to about 0.1 $R_{\odot}$ from the photosphere) and around the Sun via helioseismic holography (e.g., Lindsey & Braun, 1997; 2017).

Forecasting Status: The detection of strong concentrations of magnetic flux on the farside of the Sun via helioseismology has been demonstrated in several research papers and is routinely applied

in a research environment. The performance of the technique remains a research effort and shows promise for forecasting activity, at least in the case of large farside ARs (e.g., Liewer et al., 2017).

Forecasting Requirement: No specific requirement exists. However, reliable detection of farside activity is necessary for forecasting irradiance variations at Earth with a 7+ days horizon. Also, forecasting of AR emergence on disk is likely required for predicting eruptive activity with a 24-h+ horizon.

Measurement Gap: Only SEL measurements are currently available. LOS or vector magnetic measurements become less reliable beyond about 60° from the central meridian and magnetic equator. This reduces the resolution and reliability of farside helioseismology and the convection depths that can be probed via helioseismology. There are inconsistencies among magnetograms from different observatories which are due to different calibration schemes, and spectral lines used for the measurements. Furthermore, measurements of transverse magnetic fields are biased toward strong fields because of their sensitivity (they have a general threshold of 100–200 G).

Farside Data. Currently, we are only able to study ARs only for a limited portion of their lifetime, as they cross near the central meridian. Many ARs are not identified until they rotate onto the near side of the Sun. Forecasts of AR flaring and eruption would benefit from additional data provided by seeing the ARs on the far side of the Sun in addition to the SEL observations.

AR Emergence. Flaring and eruptive events are more frequent during the emergence of AR flux. Therefore, there is considerable interest in detecting the presence of subsurface magnetic fields to predict new flux emergence.

There has been research that suggested that time-distance helioseismic techniques may be able to detect sound-speed anomalies thought to be caused by subsurface emerging ARs (Illonidis, 2011). However, these results have been controversial and disputed as being below the noise level associated with the method (Braun, 2012).

The global interior field, embedded in the convection zone, is sheared into a toroidal configuration by the DR. This toroidal magnetic field gives rise to the ARs. Rossby waves, long theorized but only recently observed (Löptien et al., 2018; Hathaway & Upton, 2021), are essential to convection zone dynamics and are thought to be the primary mechanism for removing kinetic energy at the largest scales. These large vortical flows, caused by a balance between the Coriolis force and horizontal pressure gradients, propagate retrograde relative to the CR frame of reference and have lifetimes of at least one CR. Studies have suggested that disturbances in the DR or in Rossby waves may provide a physical mechanism for detecting fluctuations in the toroidal field that correspond to "nests" where ARs are likely to emerge (Dikpati et al., 2017).

Required Measurements (maintain):

- **SEL LOS photospheric field (B_{phot}) measurements.** These are currently provided by SDO/HMI 24×7 and by ground-based observatories. The LOS magnetic field measurements are needed to observe ARs and measure the properties, such as location, size, class of AR and the polarity inversion line. Helioseismology uses these observations to measure the local flows around the AR.

- **SEL vector B_{phot} measurements.** These are currently provided by SDO/HMI 24×7 and by ground-based observatories. These observations provide more detailed information about the structure of the magnetic field lines within the AR.

Required Measurements (Improve):

- **SEL B_{phot} fields measurements + off-SEL EUV imaging.** Brightening in EUV wavelengths is associated with the presence of ARs. The He II Ly-α wavelength has been shown to be successful as a proxy for determining the location and the amplitude of magnetic flux in an AR. These data are used to generate synthetic magnetograms of the far side of the Sun. Preference should be given to EUV imaging of the He II Ly-α line. The additional off-SEL EUV imaging should occur ***east of the SEL*** to image ARs that are ready to corotate toward Earth. However, it should be noted that EUV-derived synthetic magnetograms are not as informative as true magnetograms (as detailed magnetic topology and polarity is not obtained) and true off-SEL B_{phot} fields measurements would be preferred.
- **SEL B_{phot} fields measurements + off-SEL B_{phot} fields measurements.** Stereoscopic measurements of the B_{phot} fields will provide more coverage over the lifetime of the AR. The data from the additional vantage point can be cross-calibrated with the SEL measurements to help resolve inconsistencies in magnetic data. The additional vantage point will improve helioseismology by providing more signal to reduce the noise and by enabling the measurement of slightly longer acoustic waves. The additional off-SEL B_{phot} fields measurements should occur ***east of the SEL*** to image ARs that are ready to corotate onto the hemisphere visible to Earth (Akioka et al., 2005). Currently, the part of the solar disk around the east limb is where the photospheric measurements used by global models are the most out of date (3–4 weeks old) and for which there is most value in obtaining more recent measurements.

Required Measurements (definitive):

- **SEL B_{phot} fields measurements + 2 off-SEL B_{phot} fields measurements.** Stereoscopic measurements of the B_{phot} fields will provide coverage over most of the lifetime of the AR. The data from the additional vantage points can be cross-calibrated with the SEL measurements to help resolve inconsistencies in magnetic data. The additional vantage points will significantly improve helioseismology by providing more signal to reduce the noise and by enabling the measurement of much longer acoustic waves and thus probe deeper into the convection zone. These improvements have the potential to finally detect the signature of subsurface AR emergence. **Preferred locations are L4 and L5** to balance additional disk coverage with overlap of SEL observations (Gibson et al., 2018).

Required Measurements (close):

- **B_{phot} fields for 360° of the solar surface.** This would provide full coverage of the AR belts (both near and far sides of the Sun). This will enable the measurement of the properties of **ALL ARs over the entire lifetime** of the region. Furthermore, this will allow helioseismology to probe to the base of the convection zone.

5.3.2 AR Solar-Cycle Properties

These are observable to characterize the average, time-evolving properties of ARs needed to produce solar-cycle predictions (Jiang et al., 2014; Charbonneau, 2020). They include emergence time and rate, location, flux/area, tilt, bipole separation distance. ARs are the photospheric (i.e., solar surface) manifestations of large-scale magnetic flux tubes rising up through the turbulent convection zone (Fan, 2009), resulting in considerable scatter in AR properties. The physical picture is further confounded by the variability in these properties during the AR lifetime, from one AR to the next, and over the course of the solar cycle. AR properties are measured for each AR and when taken cumulatively, statistical values for these properties emerge (e.g., Spörer's Law and Joy's Law). These AR statistics are used to inform dynamo and surface flux transport models to aid in predicting the long-term solar-cycle variability.

Measurement Method: The spatial and magnetic properties of ARs are derived from full-disk synoptic magnetograms (vector or LOS) taken from the SEL. The statistical properties are obtained by averaging many measurements from long-term synoptic observations.

Forecasting Status: Currently these parameters are roughly defined with some solar-cycle variability (Hathaway, 2015):

1. The appearance of ARs is variable with the solar cycle, with the time between subsequent emergence occurring weeks apart during solar minimum and hours apart during solar maximum.
2. ARs emerge at all longitudes. At the beginning of the cycle, ARs emerge at midlatitudes (~30° on average) and as the cycle progresses, they tend to emerge closer to the equator (Spörer's Law). The ARs emerge in a distribution about the average latitude, with latitudinal distribution decreasing with the size of the AR. While the location appears somewhat random, it is likely tied to the location of the global toroidal field embedded in the convection zone.
3. ARs are characterized by their size in terms of total flux or area. AR fluxes range from ~10^{20} Mx up to ~10^{23} Mx and the area being proportional to the flux: 1.2 * area (10^{18} cm^2) ~flux (10^{21} Mx). Smaller magnetic regions (down to ~10^{17} Mx) do exist. These are known as ephemeral regions, are typically short lived, and are not believed to contribute significantly to the dynamo.
4. The average AR tilt is given by Joy's Law—e.g., angle between the bipolar spots (with respect to lines of latitude) is approximately equal to one half of the latitude. The tilt is thought to be caused by the Coriolis force acting on the flux tube as it rises to the surface, giving the systematic tilt. However, the flux tube is also buffeted by the turbulent convection motions as it rises, producing considerable variability about the average tilt.
5. The AR separation distance (e.g., the distance between the leading and following polarity bipoles) is proportional to the size of the AR. The flux in the leading spot is approximately given by (4×10^{20} Mx)*($s^{1.3}$), where s is the distance between the bipoles.

Forecasting Requirement: No specific requirement exists; however, improvements in forecasting these parameters will lead to improved solar-cycle forecasts. Ideally, we need well-defined parameters over the solar cycle and information on how these parameters change from cycle to cycle based on solar-cycle amplitude.

Measurement Gaps: The AR Solar Cycle Properties are statistical properties that are derived from a large number of detailed AR observations and therefore share the same measurement gaps identified for AR Emergence and Evolution data (e.g., unreliable beyond 60° from the central meridian, viewed for only a portion of the AR lifetime, as well as inconsistencies among magnetograms).

1. **Farside AR data.** All of these parameters would benefit from additional data provided by seeing the AR on the far side of the Sun. The emergence time in particular cannot be adequately assessed because many ARs are not identified until they rotate onto the near side of the Sun.
2. **AR evolution.** Many of these AR parameters are time varying, changing systematically over the lifetime of the AR. Different results for each parameter are often obtained depending on the stage of the AR evolution. To improve on these measurements, detailed studies over the entire life of the ARs are needed.
3. **Long-term synoptic studies.** AR properties are measured for each AR and when taken cumulatively, statistical values for these properties emerge (e.g., Spörer's Law and Joy's Law). Therefore, these measurements rely on long-term synoptic studies to provide sufficient data to derive these relationships.

Required Measurements (maintain):

- **Same as Section 5.3.1.**

Required Measurements (improve):

- **Same as Section 5.3.1.**

Required Measurements (advance):

- **Same as Section 5.3.1.**

Required Measurements (close):

- **Same as Section 5.3.1.**

5.3.3 High-Latitude Flows

Plasma flows on the Sun can be divided into two categories: the zonal flows and turbulent CFs. The zonal flows include the MC (Featherstone & Miesch, 2015), DR (Howe, 2009), and their residuals (e.g., the Torsional Oscillations). These large-scale surface and interior plasma flows are known to change with depth, latitude, and phase of the solar cycle. Turbulent CFs are "boiling" plasma motions caused by the large temperature gradient in the Sun's convection zone. Convective cells (Rincon & Rieutord, 2018) span the entire range of sizes between granules and giant cells,

with supergranules being the dominant convective structure. All three of the plasma flows work together to transport the Sun's magnetic field and drive the solar cycle.

Measurement Method: There are multiple techniques for measuring plasma flows on the Sun. Both the zonal flows and the CFs can be measured directly from Doppler images (Ulrich, 2010; Hathaway et al., 2015) or by tracking the motions of the supergranules in the Doppler images (Gizon & Rempel, 2008; Hathaway et al., 2013). The zonal flows at the surface can be obtained by tracking the motion of the magnetic network (Hathaway & Rightmire, 2010). Global helioseismology (Basu, 2016) and local helioseismology (Gizon & Birch, 2005) are used to measure the flows below the surface.

Forecasting Status:

1. **MC**: The MC is the weakest of the Sun's flows. It is poleward at the surface, with a peak velocity of ~20 m/s in the midlatitudes. The MC acts as a conveyor belt. The poleward flow at the surface is responsible for carrying residual magnetic flux from decaying ARs to the poles, while the meridional return flow in the convection zone sets the timing of the solar cycle.
2. **DR**: The DR is fastest at the equator and slowest at high latitudes, with a relative velocity ~200–250 m/s. Its velocity structure is well described throughout the convection zone. It is responsible for stretching the interior magnetic field around the Sun into a toroidal configuration, causing it to become stronger and rise up in the form of ARs.
3. **CF**: The turbulent CFs form cellular structures in which the plasma spreads out from upflows in the cell centers and into narrow downflow lanes at the boundaries. The convective cells exist on a spectrum of spatial, temporal, and velocity scales. At the smallest end of the spectrum are the granules, with diameters of 1000 km, velocities of 3000 m/s, and lifetimes of 10 min. At the largest end of the spectrum are giant cells. These structures are expected to have diameters of ~200,000 km and lifetimes of a few months, but their velocities are disputed. The dominant convective structure is the supergranule, with diameters of 30,000 km, velocities of 500 m/s, and lifetimes of about a day. Small magnetic elements are transported to the boundaries of each convective cell, where they become trapped in the downflow lanes and form the magnetic network on the surface of the Sun.

Forecasting Requirement: No official requirement exists so we define them here:

1. **MC**: Accuracy within ~1 m/s at all latitudes and throughout the convection zone.
2. **DR**: Accuracy within ~10 m/s at all latitudes and throughout the convection zone.
3. **CF**: Determine the nature of the convective structures at all latitudes on all spatial scales.

Measurement Gap: Only SEL observations are currently available. This limits the latitudes that the flows can be measured and the convection depths that can be probed via helioseismology.

1. **MC**: Measurements of the high latitude are conflicting, with some suggesting the presence of an equatorward meridional counter cell at the poles. The presence or absence of a polar counter cell determines the latitude at which the MC subducts before becoming equatorward within the convection zone, though the depth at which this occurs is debated. This measurement is needed to determine whether the MC sets the timing of the solar cycle.

2. **DR**: The DR is well described throughout the convection zone at all latitudes below 60°, but its structure in the polar regions is unknown (e.g., does it stay retrograde, go to zero, or turn prograde). Determining under which regime DR operates will provide important constraints on dynamo models (e.g., sets the Rossby number).
3. **CF**: The CF is already well described at the granule and supergranular scales but is disputed at the largest spatial scales (low wavenumber, e.g., "giant cells"). The size and lifetimes of the largest convective cells (in the polar regions in particular) not only determines the behavior and structure of polar vortices but also provides important constraints on dynamo models (e.g., sets the Rossby number).
4. **Temporal Variation**. While it is critical to have an explorer mission to the poles to obtain an accurate measure of the flows in the polar regions, it is also important to explore the polar regions at different phases of the solar cycle (minimum, rising phase, maximum, decaying phase) as the flow parameters are known to have a solar- component and feature observed/not observed during a single pass may disappear/appear at a later phase of the cycle.

Required Measurements (maintain):

- **SEL LOS Doppler and photospheric field (B_{phot}) measurements.** These are currently provided by SDO/HMI 24×7 and by ground-based observatories.

Required Measurements (improve):

- **High-latitude (>60°) Doppler magnetograph (MDI resolution/cadence) for at least three CRs.** These flows are very weak and three rotations of observations are needed to pull the signal out of the noise.

Required Measurements (advance):

- **High-latitude (>60°) Doppler magnetograph (HMI resolution/cadence) for multiple CRs at different phases of the solar cycle**

Required Measurements (close):

- **Continuous 4π full-disk Doppler magnetograph (HMI resolution/cadence)**

5.3.4 Polar Fields

The Sun's polar fields vary inversely in time with the solar cycle, reversing near solar maximum and peaking near solar minimum. During solar minimum, the total flux on one hemisphere is approximately 10^{22} Mx, or about the same amount of flux as a moderately sized AR (Petrie, 2015). However, the north and south poles are not perfectly in sync in amplitude or phasing; one hemisphere may briefly lead the other by a few years.

Solar minimum represents the beginning of the solar cycle and the Sun's polar magnetic fields at this time serve as the foundation for the emerging cycle, ultimately setting the amplitude of the solar cycle through the Babcock–Leighton mechanism (as described in Section 4.3). As such, the strength of the polar fields at solar minimum have become the favored and most reliable solar-cycle

predictor (Hathaway, 2015; Petrovay, 2020). Surface flux transport models and dynamo models are often used to simulate the evolution of the flux on the Sun to predict the polar fields ahead of minimum and thus extend the predictive range of using the polar fields.

Measurement Method: The polar field strength is typically obtained by calculating the axial dipole moment of the flux on the entire Sun. However, the north and south poles are not perfectly in sync in amplitude or phasing. Therefore, the polar field strength is also obtained by measuring the total flux above a given latitude (usually 55° or 60°) and averaging it over the area. The latter method is more subjective but has the benefit of providing information about the hemispheric asymmetry.

Forecasting Status: When used as a predictor of the next cycle, able to predict ~3 years in advance of solar minimum.

Forecasting Requirement: No specific requirement exists, but we want to extend the prediction window and need to know whether this is fundamentally limited by stochastic processes. High-latitude observations are needed.

Measurement Gap: Only SEL measurements are currently available. The polar fields are only observed on the northern and southern limb of the SEL magnetograms. Therefore, they share many of the same measurement gaps identified in Section 5.3.1 for AR emergence and evolution data (e.g., inconsistencies among magnetograms, unreliable beyond 60° from the central meridian, as well as transverse perspective).

1. **Measurement uncertainty.** Unlike ARs, which pass near the disk center, polar field measurements are only available at the limb. Currently we do not have an accurate measurement of the amount of flux at the poles, the inclination of the polar magnetic fields, or how the flux elements are organized. Constraining the polar fields is essential to improving our ability to make solar-cycle forecasts.
2. **Flux transport.** Without an accurate measure of the flux at the poles, we are not able to determine whether accumulation of flux solely from the remnants of ARs is sufficient to account for the total flux budget or if there is a significant amount of local flux emergence at high latitudes. Determining the flux distribution and strengths will provide valuable constraints on surface flux transport and dynamo models.
3. **Hemispheric asymmetry.** We know that the amplitude of the polar fields in each hemisphere go out of phase with one another, resulting in a hemispheric asymmetry. The Sun is tilted with respect to the ecliptic plane such that as Earth rotates around the Sun, the inclination of the Sun with respect to Earth oscillates between ±7.23°. The result is that while one pole comes into a slightly better view, we lose the other pole altogether. Since we only have a good view of one pole at a time, we are unable to access the extent of this asymmetry and how it manifests in the solar cycle. For example, solar cycle 24 had a pronounced hemispheric asymmetry in the AR emergence, which caused the amplitude of the cycle to be weaker than it would have been if the AR emergence in the hemispheres had been in sync. Further investigation is needed to determine whether an asymmetry in the polar fields can cause this to occur.
4. **Temporal variation.** While it is critical to have an explorer mission to the poles to obtain an accurate measure of the polar fields, as with the high-latitude flows, it is also important to explore the polar regions at different phases of the solar cycle.

Required Measurements (maintain):

- **Same as Section 5.3.3.**

Required Measurements (improve):

- **Same as Section 5.3.3.**

Required Measurements (advance):

- **Same as Section 5.3.3.**

Required Measurements (close):

- **Same as Section 5.3.3.**

6 Measurement Priorities

The committee's consensus on the priorities to address the measurement gaps identified in the analysis (Section 5) are presented in this section of the report. The approach to prioritization is given in Section 6.1, and the top-level measurement priorities are outlined in Section 6.2 before detailing the specific priorities for current at-risk measurements in Section 6.3. Future measurements that can lead substantial progress in SWx *-casting are presented in Section 6.4.

6.1 Approach to Measurement Gap Prioritization

The gap analysis by the committee identified a large number of important measurements spanning a wide range of wavelengths, measurement types, and approaches across SH and geospace phenomena. The charge to the committee offered no prioritization guidance (programmatic or otherwise). Hence, the committee adopted the following approach to create a balanced set of measurement priorities:

- Measurement priorities for maintaining, improving, advancing, and closing on gaps in SWx *-casting were considered separately.
- The SH and GEO subpanels prioritized their measurements separately given the different nature of the measurements. The link between the two regimes were maintained as explained in the SH/GEO prioritization approaches below.
- The subpanels weighted the measurements according to several factors. The assigned weights were used only to provide an initial ranking for further discussion:
  - The GEO prioritization considered the ***SWx hazards*** connected to each measurement; the ***science*** value; and the impact on ***NASA SWx needs***.
  - The SH prioritization considered the ***GEO prioritizations*** (thus, linking SH and GEO); the ***science*** value; and the impact on ***NASA SWx needs (exploration score).***
  - Following the initial ranking, the subpanel members evaluated the measurements lists and provided their own rankings. The average ranking, representing the consensus, was used to divide the measurements into three categories of high, medium, and low.

The committee emphasizes that the three priority categories are principally to provide some fine-grain organization to the lists. All measurements appearing in Table 5-1 and Figure 5-1 through Figure 5-10 are important by virtue of their appearing in those tables. As this is a NASA report, the committee draws attention to any novel measurements or approaches; these are highlighted in the tables below.

6.2 Top-Level Priorities for Filling Critical Observational Gaps

Based on the SWx hazard traceability diagrams presented in Section 5 and the details presented throughout this report, the current state of observable gaps were grouped, weighted, and prioritized based on the following metrics: (a) relevance to multiple SWx hazards, (b) assigned priority, (c) likelihood and consequence (see Figure 2-1), and (d) scientific merit. The results of this prioritization scheme are shown in Table 6-1 below, which consists of the seven highest priority observable/measurement categories out of over 40 observables and measurements considered. Note: particular observable quantities pertaining to each category of measurement gap are detailed further below for SH categories (Section 6.3) and geospace categories (Section 6.4).

Table 6-1. Top-ranked current SWx observation gap categories

Rank	Current Observation Gaps	Normalized Weighted Score
1	Solar/solar wind observations, including off-SEL	0.74–1.00
2	Ionospheric key observables	0.93
3	Solar wind in peri-geospace	0.83
4	Thermospheric key observables	0.64
5	Ionospheric D- and E-region EPP and E- and F-region cusp and auroral precipitation	0.55–0.60
6	Ring current and radiation belt electrons	0.58
7	Plasma sheet electrons and injections/bursts from cislunar into GEO and MEO regions	0.50

Solar and solar wind measurement made from off the SEL importantly capture solar activity around the Sun that cannot be observed from Earth, including at the Sun–Earth L1 point (~240 R_E upstream of Earth). The L4 and L5 Sun–Earth Lagrange points offer ideal locations to extend solar observable horizons around the eastern and western limbs, respectively. Because of the criticality of solar and solar wind driving all externally originating SWx, solar, and solar wind observation gaps rank high in the committee's priorities. Significant propagation uncertainties and errors occur when solar wind observations made around L1 are propagated to Earth's subsolar magnetopause. Propagation uncertainties and errors can result from finer characteristic length and temporal scales, the turbulent nature of the solar wind, and the spatiotemporal evolution of the solar wind as it propagates between L1 and Earth's magnetopause. For this reason, a dedicated and continuous solar wind monitoring system in peri-geospace (i.e., the space around geospace, approximately corresponding to cislunar range) also ranks high in this prioritization. Reducing errors in solar wind input conditions will also reduce errors in SWx predictive-model outputs that are driven by solar wind conditions.

There are also key observation gaps in solar disk and coronal monitoring from Earth (and at other solar longitudes), such as full solar irradiance from UV to X-rays (Figure 6-3 - 6-4). These gaps are of relatively high priority considering the importance of these observables as model inputs. Solar radiation monitors (SRB, flare, and SEP monitoring) also require implementing at the L4,

and L5 Lagrange points and in peri-geospace. These monitoring platforms will be of increasing importance as humanity returns to the Moon and expands its presence further to Mars and beyond.

The next highest priority measurement gaps involve ionospheric effects on satellite communications and navigation signals including the threat of spacecraft charging due to enhanced current systems and electron precipitation around LEO. Similarly, key observables for quantifying and predicting thermospheric expansion and contraction also ranked highly due to the threat of enhanced atmospheric drag affecting satellite orbit prediction and orbital lifetimes. These prediction uncertainties increase the possibility of satellite collisions, which result in proliferating debris fields around LEO that further increase the likelihood of additional collisions. In the worst-case scenario (i.e., Kessler Syndrome), a shell of debris from a runaway cascade of collisions renders LEO essentially unusable and possibly impenetrable to future missions.

The highest ranked priorities continue with EPP and auroral precipitation into the upper layers of Earth's atmosphere. These effects result in enhanced and often localized ionospheric heating and enhanced conductivity as well as thermospheric heating. Precipitating electrons and electrons corresponding to ionospheric and FAC systems also pose a hazard to spacecraft surface and subsurface/hybrid charging in the LEO environment. Filling these measurement gaps will require new and innovative solutions. This is because all of these effects can be highly localized (<100-km scales) and are yet distributed over the globe. Solutions include the possible use of hosted payloads and of data buys from commercial spacecraft in the LEO environment. Thus, future observatory systems to fill the related critical observation gaps must rely on a network of many observatories providing a combination of in situ and remote sensing observations.

With the loss of NASA's Van Allen Probes, there are several major observational gaps left in geospace and peri-geospace (including the lunar and cislunar environments) concerning various radiation hazards to both crewed (including both the spacecraft and the astronauts onboard) and robotic spacecraft. The final categories in the highest priority list pertain to those hazards and prioritize continued, comprehensive monitoring of key observables in Earth's ring current and radiation belts plus energetic electrons in the near-Earth plasma sheet and injections and bursts of energetic electrons from cislunar space into GEO and MEO.

6.3 Priorities for Maintaining Current Status

6.3.1 Solar and Heliospheric Priorities

The mostly green "maintain" column in Table 5-1 indicates that the SH measurements required to maintain the current *-casting state are mostly available. Solar disk and coronal coverage are provided by both NASA and NOAA assets both current (SDO, LASCO, GOES) and future (SWFO-L1, GOES, ground-based magnetographs). There are, however, several measurements that are either missing now (red) or will become unavailable in the near future. They are shown on Table 6-2. The prioritization is driven mostly by the use of these measurements.

Table 6-2. Priority list of measurement gaps in SH quantities required for maintaining current SWx *-casting capabilities

Measurement	Main Use	Notes
Off-SEL VIS coronagraphic imaging to >30 $R_{\odot}$	ToA, mass density	Useful >30°–40° from SEL; only available from STEREO-A (14+ years in operation), which will be within 30° of the SEL in 3/2022–10/2024
Protons >300 MeV	All SEP parameters	High proton energies are not covered by current payloads
24×7 <10-MHz dynamic spectra with <1 h latency	Eruptive event proxy	Reliance on research missions prevents robust use for operations

Off-SEL coronagraph images from the STEREO spacecraft have been used widely in SWx research and operations but they lose their utility within ~30°–40° of the SEL because the views of the transients become similar to SEL coronagraph views. Off-SEL imaging is currently provided only by the aging STEREO-A spacecraft (launched in 2006) which will be within 30° of Earth from March 2022 to October 2024. The next planned off-SEL imaging will be from the ESA L5 Carrington mission scheduled for launch no earlier than 2027, so there is potential for a long gap in off-SEL observations, if STEREO-A does not survive.

High-energy protons are of particular concern for cislunar space exploration as they arrive at 1 AU as fast as 12 min and can be used to inform nowcasts for the intensity and fluence of the developing SEP event.

Finally, low-frequency radio spectra are commonly used to detect emissions from solar eruptions, such as Type II/III bursts that are proxies for the CME speed or SEP productivity. Frequencies above ~10 MHz can be measured on the ground, but these correspond to locations at most a couple solar radii from Sun center. Emissions farther from the Sun, extending into interplanetary space, are emitted at lower frequencies and are detected by several NASA spacecraft (Wind, STEREO-A, Parker Solar Probe). These are research spacecraft, however, with generally long latencies between data acquisition and data release for analysis that prevent the use of these measurements for SWx forecasting.

6.3.2 Geospace Priorities

Table 6-3 shows the currently available, on-orbit assets that provide data that are valuable for SWx *-casting. These have been ranked in priority based on the details in the SWx hazard block diagrams shown in Section 5. It should be noted *and stressed* here that DMSP and POES are discontinued programs. DMSP has a follow-on weather satellite program (DoD/United States Space Force [USSF]) that will carry energetic charged particle sensors. There is no known current plan for a follow-on program for POES (NOAA). With the loss of DMSP and POES in the near future, a number of critical ionospheric and thermospheric observational gaps will open up in the polar LEO environment. Many of the rest of these assets/missions are NASA science missions and offer only very partial coverage compared to that needed for an effective SWx observatory network.

Table 6-3. Priority list of measurement gaps in geospace quantities required for maintaining current SWx *-casting capabilities

Ranked Priority	Assets/Mission	Observable	Relevant SWx Hazard	Real-Time Availability (within 10 min)?
1	DMSP	F-, E-, D-region plasma density, F- and E-region ion velocity and E-field, F-region ion and neutral composition, plasma temperature, cusp and auroral precipitation, E-region auroral precipitation, E- and D-region EPP, ionospheric currents and conductivity, neutral composition	1. Ionospheric disturbances 2. Thermospheric expansion 3. GICs	No (>2-h latency)
2	POES/MetOp	F-region cusp and auroral precipitation, E-region auroral precipitation, E- and D-region EPP, >1 MeV electrons and ions	1. Ionospheric disturbances 2. Thermospheric expansion 3. GICs 4. Radiation effects: surface charging, SEE, ETD	No (90-min latency)
3	ICON	F- and E-region E-field and ion velocity and neutral winds, F-region ion and neutral composition and ion temperature, neutral composition	1. Ionospheric disturbances 2. Thermospheric expansion	Unknown
4	SWARM	F-region plasma density, ionospheric currents, neutral density	1. Ionospheric disturbances 2. Thermospheric expansion 3. GICs	Unknown
5	GOLD	F-region ion and neutral composition, ionospheric conductivity (from FUV)	1. Ionospheric disturbances 2. Thermospheric expansion	Unknown
6	COSMIC-2	F-, E-, D-region plasma density, F- and E-region ion velocity and E-field, F-region ion temperature	1. Ionospheric disturbances 2. Thermospheric expansion	Unknown
7, 8	GOES	10s to 100s keV electrons and ions, >1 MeV electrons and ions	Radiation effects: surface and internal charging, SEE, ETD	Yes
7, 8	CubeSats	GNSS-RO (density), F-, E- and D-region cusp, auroral, and EPP	1. Ionospheric disturbances 2. Thermospheric expansion 3. GICs	No
9–14	MMS, THEMIS, LANL-GEO, GPS, AMPERE, TIMED	Tens to hundreds of keV electrons and ions, >1 MeV ions and electrons, ionospheric currents, F-region ion and neutral composition	1. Ionospheric disturbances 2. Thermospheric expansion 3. GICs 4. Radiation effects: surface and internal charging, SEE, ETD	No
15	TWINS (in situ)	>1 MeV electrons and ions	Radiation effects: SEE and ETD	No
16–19	REACH, JASON, GRACE-FO, various GNSS-Rxs	>1 MeV electrons and ions, F-, E-, and D-region plasma density, neutral density	1. Ionospheric disturbances 2. Thermospheric expansion 3. Radiation effects: surface and internal charging, SEE, ETD	Varies *REACH could be made available with negotiations with USSF
20	LRO	>1 MeV ions	Radiation effects: SEE, ETD	No

6.4 Priorities for Improving *-casting Status

The committee has also identified several measurements that can impact SWx *-casting significantly by filling important gaps in our knowledge of the Sun–Earth system and the inner heliosphere, more generally. The prioritized measurements are discussed separately for SH and geospace in the rest of the section.

6.4.1 SH Priorities

The measurements are taken from the respective columns ("improve," "advance," and "close") of Table 1-1, consolidated for duplicates, and prioritized in three tiers ("high," "medium," and "standard"). The tiers are delineated by different hues based on their science value and relevance to space exploration and geospace inputs. Table 6-3, Table 6-4, and Table 6-5 summarize the list for the three impact categories ("improve" to "closure"). Novel measurement techniques are shown in blue text.

Table 6-4. SH priorities for improving, advancing, and closing critical gaps prohibiting advancement of SWx *-casting

ID	Measurement	Notes
	Improve	
I1	Off-SEL LOS photospheric magnetic field	Critical modeling gap; relevance to ~all SH SWx quantities; vector filed strongly preferred
I2	Off-SEL EUV disk imaging + VIS imaging to >80 $R_\odot$	Critical modeling gap; important to space exploration
I3	Multipoint (grid) in situ particles & fields, upstream of L1 (within 0.9 AU)	Direct impact to SWx forecasting accuracy; critical for model validation; novel science capability for transients
I4	2-viewpoint off-SEL (symmetric, e.g., L4/L5) VIS imaging to >80 $R_\odot$	Improves on I2; critical to space exploration
I5	Off-SEL vector photospheric magnetic field	Improves on I1; important for prediction studies
I6	SEL vector photospheric + chromospheric magnetic field	Improves on I1; important for prediction studies; can be made (partially) from the ground or suborbital
I7	Off-ecliptic (>60°) vector photospheric magnetic field	Improves on I1; critical modeling gap; partially satisfied by Solar Orbiter
I8	EUV disk imaging of hot plasmas (~10 MK)	Detection of coronal 'sigmoids'; Important for prediction
I9	Off-SEL SXR irradiance	Important for eruptive energetics budget, SEP forecasting schemes, thermospheric modeling
I10	Off-limb UV/EUV/NIR spectroscopy	Coronal and CME magnetic field, eruption energetics
I11	Decametric radio (<10 MHz) with 15-min latency	Eruption/SEP proxy
I12	EUV on-disk stereoscopy (2°–10° angular separation)	Pre-eruption magnetic topology; flare/CME prediction
I13	HXR imaging spectroscopy	Eruption energetics, SEPs
	Advance	
A1	2-viewpoint off-SEL (symmetric, e.g., L4/L5) VIS imaging to >80 $R_\odot$ + LOS B_{phot} + upstream in situ (w/in 0.9 AU)	Combined I4,I1,I3 has stronger impact on SWx *-casting than the individual measurements
A2	2-viewpoint off-SEL (symmetric, e.g., L4/L5) VIS imaging to >80 $R_\odot$ + EUV disk imaging + radially distributed (0.7–1 AU) in situ particles & fields	Combined I4,I2, I3 variant, focused on IP transport
A3	2-viewpoint off-SEL (symmetric, e.g., L4/L5) + EUV (incl. hot plasmas) disk imaging + vector B_{phot}	Combined I4, I2 + I8, I5, focused on eruption sources, SEPs
A4	Multipoint (grid) in situ upstream of L1 (<0.9 AU, usually)	I3 variant with higher measurement resolution
A5	Off-ECL (>60°) vector photospheric magnetic field	Improves on I1; critical modeling gap; requires longer high-lat time series than possible from Solar Orbiter or a potential SOLARIS pathfinder
A6	Off-limb Ly-α spectroscopy (κ-distribution)	Remote sensing of "seed" particles; potentially important for space exploration
A7	Off-ecliptic EUV disk + VIS imaging to >80 $R_\odot$	CME/shock/SEP IP propagation; critical for space exploration
A8	Decametric radio (<10 MHz) with 1-min latency	Eruption/SEP proxy
A9	SXR-NUV disk imaging	Sources of solar irradiance/eruptions
A10	Off-SEL HXR imaging spectroscopy	Eruption energetics; SEPs
A11	Complete spectral irradiance <300 nm	Critical for modeling of thermosphere & ionosphere

ID	Measurement	Notes
	Close	
C1	4π coverage of vector B_{phot} + Doppler + EUV disk + VIS imaging >20 $R_\odot$	Closes most critical gaps on solar drive inputs for geospace and space exploration
C2	3 off-SEL (120° apart) VIS img > 20 $R_\odot$ + off-ECL VIS imaging to >80 $R_\odot$ + >67% coverage of LOS B_{phot} + strategically distributed in situ particles & fields	C1 variant focused on IP and SEP propagation and space exploration
C3	Multi-height vector magnetic field	Possible closure on eruption energetics and hence eruption prediction (hours to minutes); critical for space exploration
C4	Complete spectral irradiance <300 nm at 0.1-nm res	Near closure for solar irradiance input to atmospheric models
C5	Decametric radio (<10 MHz) with 1-min latency	Development of operational proxies for CME/SEP phenomena

Figure 6-1 provides a visual overview of the table *improve* and *advance* priorities. It demonstrates the need for spatial coverage of the inner heliosphere using strategically selected locations and measurement complements.

The measurements required to provide *closure* to several of the open research issues and forecasting gaps that were identified in Table 5-1 and summarized in Table 6-4 are represented visually in Figure 6-2.

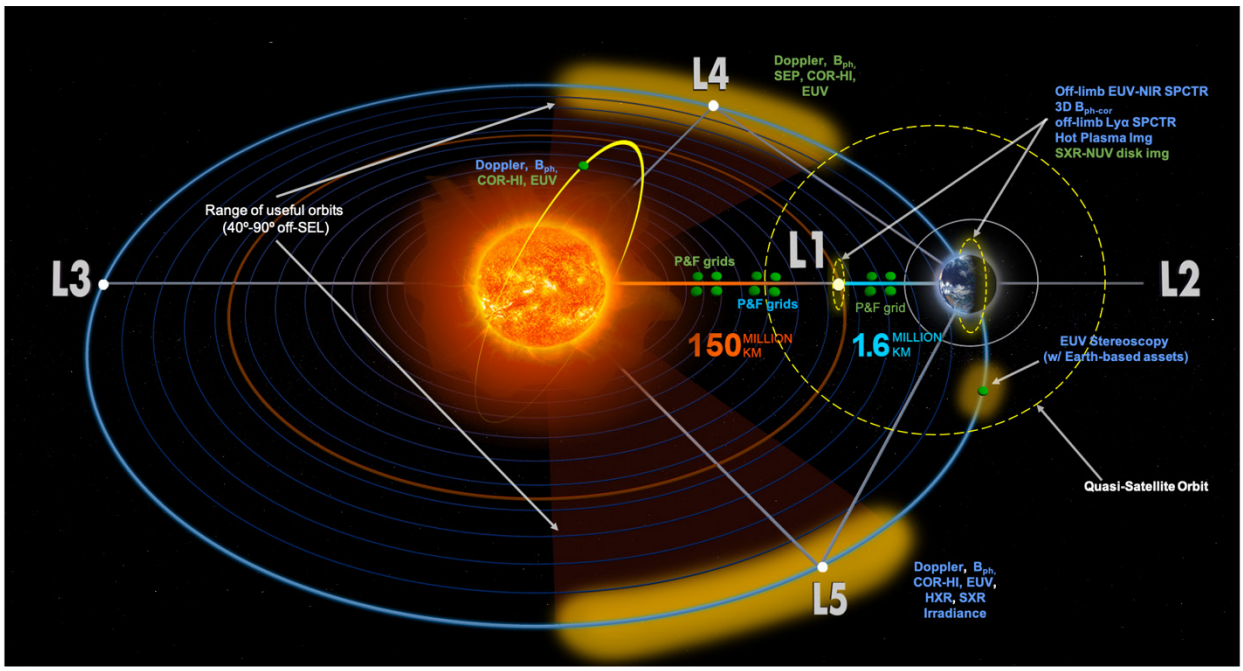

Figure 6-1. Visual representation of the locations and types of measurements required to significantly advance SWx understanding and forecasting capabilities. Details are provided in Table 6-4 and Section 5.

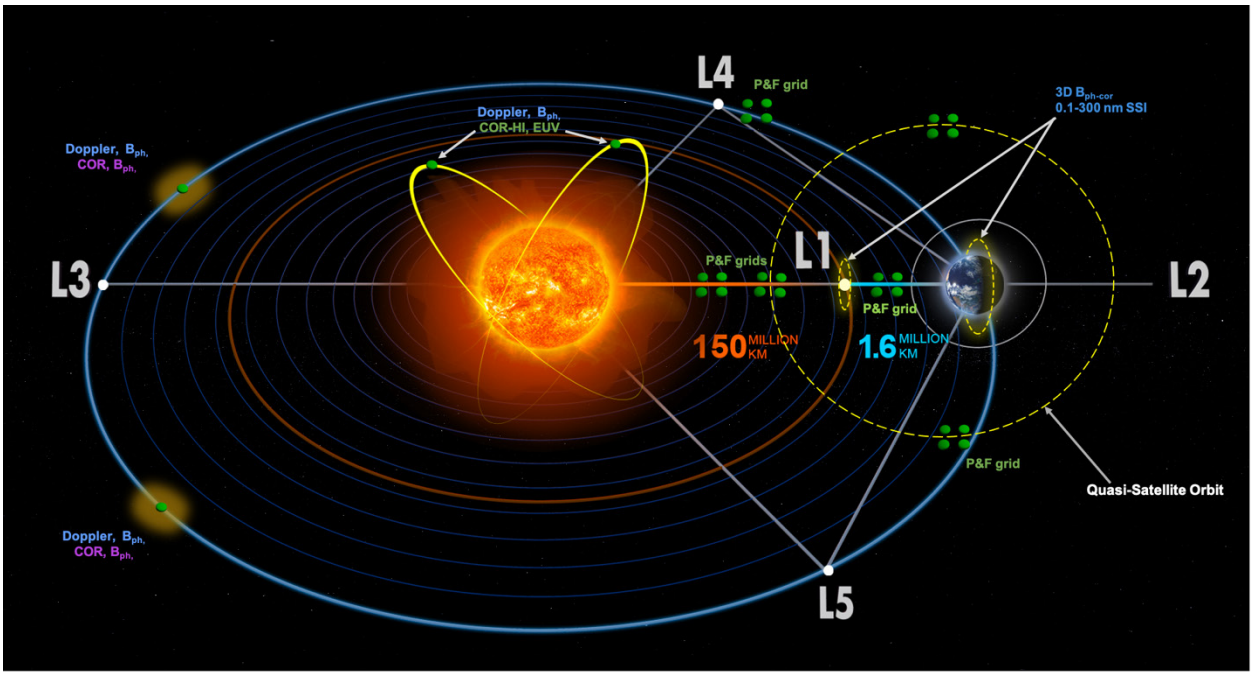

Figure 6-2. Visual representation of the locations and types of measurements that can lead to closure for several SWx research and forecasting issues. Details are provided in Table 6-4 and Section 5.

6.4.2 Geospace Priorities

Similar to the SH measurement priorities, Table 6-5 lists the geospace requirements from Section 5 recommended as highest priority to consider filling for improved SWx *casting:

Table 6-5. Geospace priorities for improving, advancing, and closing critical gaps prohibiting advancement of SWx *-casting

Improve/Advance/Close	Description/Requirements
Ionospheric Key Observables	
Improve	F-region: Currently the DMSP and NOAA satellites are confined to limited local time sectors; an expansion of local time coverage is critically needed.
	F-region: To better understand EPP, it is important to measure pitch angle resolved, differential energy spectra of the precipitating particles, which are currently not available from DMSP and NOAA-POES.
	F-region: Continue to enhance the network of single-point LEO observations through CubeSats, smallsats, and other means to characterize key observables of the F-region ionosphere (in situ and/or remote sensing), including at least plasma density, E-fields and ion velocities, neutral winds, particle precipitation, and ion and/or neutral composition.
	F-region: Any one or more of the “close” observations described below added to existing observatories.
	E-region: Continue to enhance the network of single-point LEO observations through CubeSats, smallsats, and other means to characterize the precipitation of auroral and energetic particles (in situ measurements) or retrieve the resultant conductivity enhancements in the auroral zone (remote sensing), including at least auroral imaging, plasma density, E-fields and ion velocities, neutral winds, and/or EPP.
	E-region: Improve UV imaging platforms at MEO altitudes to demonstrate capabilities to predict thermospheric heating and density enhancements.

Improve/Advance/Close	Description/Requirements
	D-region: Continue to enhance the network of single-point LEO observations through CubeSats, smallsats, and other means to characterize the precipitation of SEPs and energetic particles (in situ measurements), including at least plasma density and EPP.
Advance	F-region: Multiple of the "close" observations described below distributed over all latitudes and multiple local times added to existing observatories.
	E-region: Develop ≤100 km spatial resolution, 1–5 minute temporal resolution auroral E-region characterization, including relevant auroral and EPP, in each hemisphere to verify capability, with real-time access through orbital communications networks.
	E-region and D-region: SEP forecast from a solar active region monitor.
	D-region: Develop ≤100 km spatial resolution, 1–5 minute temporal resolution SEP and radiation belt EPP monitors distributed around MLT and spanning polar latitudes.
Close	F-region plasma density (in situ plus remote sensing profiles), electric fields, plasma velocities, neutral winds, ion and neutral composition, and cusp and auroral electron and proton precipitation from a network of observatories enabling regular (daily or more frequently), full globe observations at ≤100 km spatial resolution and real-time data transmission.
	E-region: Continuous auroral imaging of both hemispheres from observatories in MEO/HEO dedicated to providing continuity in measurements (spatial and temporal). Full coverage in both hemispheres at 100 km spatial resolution and real-time data transmission would allow immediate nowcast of auroral activity and, with the buildup of modeling capability, an hour advance prior to the arrival of auroral effects (e.g., heating and EPP) and neutral density perturbations at middle and low latitudes, after which all satellite orbits will be affected.
	E-region: Continuous ≤100 km spatial resolution, real-time data transmission from cusp, auroral, ring current, and radiation belt EPP monitors distributed around MLT and spanning polar latitudes.
	D-region: Continuous ≤100 km spatial resolution, real-time data transmission from SEP and radiation belt EPP monitors distributed around MLT and spanning polar latitudes.
	E-region and D-region: SEP forecast from solar active region monitors spanning beyond the eastern and western limbs.
Thermospheric Key Observables	
Improve	Continue to enhance the network of single-point LEO observations through CubeSats, smallsats, and other means to characterize key observables of the thermosphere (in situ and/or remote sensing), including at least neutral density, temperature, composition and wind, ionospheric E-field, velocity, and current, and/or EPP.
	Dedicate simple missions to characterize orbital effects and atmospheric drag to support model verification/validation.
Advance	Progress toward populating the network of observatories defined in the close requirements listed below.
Close	Continuous ≤100 km spatial resolution, real-time data transmission from neutral density, temperature, composition and wind, ionospheric E-field, velocity, and current, and energetic particle precipitation monitors distributed around MLT and spanning polar latitudes.
EPP	
	See ionosphere and thermosphere above, and ring current and radiation belt elections below.
Ring Current and Radiation Belt Electrons	
Improve	Additional observatories measuring the ring current and radiation belt EPP in the LEO environment at a range of altitudes (~300 km≤ alt ≤ 1300 km), all geographic longitudes, and geographic latitudes up to at least ~75°.
	Additional observations measuring ~keV to ~hundreds of keV electrons and protons around more MLT at GEO.
Advance	Inner Belt: Additional observatories measuring differential intensity energy spectra and angular distributions of hundreds of keV to multiple MeV electrons and 1 MeV to GeV protons and heavy ions near the magnetic equator ranging from $1.1 \leq L < 3$.
	Outer Belt: Additional observatories measuring differential intensity energy spectra and angular distributions of tens of keV to multiple MeV electrons and chorus, EMIC, and hiss waves near the magnetic equator ranging from $2.5 \leq L < 8$.
Close	Continuous ≤100 km spatial resolution, real-time data transmission monitoring ring current and radiation belt EPP in the LEO environment at a range of altitudes (~300 km ≤ alt ≤ 1300 km), all geographic longitudes, and geographic latitudes up to at least ~75°.

Improve/Advance/Close	Description/Requirements
	Ring Current: In situ ring current observations (differential intensities of ~keV to ~100 keV electrons, protons, and heavier ions) from multiple, near-equatorial GTO spaced around several MLT and from several MLT at GEO.
	Outer Belt: Multipoint observatories simultaneously measuring differential intensity energy spectra and angular distributions of tens of keV to multiple MeV electrons and chorus, EMIC, and hiss waves near the magnetic equator ranging from $2.5 \leq L < 8$ spaced in at least 6 MLT sectors spanning 24-hours MLT and phased to enable full radial distributions of the outer belt electrons at least once per hour.
Injections and Plasma Sheet Electrons	
Improve	Accessibility to GPS and LANL-GEO observations in near-real-time.
	Reduced latency on observations from THEMIS and MMS.
	Additional observations measuring ~keV to ~100 keV electrons and protons around more MLT at GEO.
Advance	The above "improved" requirements plus any one or more of the following "close" requirements.
Close	At least one observatory measuring ~keV to ~MeV electrons per MLT-hour around GEO.
	~keV to ~MeV electron differential intensity observations from a high-inclination MEO constellation like GPS.
	~keV to ~MeV electron differential intensity observations from a network of near-equatorial HEO spacecraft (like THEMIS and MMS but with apogees inside of ~10 R_E geocentric distance) spaced around several MLT.

7 Lessons Learned and Findings

Sections 5 and 6 constitute the committee's response to the tasks assigned to it by HPD.

The measurement gaps are summarized in Table 5-1 (for SH) and Figure 5-1 through Figure 5-10 (for geospace) and their prioritization is discussed in Section 6.

In addition, the deliberations during the gap analysis and the study of the final measurement lists provided the committee with several lessons learned and findings. A distillation of these findings is given below in the hope it will be useful to the readers of this report.

Our main findings from the gap analysis are as follows:

- Most of the observational gaps can be addressed with *current* technology and capabilities. The gaps most often arise from sparse spatial/temporal/spectral coverage rather than lack of measurement capability.
- The lists reveal that increasing the impact level (from "improve" to "close") rely on increasingly diverse measuring systems. In other words, concrete advances in SWx *-casting require a systems approach; namely, *coordinated concurrent* measurements along three axes:
  - The same measurement types made from different locations (distributed)
  - The same measurement type made in finer grids (multipoint)
  - Complementary and supplementary measurements made in different regimes (imaging + in situ; SEL heliospheric + magnetospheric, off-SEL heliospheric, etc.)
- An effective systems approach requires a *long-term strategy and implementation plan* to be successful. The system can be built up over time, as resources become available, in a coherent and orchestrated manner.
- *Novel measurement capabilities* could result in big science and operational payoffs with current technologies and manageable risk (e.g., remote sensing of "seed" particle distributions via Ly-α spectroscopy, distributed in situ measurements of incoming solar wind within 0.7–1 AU,

high-heliolatitude solar and in situ observations over many rotations). This is an area where NASA excels.

- Important information for the gap analysis was not always available in the open literature. For example, the committee could not identify the forecasting requirements or forecasting status for some parameters (e.g., SXR peak intensity) nor locate studies to support specifications for some measurements (e.g., number of in situ measurements for robust reconstruction of CME B_z or optimal separations for SEP measurements). Furthermore, the committee was not in a position to quantify the impact on SWx forecasting from the mitigation of any given gap, other in the qualitative manner of "improve" to "close." This quantification and fine-tuning of many of the suggested "required measurements" could be achieved via OSSEs. Such studies could quantify the impact of a given measurement in SWx forecasting, help define the measurement-to-model-to-product flow (e.g., data assimilation techniques) and assist in developing infrastructure plans.
- Consider whether/where modeling can provide sufficient substitute for a missing/incomplete measurement. Such models may exist or can make good Living With a Star (LWS) or Space Weather Research-to-Operations (R2O) projects. For example, could models based on photospheric magnetic field measurements replace direct solar wind or EUV (or other wavelength) irradiance measurements for some purposes?
- The SH gap analysis identified several measurement types appearing repeatedly as "required measurements" in Section 5.1. This can also be gleaned from an inspection of Table 5-1. Their popularity signifies a wide-ranging SWx impact. In other words, this measurement set can be considered as the "backbone" or "core" set of measurements for addressing SWx issues. These measurement types are:

    - Photospheric vector magnetic fields
    - EUV disk imaging (in several wavelengths)
    - VIS coronagraphic imaging (overlap with EUV up to at least 15 $R_\odot$)
    - SXR intensity time profile
    - SXR-EUV irradiance
    - In situ P&F (including energetic particles)

- In geospace, the "backbone" measurements are more specific to different orbital regimes; for example:

    - Whenever possible, LEO spacecraft should carry core instrumentation for critical ionosphere and thermosphere observation gaps (including ionospheric disturbance, thermospheric expansion, GIC, and radiation hazards; see Figure 5-1 through Figure 5-9)
    - Whenever possible, GTO, MEO, GEO, and HEO spacecraft should carry core instrumentation for critical radiation belt and ring current observation gaps (i.e., to better diagnose and predict radiation hazards; see Figure 5-6 through Figure 5-9)
    - All crewed spacecraft (or lunar station or vehicle) should carry core instrumentation for monitoring and quantifying radiation hazards to both the spacecraft (or lunar station or vehicle) and astronauts onboard
    - Whenever possible, observables that can contribute as real-time boundary conditions for operational models (e.g., solar wind in peri-geospace as a real-time boundary condition for magnetosphere-ionosphere-thermosphere systems models) should also be improved

and populated; such real-time, observation-driven model boundary conditions should lead to improved performance and accuracy of nowcasting and forecasting models

Pathways to more efficient SWx *-casting:

- A SWx beacon capability for near-real-time data availability should be a requirement for all NASA missions with relevant SWx observations.
- Innovative solutions and strategic agreements and partnerships could be established to benefit from available rideshare and hosted-payload opportunities to help fill critical SWx observational gaps.
- A clearinghouse could be created to process SWx-relevant measurements and data from commercial operators or other sources.
- Commercial opportunities could be encouraged to produce SWx products from payloads owned and operated by commercial operators; such an approach may encourage the deployment of more SWx-relevant packages on commercial spacecraft.
- Some measurements (or derived data products) could be standardized to benefit data assimilation and model development.
- A set of baseline observational requirements for SEP measurements can be defined toward populating geospace, peri-geospace, and the heliosphere for improved *-casting of SEP access (and thus corresponding radiation hazard) to any location around geospace and the heliosphere.
- The value of OSSE techniques can be applied for optimizing the number and location of measurements in the heliosphere or geospace, for the multipoint measurements found in this analysis.
- The systems approach to SWx data processing and modeling can be expanded. Streamlined open-access interfaces for ingesting data into models, for model integration across the heliophysics regimes, and for modeling outputs to ease and speed up validation, evaluation, and research in general.
- All SWx data can be made openly available in near real time to encourage researchers to improve model development.
- An interactive set of visualization tools can be designed to show the system of SWx observatories throughout geospace and the heliosphere and plot data in near real time.

Appendix A. Acronyms

Acronyms			
ACE/CRIS	Advanced Composition Explorer/Cosmic Ray Isotope Spectrometer	LWS	Living With a Star (program)
AL	Auroral (Electrojet) Lower Index	MAE	Mean Absolute Error
APL	Johns Hopkins Applied Physics Lab	MC	Meridional Circulation
AR	Active Region	MEO	Medium Earth Orbit (apogee between LEO and GEO)
ASI	All Sky Imager	MF	Medium Frequency
BSS	Brier Skill Score	MFR	Magnetic Flux Rope
CBE	Current Best Estimate	MHD	Magnetohydrodynamic
CF	Convective Flow	MLat	Magnetic Latitude
CIR	Corotating Interaction Region	MLE	Mean Log Error
CME	Coronal Mass Ejection	MLI	Multilayer Insulation
COSPAR	Committee on Space Research	MLT	Magnetic Local Time
CR	Carrington Rotation	MMS	Magnetospheric Multiscale
DMSP	Defense Meteorological Satellite Program	MUSER	Mingantu Spectral Radioheliograph
DoD	Department of Defense	NAOJ	National Astronomy Observatory of Japan
DR	Differential Rotation	NiCT	National Institute of Information and Communications Technology
DSCVR	Deep Space Climate Observatory	NOAA	National Oceanic and Atmospheric Administration
D_{st}	Disturbance Storm-Time	NOx	Nitrous Oxide, in particular odd-reactive nitrogen
EIC	Equivalent Ionospheric Current	NSF	National Science Foundation
EM	Electromagnetic	OSSE	Observing System Simulation Experiment
EMIC	Electromagnetic Ion Cyclotron	P&F	Particles and Fields
ENA	Energetic Neutral Atom	PCA	Polar Cap Absorption
EOVSA	Expanded Owens Valley Solar Array	PIL	Polarity Inversion
EPP	Energetic Particle Precipitation (into Earth's atmosphere)	POD	Precision Orbit Determination
Es	Sporadic E-layer	POES	Polar Operational Environmental Satellites
ESA	European Space Agency	R1/R2	Region-1/-2 Currents
ETD	Event Total Dose	R2O	Space Weather Research-to-Operations (program)
EUFHORIA	European Heliospheric Forecasting Information Asset	R_E	(mean) Earth Radius (1 R_E = 6378.1 km)
EUV	Extreme Ultraviolet (wavelengths)	RO	Radio Occultation
EUVS	EUV Spectrometer	$R_\odot$	Solar Radius (1 $R_\odot$ = 6.957 × 10^5 km)
EVA	Extravehicular Activity	RSTN	Radio Solar Telescope Network
FAC	Field-Aligned Current	SDI	Scanning Doppler Imager
FAR	Fasle Alarm Ratio	SDO/AIA	Solar Dynamics Observatory/Atmospheric Imaging Assembly
FASR	Frequency-Agile Solar Radiotelescope	SED	Storm-Enhanced Density
FEMA	Federal Emergency Management Agency	SEE	Single Event Effect
FISM	Flare Irradiance Spectral Model	SEM/EPS	Space Environment Monitor-Energetic Particle Sensor
FOV	Field of View	SEL	Sun–Earth Line

Acronyms			
FPI	Fabry-Perot Interferometer	SEP	Solar Energetic Particles
FUV	Far Ultraviolet (wavelengths)	SH	Solar and Heliospheric
GBM	Ground-Based Magnetometer	SIDC	Solar Influences Data Analysis Center
GBO	Ground-Based Observatory	SILSO	Sunspot Index and Long-term Solar Observations
GCR	Galactic Cosmic Rays	SIR	Stream Interaction Region
GEO	Geosynchronous Earth Orbit (~36,000-km altitude)	SoA	Speed-on-Arrival
GIC	Geomagnetically Induced Current	SNR	Signal-to-Noise Ratio
GOES	Geostationary Operational Environmental Satellites	SRB	Solar Radio Burst
GLE	Ground Level Enhancement	SSI	Solar Spectral Irradiance
GNSS	Global Navigation Satellite System	SSN	Sunspot Number
GTO	Geosynchronous Transfer Orbit	SUSANOO-CME	Space-weather-forecast-Usable System Anchored by Numerical Simulations and Observations
HCS	Heliospheric Current Sheet	SUVI	Solar Ultraviolet Imager
HEO	High Earth Orbit (apogee >GEO)	SW	Solar Wind
HF	High Frequency	SWFO	Space Weather Follow-on
HI	Heliospheric Imager	SWx	Space Weather
HMI	Helioseismic and Magnetic Imager	SWxSA	Space Weather Science Application
HOx	Hydroxyl, in particular odd-reactive hydrogen	SXR	Soft X-rays
HPD	NASA's Heliophysics Division	TAD	Traveling Atmospheric Disturbance
HSS	High Speed Stream	TBD	To Be Determined
HXR	Hard X-rays	TEC	Total Electron Content
ICME	Interplanetary Coronal Mass Ejection	TID	Total Ionizing Dose
IMAP	Interstellar Mapping and Acceleration Probe	TNID	Total Non-Ionizing Dose
IMF	Interplanetary Magnetic Field	ToA	Time of Arrival
IR	Infrared	TSS	True Skill Statistics
ISS	International Space Station	USSF	United States Space Force
IP	Interplanetary	UV	Ultraviolet
IPS	Interplanetary Scintillation	VHF	Very High Frequency
ISR	Incoherent Scatter Radar	VIS	Visible
K_p	Planetary K-index	VLF	Very Low Frequency
LANL	Los Alamos National Laboratory	WAAS	Wide Area Augmentation System
LASCO	Large Angle and Spectrometric Coronagraph	WISPR	Wide-Field Imager for Parker Solar Probe
LRO	Lunar Reconnaissance Orbiter	WSA	Wang-Sheeley-Arge (Model)
LTO	Lunar Transfer Orbit	XRT	X-ray Telescope